THE UNIVERSITY OF TEXAS AT AUSTIN
**CENTER FOR TRANSPORTATION RESEARCH**

# Efficient Model for Predicting Friction on Texas Highway Network

Christian Sabillon
Joaquin Hernandez
Ruohan Li
Robing Huang
Jorge A Prozzi

# Technical Report Documentation Page

| 1. Report No.<br>FHWA/TX-22/0-7031-1 | 2. Government Accession No. | 3. Recipient's Catalog No. | |
|---|---|---|---|
| 4. Title and Subtitle<br>Efficient Model for Predicting Friction on Texas Highway Network | | 5. Report Date<br>  Submitted: December 2021 | |
| | | 6. Performing Organization Code | |
| 7. Author(s)<br>  Christian Sabillon, Joaquin Hernandez, Ruohan Li, Robing Huang, Jorge A Prozzi | | 8. Performing Organization Report No.<br>  0-7031-1 | |
| 9. Performing Organization Name and Address<br>  Center for Transportation Research<br>  The University of Texas at Austin<br>  3925 W. Braker Lane, 4th Floor<br>  Austin, TX 78759 | | 10. Work Unit No. (TRAIS) | |
| | | 11. Contract or Grant No.<br>  0-7031 | |
| 12. Sponsoring Agency Name and Address<br>  Texas Department of Transportation<br>  Research and Technology Implementation Division<br>  125 E. 11th Street<br>  Austin, TX 78701 | | 13. Type of Report and Period Covered<br>  Technical Report<br>  September 2019 – December 2021 | |
| | | 14. Sponsoring Agency Code | |
| 15. Supplementary Notes<br>  Project performed in cooperation with the Texas Department of Transportation and the Federal Highway Administration. | | | |

16. Abstract

The objective of this project was to develop a model to predict friction that could be applied at the network level to overcome some of the issues associated with friction measuring equipment. This project developed an instrument that can collect high-resolution surface profiles to determine macrotexture and microtexture under different conditions and on different surface types. These data were used to develop a model to predict friction and skid number with a high degree of accuracy. The instrument is able to collect data at highway speed, allowing accurate texture data collection on the entire network on an annual basis, and is small enough to attach to any surveying vehicle, so texture data can be collected as part of other operations, eliminating the need for an independent data collection effort. The development of this instrument provides not only savings but also enhances operational safety. The model was calibrated for 29 pavement sections in the Austin District, so the researchers recommend implementing the findings of this project and extending the calibration of the model to more pavement sections around the state.

| 17. Key Words<br>  Pavement surface, microtexture, macrotexture, friction, skid number, prediction modeling | | 18. Distribution Statement<br>No restrictions. This document is available to the public through the National Technical Information Service, Alexandria, Virginia 22312; www.ntis.gov. | |
|---|---|---|---|
| 19. Security Classif. (of report)<br>  Unclassified | 20. Security Classif. (of this page)<br>  Unclassified | 21. No. of pages<br>  151 | 22. Price |

Form DOT F 1700.7 (8-72) Reproduction of completed page authorized

# Efficient Model for Predicting Friction on Texas Highway Network

Christian Sabillon
Joaquin Hernandez
Ruohan Li
Robing Huang
Jorge A Prozzi

# Disclaimers

**Author's Disclaimer**: The contents of this report reflect the views of the authors, who are responsible for the facts and the accuracy of the data presented herein. The contents do not necessarily reflect the official view or policies of the Federal Highway Administration or the Texas Department of Transportation (TxDOT). This report does not constitute a standard, specification, or regulation.

**Patent Disclaimer**: There was no invention or discovery conceived or first actually reduced to practice in the course of or under this contract, including any art, method, process, machine manufacture, design or composition of matter, or any new useful improvement thereof, or any variety of plant, which is or may be patentable under the patent laws of the United States of America or any foreign country.

# Engineering Disclaimer

NOT INTENDED FOR CONSTRUCTION, BIDDING, OR PERMIT PURPOSES.

Research Supervisor: Jorge A Prozzi

# Acknowledgments

# Table of Contents

# List of Figures

# List of Tables

# List of Terms

| | |
|---|---|
| $C_m$ | Cross width mean |
| $C_s$ | Cross width skewness |
| $C_v$ | Cross width variance |
| $R_a$ | Absolute height average |
| $R_k$ | Kurtosis |
| $R_r$ | Solidity factor |
| $R_s$ | Skewness |
| $R_t$ | Ten-point mean roughness |
| $R_v$ | Height variance |
| $R_z$ | Maximum height |
| AIMS | Aggregate Imaging system |
| BPN | British Pendulum Number |
| BPT | British Pendulum Test |
| CTM | Circular Track Meter |
| DFT | Discrete Fourier Transform |
| DFT | Dynamic Friction Tester |
| DMS | Dense mix surfaces and stone matrix asphalt mixes |
| GN | Grip Number |
| HM CS | High macrotexture chip seal |
| LLS | Line Laser Scanner |
| LM CS | Low to medium macrotexture chip seal |
| LWT | Locked Wheel Tester |
| MAR | Missing at random |
| MCAR | Missing completely at random |
| MNAR | Missing not at random |
| MPD | Mean Profile Depth |
| MTD | Mean Texture Depth |
| OMS | Open-graded surfaces |
| PFC | Porous Friction Course |
| PSD | Power Spectral Density |
| PSV | Polished Stone Value |
| RMS | Root Mean Square |
| SCBW | Split Cosine Bell Window |
| SN | Skid Number |
| SOFA | Sabillon-Orellana Filtering Algorithm |
| SPT | Sand Patch Test |
| $SV_2$ | Two-point slope variance |
| $SV_6$ | Six-point slope variance |

# Chapter 1:   Literature Review

## 1.1   Pavement Texture

Pavement texture is defined by the irregularities on a pavement surface that deviate from a true perfectly flat surface. The texture of a pavement has been deemed one of the most important characteristics of the road surface given that it determines most tire/pavement interactions such as: noise, friction, rolling resistance, etc. (Maguire and Carme, 2015). Pavement texture typically requires specialized equipment and mathematical tools in order to be characterized.

A linear profile is the simplest representation of pavement texture. The profile is a two-dimensional representation of the surface texture obtained using a sensor device, such as a laser, that is described by two coordinates: distance and height, in the longitudinal and vertical directions, respectively (Zuniga-Garcia, 2017). Profiles can be considered stationary, random functions of the distance along the surface (Sanberg, 1987). Using Fourier analysis, these functions can be mathematically represented as a series of sines and cosine waves of various amplitudes and spatial frequencies or wavelengths. The texture wavelength is the spatial period of a wave. Typically, the wavelength is symbolized by the Greek letter lambda ($\lambda$) and reported in units of length (m or mm.). The spatial frequency ($f_s$) is defined as the inverse of the wavelength and given in cycle per meter. The texture amplitude is defined as the peak-to-peak height difference (Zuniga-Garcia, 2017). **Figure 1.1** illustrates the main parameters on a linear texture profile. Advances in technology allow for the measurement and analysis of 3D surface profiles. Profiles collected along the transverse direction of the pavement are also known as cross-sectional pavement profiles in the literature.
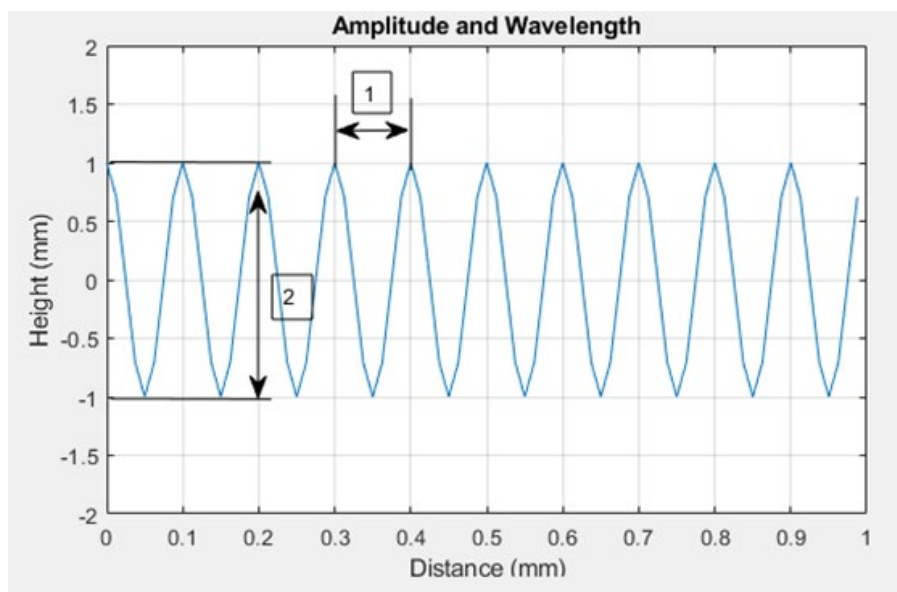


*Figure 1.1* *Basic terminology: wavelength (1), amplitude (2)*

### 1.1.1 Surface Texture Components

For the purpose of facilitating analysis, the irregularities of the pavement surface are usually divided into four components: unevenness or roughness, megatexture, macrotexture, and microtexture. Each category is a function of the domains of texture wavelengths or spatial frequency, given that they are related by the relation $f_s = 1/\lambda$ (Serigos et al., 2016). **Figure 1.2** illustrates the surface texture spectrum with the four main texture components and their respective wavelength or spatial frequency domain.



| *Unevenness or Roughness* | *Megatexture* | *1st Decade Macrotexture* | *2nd Decade Macrotexture* | *1st Decade Microtexture* | *2nd Decade Microtexture* |
|---|---|---|---|---|---|
| 500 mm | 50 mm | 5 mm | 0.5 mm | 0.05 mm | Wavelength (λ) |
| 2 cycles/m | 20 cycles/m | 200 cycles/m | 2,000 cycles/m | 20,000 cycles/m | Spatial Frequency (f$_s$) |
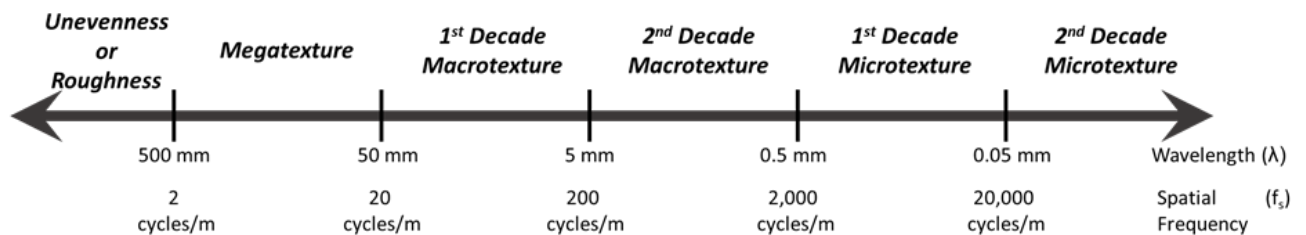
*Figure 1.2 Definition of fundamental texture classes, as a function of the wavelengths or spatial frequency*

Unevenness, also referred to as roughness, is the texture component that describes the irregularities in the pavement surface that affect the ride quality, smoothness, and serviceability. Its reference length would be equivalent to a short stretch of road. (AASHTO, 2008; Zuniga, 2017). Megatexture is defined by the distress, defects, or waviness of the road surface, and its wavelengths are in the same order of size as the tire/pavement interface. This type of texture is typically the easiest to appreciate with the naked eye. Examples of megatexture include ruts, potholes, and major joints and cracks (AASHTO, 2008). Macrotexture refers to the large-scale texture of the pavement surface due to the aggregate particle size and arrangement. In flexible pavements, mixture properties such as aggregate shape, size, and gradation control the macrotexture. In rigid pavements, the method of finishing the surface is what controls the macrotexture. This includes methods such as dragging, tinning, grooving width and spacing, and direction of the texturing. State-of-the-art practice methodologies used for measuring pavement texture at highway speed typically account only for macrotexture (AASHTO, 2008, Zuniga, 2017, Serigos et al., 2016). Microtexture alludes to the sub-visible or microscopic asperities of the aggregate surface, which control the contact between the tire rubber and the pavement surface (Serigos et al., 2016). Microtexture is a function of the individual aggregate particle mineralogy and petrology, the aggregate source (natural or manufactured), and is affected by the environmental effects and the action of traffic (Zuniga, 2017).

Each of the four texture components influence the interaction tire/pavement to varying degrees. Smit reported that the unevenness of the pavement plays a

significant role in the rolling resistance of the pavement, while the megatexture influences both rolling resistance and tire/pavement noise (Smit, 2008). However, the two components that seem to have a significant influence on a variety of surface characteristics (such as tire/pavement noise and skid resistance) are microtexture and macrotexture. Serigos and Zuniga agreed that when microtexture and macrotexture were taken into consideration on skid resistance correlation models, together they can account for at least 70 percent of the total variance in skid resistance on the road (Serigos et al., 2016; Zuniga, 2018). Furthermore, most traffic noise analysis research indicates that the peak of traffic noise occurs within the macrotexture wavelength spectrum although it is still not fully understood how those two parameters interact (Smit et al., 2016).

## 1.1.2 Summary Statistics

Summary statistics are the base of pavement texture characterization. Each component of pavement texture is associated with specific parameters that provide a general description for the texture profile. At the unevenness and megatexture levels, the most common and well-defined parameter is the International Roughness Index (IRI). Examples of parameters used at the macrotexture level include the mean profile depth (MPD) and the mean texture depth (MTD). In practice, either of these parameters is used to describe the pavement texture, however using only one of these texture statistics provides an incomplete description of the height distribution along the pavement profile. Pavements with similar MPDs can have completely different textures hence, additional parameters, such as kurtosis or skewness, can be used to provide a more comprehensive characterization. Microtexture is the hardest component to characterize in the field. Currently, there are no standardized methods to characterize this level of texture, but the same parameters used to characterize macrotexture could be defined at smaller wavelengths to characterize microtexture.

The set of statistics used to quantify pavement texture can be broken down into two main categories: spatial and spectral parameters. Spatial parameters are those which are calculated in the spatial domain and are scale dependent, meaning the same parameters are defined separately at different levels of texture. For example, MPD can be defined at both the macro and microtexture scale. In contrast, spectral parameters are calculated in the frequency domain and considered to be scale independent. They are estimated along a wide range of texture wavelengths in order to avoid complexity of defining the same parameters at different scales (Serigos et al., 2016).

### 1.1.2.1    Spatial Parameters

Spatial texture parameters are divided into four categories: amplitude, spacing, hybrid, and functional parameters. Amplitude parameters, also known as height parameters, consist of the statistical distribution of height values along the z-axis. Spacing parameters consider the periodicity of the data within the

distribution. Hybrid parameters are a combination of spacing and amplitude. Functional parameters give information about the surface structure based on the material bearing ratio curve. The bearing ratio curve is the cumulative probability distribution of the amplitude distribution function which gives the probability of a texture profile having a certain height, Z, at any position X. A summary of the most commonly used spatial parameters found in the literature is shown in **Table 1.1**, where $h_i$ represents the height of the measured profile, N the number of coordinates, and $\Delta x$ the horizontal distance between coordinates.

**Table 1.1 Spatial texture parameters used for pavement texture characterization (Zuniga, 2017)**

| Statistic | Equation |
|---|---|
| Mean Profile Depth (MPD) | $MPD = \dfrac{1}{2}\left[\max(h_1, \ldots, h_{N/2}) + \max(h_{N/2}, \ldots, h_N)\right]$ |
| Height Average (Ra) | $R_a = \dfrac{1}{N}\sum_{i=1}^{N}|h_i|$ |
| Maximum Height (Rz) | $R_z = \max(h_i) - \min(h_i), i = 1,2,\ldots,N$ |
| Root Mean Square (RMS) | $RMS = \sqrt{\dfrac{1}{N}\sum_{i=1}^{N}h_i^2}$ |
| Skewness (Rsk) | $R_{sk} = \dfrac{1}{RMS^3}\left(\dfrac{1}{N}\sum_{i=1}^{N}h_i^3\right)$ |
| Kurtosis (Rku) | $R_{ku} = \dfrac{1}{RMS^4}\left(\dfrac{1}{N}\sum_{i=1}^{N}h_i^4\right)$ |
| Two-Point Slope Variance (SV2pts) | $SV_{2pts} = \sqrt{\dfrac{1}{N}\sum_{i=1}^{N}\left(\dfrac{h_i - h_{i+1}}{\Delta x}\right)^2}$ |
| Six-Point Slope Variance (SV6pts) | $SV_{6pts} = \sqrt{\dfrac{1}{N}\sum_{i=1}^{N}\left(\dfrac{h_{i+3} - 9h_{i+2} + 45h_{i+1} - 45h_{i-1} + 9h_{i-2} - h_{i-3}}{60\Delta x}\right)^2}$ |

## 1.1.2.2 Spectral Parameters

Spectral parameters refer to parameters obtained in the frequency domain. Obtaining spectral parameters requires the use of Fourier analysis to examine the surface texture. A Fourier transform can decompose a texture profile into a function of sinusoidal waves. A common approach is to determine the parameters from the texture spectrum. The technical specification ISO 1373-4

(2008) describes the procedure to obtain the texture spectrum expressed in octave or one-third octave bands. The parameter used to characterize the texture spectrum is known as the texture level ($L_{tx,\lambda}$). The texture level is a logarithmic transformation of an amplitude representation of the texture profile having a center wavelength equal to lambda ($\lambda$) and reported in units of decibels (dB). This approach has been mainly used to find correlations between tire/pavement noise and the pavement texture, however, it has also been used in research studies intended to correlate texture and friction (Sandber and Descornet, 1980; Miller et al., 2011).

Another approach, known as Power Spectral Density (PSD), has commonly been used to analyze pavement texture in the frequency domain. The PSD is a description of how the energy of a pavement texture profile is distributed over the different frequencies. The PSD is obtained by applying a Fourier transform to the linear profile of a pavement surface to decompose it into a series of sinusoidal functions with discrete frequencies. Because so many sinusoids must be added together to build complex road profiles, individual amplitudes are almost always small. Hence, the Fourier transform is adjusted to show how the variance of the profiles is distributed over a set of sinusoids. This adjustment is known as the Power Spectral Density (Sayers and Karamihas, 1998). Serigos et al (2014) used the slope and intercept of the linearized PSD curve to characterize the surface macro and microtexture. The study observed a strong correlation between the log of the PSD and the log of the frequency in most of their sampled test surfaces.

Wavelet transform (WT) or wavelet analysis is an analytical developed to overcome the shortcomings of the Fourier transform. Wavelets are functions that satisfy certain mathematical requirements used to represent data. The wavelet transform can be used to decompose a signal into different frequency components and then, present each component with a resolution matched to its scale. The major advantage of the WT is that it allows for the analysis of a localized area of a larger signal hence, it can capture revealing aspects of the data that other signal analysis techniques might miss, such as, trends, breakdown points, discontinuities in higher derivatives, etc. In road roughness analysis, the wavelet analysis can reveal localized surface irregularities such as surface depressions, potholes, surface heaving and bumps (Wei et al, 2002).

Other studies have used fractal and multi-fractal theory to characterize texture. Fractal is a mathematical set that has a fractal dimension which usually exceeds its topological dimension and may be nonintegral (Mandelbrot, 2004; Mandelbrot, 1983). Fractals are typically self-similar patterns. Self-similarity means that they are "the same from near as from far". The fractal theory for pavement assumes that texture irregularities follow approximately the same pattern at different scales. Therefore, patterns observed at a lower frequencies could repeat at higher frequencies. In order to appreciate the similarity of the

texture patterns at different levels, the patterns need to be scaled by different factors known as the fractal dimension in the coordinate axis (Rajaei, 2017). Villani et al (2014) evaluated pavement surface friction properties using fractal analysis and developed a methodology that allows for the selection of aggregate type and mix design recipe for optimized skid resistance performance.

The spectral parameters described above are constructed from solid physical bases but are too complex for Pavement Engineers to use on a routine basis, as the statistics accompanying the models require significant time to be computed (Kane at al, 2015). To overcome this issue, new simpler approaches based on modern signal processing techniques have been developed. Among these techniques the simplest and most promising one is known as the Hilbert-Huang Transform (HHT) (Huang and Pan, 2006). The HHT is an empirical approach rather than a theoretical approach (like the Fourier or Laplace transform) that provides a way to decompose a signal into a set of functions and obtain instantaneous amplitudes and frequencies.

## 1.1.3 Texture Measurements

In terms of texture, there is wide variety of techniques and equipment used to measure texture based on the texture component of interest. Typically, transportation agencies collect data for roughness, megatexture and macrotexture for pavement management purposes. However, no standard has been developed to measure microtexture in the field so numerous efforts and research studies are being conducted to develop an affordable, efficient and reliable way to measure the finest component of the surface profile (Zuniga, 2017).

### 1.1.3.1      Roughness/Unevenness and Megatexture Levels

A topological survey can be used at the unevenness level to describe the pavement texture by obtaining the International Roughness Index (IRI). IRI was developed in 1986 by the World Bank as one the first standardized primary indicator for the serviceability of highway network to road users (Sayers et al., 1986). The index measures pavement roughness in terms of the number of inches per mile (in/mi) or meters per kilometer (m/km) that a theoretical car model "jumps" as the van is driven along the roadway. **Figure 1.3** shows a schematic of a Road Surface Tester (RST), a survey vehicle used to measure IRI. The measurements of IRI are typically within a wavelength range of 1.3 to 30 meters. (Sayers et al., 1986). In addition, these measurements can be further used to characterize the pavement at the megatexture level using the highest resolution possible. An alternative way to characterize pavement at the megatexture level is to use a similar survey vehicle to collect pavement rut depths. Rutting is a surface depression in the wheel path that results from the accumulation of plastic strains or permanent deformation occurring in the different layers of the pavement structure due to the action of repeated traffic loads (Little et al., 2018)
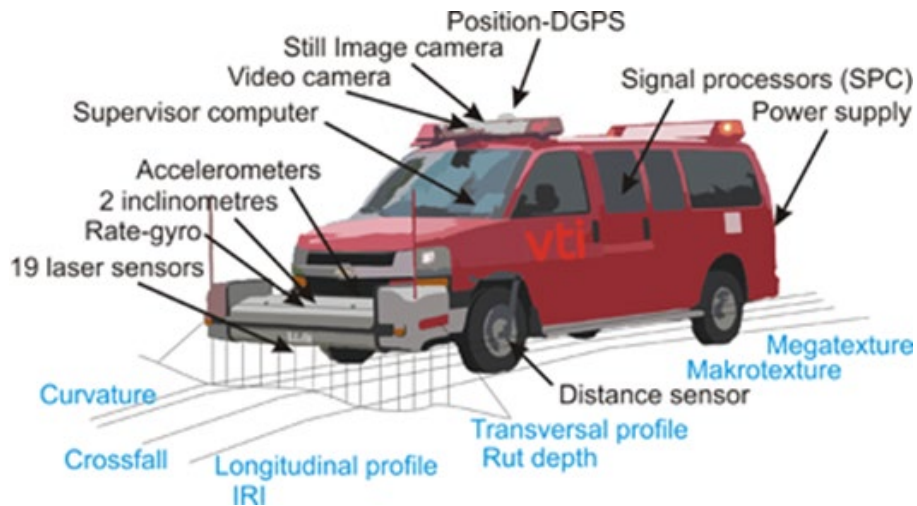
**Figure 1.3** *Schematic of a RST used to measured IRI and rut depth (VTI, 2021)*

### 1.1.3.2 Macrotexture Level

Measurements taken on the macrotexture level can be collected in two different ways: with on-spot or in motion measurements. On-spot measurements typically require traffic control in order for technicians to collect the data in a safely manner and a significant number of measurements to get a representative sample for the pavement. Examples of on-spot measurements involve volumetric techniques such as the Sand Patch Test (SPT) or non-contact measurements such as the Circular Track Meter (CTM). In-motion testing typically involves taking continuous measurements on the pavement as a vehicle or trailer equipped with proper instrumentation drives on the road. While these test methods do not require traffic control, current laser technology does not have a high enough resolution and sampling frequency to capture microtexture while driving at highway speeds. An example of in motion testing methods is the Laser Crack Measurement System (LCMS)

### *1.1.3.2.1 Sand Patch Test (SPT)*

Some of the most common volumetric techniques used to measure macrotexture on pavement are the SPT, grease patch test and outflow meter test. Out of the three, the SPT is the simplest and most commonly used by transportation agencies around the world. The method involves applying a known volume, which is typically 25 mm$^3$, of either solid glass spheres of uniform size or Ottawa natural silica sand on a relatively uniform, not distressed section of the pavement surface. The sand is later spread in a circular motion with a spreading tool, as shown in **Figure 1.4**. Once the roughly circular patch of sand is made, four equally spaced diameters are measured and averaged to compute the area of the sand patch. The known volume of sand is then divided by the area of the circle using **Equation 1.1** and reported as the mean texture depth (MTD) (ASTM E965, 2019). The grease patch method is a variation used by NASA in which grease is used instead of sand or glass spheres (Zuniga, 2017). The outflow meter

7

is a transparent vertical cylinder that is placed on the top of the pavement surface, it is filled with water and the time for the water level to fall by a fixed amount is measured and reported as the outflow time (ASTM E2380, 2015).

$$MTD = \frac{4V}{\pi D^2}$$ (1.1)

where $V$ is the sample volume for the material in mm$^3$ and D is the average diameter covered by the material in mm.



**Figure 1.4** *SPT equipment (left), and field data collection (right)*

An alternative to indirect measurements of the texture profiles involves more modern techniques using non-contact lasers, such as the Circular Track Meter (CTM) or the Laser Texture Scanner (LTS) (Zuniga, 2017). The information collected from these devices can be used to compute various profile statistics such as the mean profile depth (MPD) and the root mean square (RMS), as defined in Table 1.1.

### 1.1.3.2.2 Circular Track Meter (CTM)

The CTM is a device used to measure MPD and RMS. It consists of a laser displacement sensor that is mounted on an arm that rotates clockwise at a fixed elevation from the measured surface and a notebook computer that is used to control the device and save all the processed data as shown in **Figure 1.5** *CTM (left), and CTM segments*5. The device measures a 2D profile of a circle 284 mm in diameter and 892 mm in circumference. The profile is divided into eight segments with an arc length of 111.5 mm. The MPD is determined for each of the segments of the circle and the MPD reported as the average of the eight segments (ASTM 2157, 2015). The device later proceeds to calculate the RMS for the profile using the equation for RMS provided in **Table 1.1**. A major drawback of the CTM arises when measuring textures of concrete pavement. Given that the system measures texture along a circumference, it makes it difficult to measure longitudinal and traverse texture separately. These two types of textures are very important for rigid pavements, so it is recommended that

other techniques be used for that type of analysis. Another significant drawback is that it is time consuming for data collection purposes.



**Figure 1.5** *CTM (left), and CTM segments (right)*

## 1.1.3.3 Microtexture Level

There are other powerful laser devices capable of scanning and characterizing pavement texture at a macrotexture level, but the vertical and lateral resolution of these sensors is so high that they can also capture the first decade of aggregate microtexture. Currently, there are no standard methods to measure microtexture of pavements, but there have been multiple attempts at measuring microtexture using this advanced laser technology.

### 1.1.3.3.1 Line Texture Scanner (LTS)

The LTS is a lightweight and portable equipment designed to scan pavement surface coordinates in order to characterize its texture contents. It uses a laser sensor to scan the surface coordinate of parallel straight lines with a sampling rate of one point every 0.015 mm and a maximum scan area of 100 by 75 mm. The LTS computes the MPD, RMS, texture profile index, and estimated texture depth (ETD), which is an estimation of MTD based on MPD using an empirical equation, as shown in **Equation 2.2**. The resolution of the device allows it to measure and describe the two decades of macrotexture and the first decade of microtexture. However, scans performed at the highest resolution can take approximately two hours, making it impractical for field studies (Serigos et al., 2014). Zuniga (2017) also reports that the device is also not as reliable as the CTM, and researchers have experienced many operational problems with the LTS. **Figure 1.6** illustrates the LTS device along with the scanned 3D surface profile plot.

$$ETD = 0.2 + 0.8 * MPD \qquad \textbf{(1.2)}$$

where MPD and ETD are both measured in units of mm.
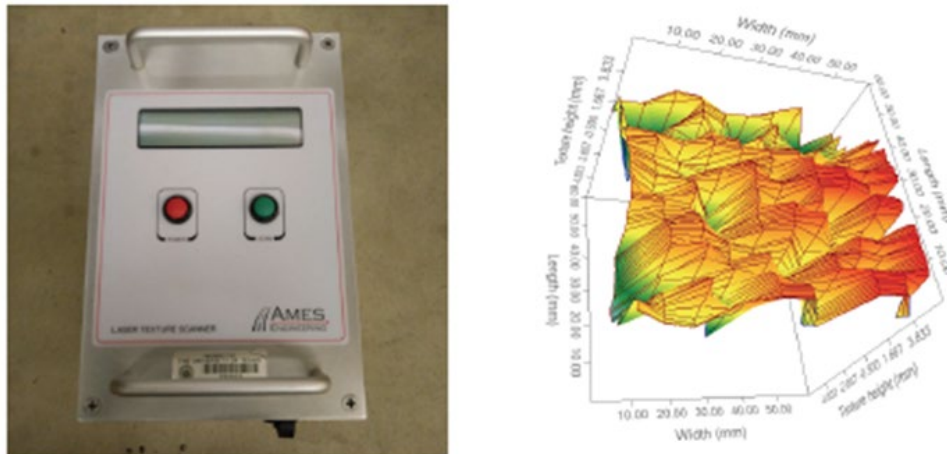


**Figure 1.6** *LTS (left), and 3D plot of measured surface (right) (Zuniga, 2017)*

### 1.1.3.3.2     Line Laser Scanner (LLS)

The LLS is a surface profiling system developed by the University of Texas at Austin to characterize macro- and microtexture (**Figure 1.7**). The device consists of a high-resolution line-laser scanner and a translation stage. The LLS can collect a maximum of 800 points in the transverse direction and up to 600 mm in the longitudinal direction. The equipment has an improved sampling rate that allows for the characterization of the two decades of macrotexture the first decade of microtexture (Zuniga, 2017). The main advantage that the LLS has over the LTS is its speed. The LLS can scan a wider area at a very high resolution in 15 seconds as opposed to two hours. Zuniga stated that not only is the LLS more efficient and reliable than both the LTS and CTM, but it also has a higher vertical resolution of 0.5 microns compared to the 15 and 3 microns of the LTS and CTM, respectively. The equipment is suitable to be used out in the field, so long as a covering mat can be placed over the translation stage to prevent sunlight from affecting the measurements of the lasers (Zuniga, 2017).



**Figure 1.7** *LLS (left), and field operation (right)*

### 1.1.3.3.3    LS-40 Portable 3D Surface Analyzer

The LS-40 is a portable 3D laser scanner (**Figure 1.8**) with ultrahigh resolution capable of scanning a 4.5 in. by 4 in. pavement surface and collect 3D texture data with a height resolution of 0.01 mm and a lateral resolution of 0.05 mm (Li et al. 2017). The 3D surface data provided by the LS-40 is used to calculate MPD and RMS by processing thousands of profiles over the entirety of the scanned surface according to the specifications of ASTM-1845 (2015). This piece of equipment can be used both under laboratory and field conditions to collect 2,048 by 2,448 cloud points for pavement texture characterization. Li et al. (2017) report that the LS-40 is not capable of providing detailed 3D texture scans with a resolution high enough to reach the first decade of microtexture, but it can provide other pavement surface features such as the aggregate form factor and multiple aggregate contour measurements to estimate characteristics at the microtexture level.



**Figure 1.8** *LS-40 Portable 3D Surface Analyzer (left), 3D surface scan (right) (Li et al., 2017)*

Another approach to circumvent the difficulties of measuring pavement microtexture is to use other measurements as surrogates for microtexture. Examples of alternative measurements for microtexture include the polish resistance of the aggregates, the British Pendulum Number (BPN) and image analysis techniques.

### 1.1.3.3.4    Polished Stone Value (PSV)

The PSV of aggregates is measured using a standardized test (BSI, 2013) where samples of aggregate are set in resin to form specimens that are mounted on the circumference of a wheel (**Figure 1.9**). This is then rotated for a period of time while a rubber tire is loaded onto the aggregate surface and a polishing medium trickled into the interface. At the end of the polishing process, the skidding resistance of the specimens is measured and compared with the results from specimens made with a control stone to calculate the PSV (Roe and Hartshorne, 1998). This measurement quantifies the resistance of an aggregate to the polishing action of vehicle tires under conditions similar to those occurring on a road surface. In the early 1970s, a relationship was established to predict

skidding resistance, in terms of side friction coefficient, from the PSV of the aggregate and expected traffic level in terms Average Daily Traffic (ADT) (Szatkowski and Hosking, 1972). However, it has been found that under certain circumstances the skid resistance achieved in practice does not match the one predicted by the relationship, and these discrepancies have given cause for concern. Furthermore, present-day traffic levels frequently require extrapolation of the original formula beyond the range of the data on which it was based. This can lead to over-optimistic or -pessimistic predictions of performance. Hence a good proportion of modern-day skid prediction research has emphasized updating the empirical relationship between PSV and skid resistance for a wider array of traffic levels and aggregate types (Roe and Hartshorne, 1998).



**Figure 1.9** *Accelerated polishing machine and aggregates (Roe and Hartshorne, 1998).*

### *1.1.3.3.5     Aggregate Imaging System (AIMS)*

The AIMS is a system that uses image analysis techniques to analyze the particle geometry of coarse and fine aggregate through three independent properties: form, angularity, and surface texture. The equipment consists of a camera, two different types of lighting schemes, and microscope technology (Masad, 2005), as shown in **Figure 1.10**. The AIMS analyzes the captured images of the aggregates using different techniques for each of the independent properties. The Wavelet method is used to analyze the aggregate texture; the gradient method and radius method are used to analyze the angularity of the aggregate; and the three-dimensional form of the aggregate is analyzed using sphericity and shape factors (Masad, 2005).

**Figure 1.10** *AIMS device*

## 1.2   Pavement Friction and Skid Resistance

Pavement friction is defined as the force that is generated as a result of vehicle tires rolling or sliding over a pavement surface. This force resists the relative motion between the tire and the pavement (Hall et al., 2009). Friction is typically characterized by the non-dimensional friction coefficient, which is the ratio of the tangential friction force to the perpendicular force applied on the pavement, as per **Equation 1.3**.

$$\mu = \frac{F_t}{F_v} \qquad\qquad (1.3)$$

where $\mu$ is the friction coefficient, $F_t$ is the tangential (tractive) force applied at the tire/pavement interface, and $F_v$ is the dynamic load on the tire perpendicular to the pavement.

Skid resistance is defined as the ability of the traveled surface of the pavement to prevent loss of tire traction (AASHTO, 2008). Skid resistance of pavements plays a critical role in road safety. Even with the high degree of complexity involved in highway crashes, the potential causes of these accidents can still be classified into three broad categories: driver related, vehicle related and road condition related (Noyce et al., 2005). Transportation agencies have little to no control over factors such as driver behavior, vehicle malfunctions or severe weather; however, they do have some control over pavement skid resistance. Several studies have shown that as the pavement skid resistance decreases the number of accidents on the road increases. Hence proper monitoring and

management of skid resistance in the highway network is required to control and reduce the number of road accidents (Serigos, 2016).

## 1.2.1 Friction and Skid Resistance Characterization

Most of the frictional force generated on the pavement is due to acceleration, braking or steering of the vehicles tires against the pavement (Flintsch et al., 2012). Two types of friction that are typically measured by transportation agencies are the longitudinal and side force friction. Longitudinal friction develops along the driving direction and has two extreme modes of operation: free-rolling (no braking), and constant brake. For free-rolling mode, the speed between the tire circumference and the pavement is equal to zero; this speed is also known as slip speed. Whereas in the constant break mode the slip speed increases from zero to the potential maximum of the speed of the vehicle (Flintsch et al., 2012). For any condition in between, the slip speed is known as variable slip speed and is measured as a percentage of the maximum speed of the vehicle. Side forced friction is the force generated as a result of the vehicle tires changing direction or compensating for pavement cross-slope or the effects of wind on the vehicle (AASHTO, 2008). The basic relationship between the forces acting on the vehicle tire and the pavement surface as the vehicle steers around a curve, changes lanes, or compensates for lateral forces follows **Equation 1.4** (Hall, Smith and Littleton, 2008).

$$F_S = \frac{V^2}{15R} - e \qquad\qquad \textbf{(1.4)}$$

where $F_s$ is the side friction, $V$ is the vehicle speed in mph., $R$ is the radius of the path of the vehicle's center of gravity in ft., and $e$ is the pavement super-elevation in ft./ft.

The skid resistance of a pavement is often represented by a parameter called the skid number (SN). The SN is determined by performing pavement friction testing using the locked-wheel method. As describe in ASTM E 274 (2015), the skid number will equal to the force required to slide a locked test tire at a given speed, divided by the effective wheel load and multiplied by 100. SN can also be estimated by multiplying the coefficient of friction by 100. This parameter is highly dependent on the texture of the pavement surface, and it is highly sensitive to wetness, pavement distresses, and temperature (Zuniga, 2017; Serigos 2016).

### 1.2.1.1      Friction Mechanisms

The frictional forces that develop between the pavement surface and a skidding vehicle tire are the result of a complex interaction of mechanisms such as: hysteresis, adhesion, abrasion and shear of the tire material. However, the

hysteresis and adhesion mechanisms account for the most significant contributions in the development of frictional forces at the pavement-tire interface (**Figure 1.11**) (AASHTO, 2008; Hall et al, 2009; Choubane et al., 2004).
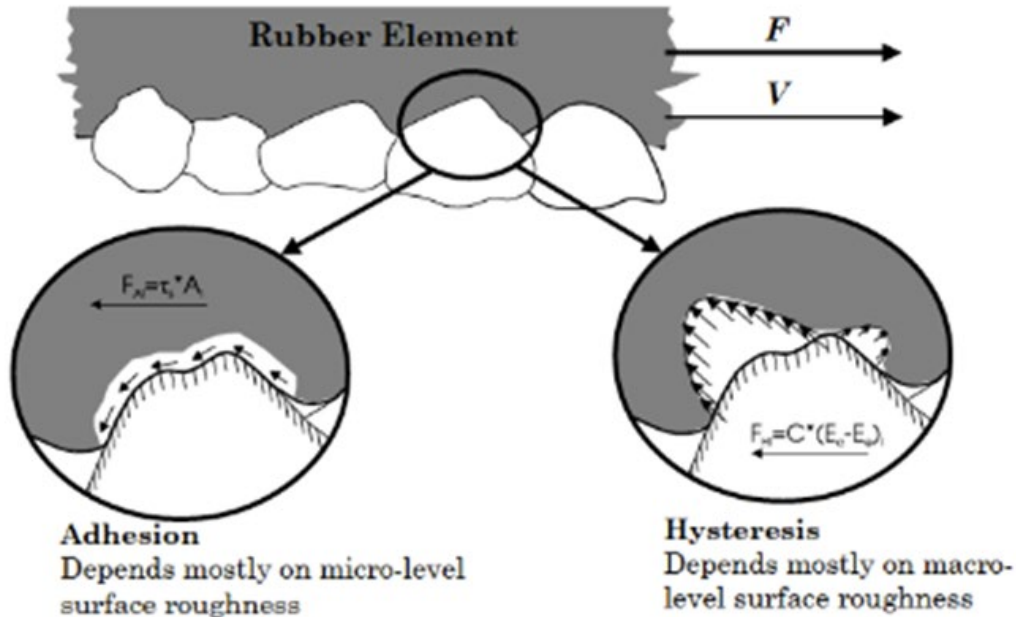


**Figure 1.11** *Frictional forces between pavement and vehicle (Hall et al., 2009)*

The adhesion component of the frictional force relates to the contact area between the rubber tire and the pavement surface. It is a result of Van der Waals forces developed at the tire-pavement interface. Van der Waals forces reflect the small-scale interlocking of microstructures as the micro-asperities of the two surfaces come in contact with one another (Hall et al, 2008). Adhesion is a function of the interface shear strength and the contact area. It is very sensitive to changes in the microtexture of the aggregate particles. This mechanism typically dominates on smooth-texture and dry pavements (AASHTO, 2008; Hall et al, 2009). The hysteresis mechanism results from the energy dissipation due to the bulk deformation of the rubber tire around bulges and depressions in the pavements surface as it traverses along the road. This deformation is commonly referred to as enveloping of the tire around the texture. As a tire compresses against the pavement, the stress distribution causes the deformation energy to be stored within the rubber. When the tire relaxes, a fraction of the stored energy is recovered while the remaining portion is lost in the form of heat (hysteresis), which is irreversible. It is this loss that leaves a net-frictional force that aids in stopping the forward motion of vehicles (NASEM, 2009). Unlike adhesion, hysteresis is most responsive to the macrotexture at the pavement surface and typically dominates under wet conditions and on rough-textured pavements. (AASHTO, 2008; Hall et al, 2009; Henry, 2000).

The coefficient of friction is a function of the slip speed of the vehicle (Henry, 2000). As seen in **Figure 1.12**, the coefficient of friction grows rapidly with increasing tire slip until it reaches the peak friction value. This value is highly dependent on microtexture and will typically occur at the critical slip which is a range from 10 to 30 percent slip (Hall et al, 2009). Any further increase in tire slip results in a decrease in the coefficient of friction until it reaches a value known as the coefficient of sliding friction. This occurs once the wheel is fully locked and the tire starts skidding over the pavement surface (Hall et al, 2009; Flintsch et al, 2012). The macrotexture of the pavement controls the slope at which the coefficient of friction drops after reaching its peak. The higher the macrotexture of the pavement, the shallower the slope and the smaller the loss in the coefficient of friction (Hall et al., 2009).
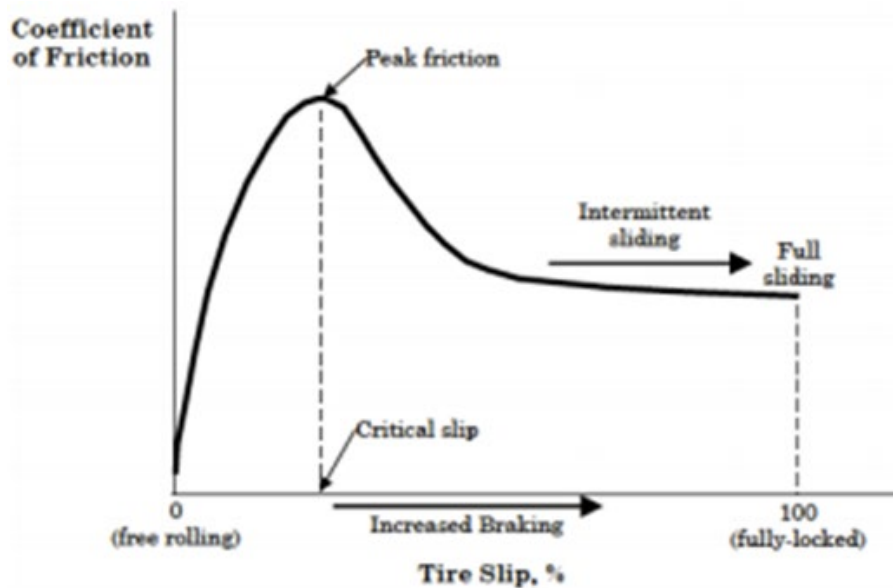


**Figure 1.12** *Friction coefficient and slip speed curve (Hall et al., 2009)*

## 1.2.2 Skid Resistance Measurement: Operational Principles and Equipment

Friction measuring devices utilize the main principle of a rubber sliding over the road surface and measuring the reaction force. The major operating principles of frictional measurement equipment for pavements are the slider, longitudinal friction coefficient (LFC) and side force coefficient (SFC) principles.

The slider principle encompasses devices used for stationary testing. It entails the use of a slider attached either to the foot of a pendulum arm or to a rotating head, which slows down on contact with the pavement surface. The rate of deceleration is used to derive a value representing the skid resistance of the road (Flintsch et al., 2012). Typically, slider operational devices are used to measure low-speed skid resistance of pavements. They are also characterized for being

stationary, relatively inexpensive and require traffic control in order to be safely operated in the field. The longitudinal friction coefficient is represented as the ratio of vertical forces to drag forces and its principle consists of the application of a braking force to a test wheel so that it rotates more slowly than the forward speed of the vehicle. This makes the test wheel slip over the surface and allows for the development of frictional forces. LFC principle-based devices are divided into three modes: locked-wheel, fixed-slip and variable-slip, each one having a different percentage of tire slip. All the test methods that are LFC-based consist of pulled device methods that utilize one or two full-scale test tires to measure friction properties. The side friction coefficient is represented as the ratio of vertical forces to sideway forces and its principle consists of using side-forced friction testers that use an instrumented measuring wheel set at an angle, known as slip angle, to the direction of travel of the vehicle. The slip angle induces friction between the tire and pavement as it makes the tire slip over the road surface (Flintsch et al., 2012). The following subsections describe the most commonly used equipment to measure pavement surface friction.

## 1.2.2.1 The British Pendulum Test (BPT)

The BPT is a manually operated test that provides an on-spot measurement of the surface friction. It evaluates skid resistance at low speeds by measuring the friction coefficient at a skidding speed of approximately 10 km/h (6 mph) (Henry, 2000), but some can go up to 12.5 km/h (7.8 mph). The test consists on using a pendulum-type tester with a standard rubber slider and a drag pointer. After calibration, the pendulum is raised to a locked position and then released to allow the slider to swing and slip on the pavement surface that has been manually wetted. A drag pointer swings along with the pendulum and indicates the British Pendulum Number (BPN) once the pendulum reaches its highest point on the first swing. The more friction the pavement has, the more it retards the swing of the pendulum, hence the higher the BPN reading. (ASTM E 303, 1998). BPN measurements are used as a surrogate of microtexture measurements, given that microtexture plays a very significant role at low-speed friction (Zuniga, 2017). **Figure 1.13** illustrates the BPT equipment used during field operation.



*Figure 1.13 BPT (left) and field operation (right)*

### 1.2.2.2 Dynamic Friction Tester (DFT)

The DFT is a modular system that is controlled electronically to measure friction by the slider principle. It measures the torque required to rotate a horizontal spinning disk fitted with three spring-loaded rubber sliders in a circular path as it contacts the pavement surface. Water is introduced in front of the slider by means of an elevated water tank to emulate wet weather conditions, as shown in **Figure 1.14**. The results for this test are typically recorded at speeds of 20, 40, 60 and 80 km/h (12, 25, 37 and 50 mph) and later plotted to obtain a speed versus friction relationship (AASHTO, 2008). Studies have shown that the values of DFT friction, when slip speed is 12 mph, are highly correlated with BPN (Wambold et al, 1998). Like the BPT, one of the main drawbacks of the DFT is that it requires traffic control in order to be safely operated in the field on in-situ surfaces.
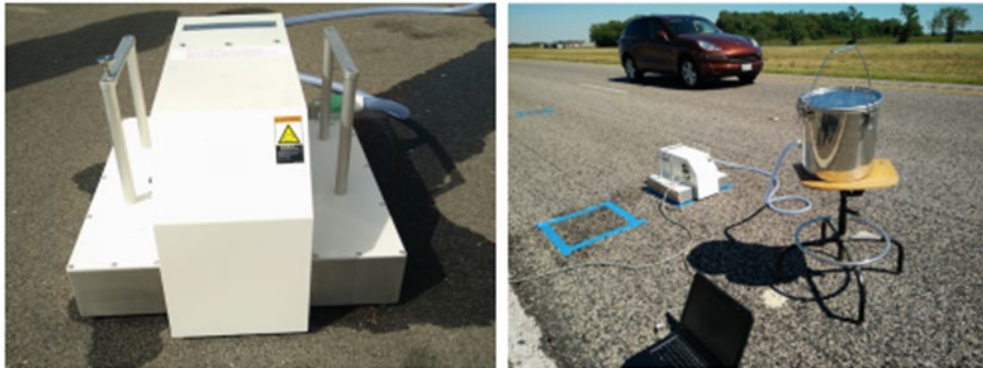


*Figure 1.14 DFT (left) and field operation (right) (Zuniga, 2017)*

### 1.2.2.3 GripTester and Micro-GripTester

The GripTester and Micro-GripTester are a type of continuous friction measuring equipment capable of dynamically measuring the longitudinal skid resistance coefficient of the pavement in terms of Grip Number (GN), or the coefficient of friction. These devices used fixed slip mode for measuring friction experienced by vehicles with ABS braking system. They are characterized by maintaining a constant slip that is typically between 10 and 20 percent as a vertical load is applied to the test tire (Henry, 2000). They have a single measuring wheel, fitted with a special smooth tire mounted on an axle designed to measure both the horizontal drag force and the vertical load force (Thomas, 2008). The difference between the GripTester and the Micro-GripTester is the scale of the device. The GripTester is towed behind a vehicle and uses measurement speeds that range from 5 to 100 km/h (3 to 62 mph) (Kogbara et al., 2016). The micro-GripTester is push manually by a technician at an average speed of 0.7 m/s (2.3 ft/s). **Figures 1.15** and **1.16** display the GripTester and Micro-GripTester devices, respectively, and their operation in the field.

**Figure 1.15** *GripTester device (left) and field operation (right).*



**Figure 1.16** *Micro-GripTester device (left) and field operation (right)*

### 1.2.2.4    Locked-Wheel Skid Tester (LWT)

The LWT is the most commonly used method for measuring pavement friction at high-speeds in the United States (**Figure 1.17**) (ASTM E 274, 2015; Henry, 2000). It is meant to test the frictional properties of the surface under emergency braking conditions for vehicles without anti-lock braking systems (ABS) by testing under a locked wheel mode. This implies that the wheel cannot rotate hence the slip speed of the tire equals the vehicle speed (Henry, 2000). The skid device consists of a smooth reference tire (ASTM E 524-08, 2015) locked into a device that is installed on a trailer that includes a water distribution system connected to a water tank placed on the moving vehicle. The trailer is then towed behind the vehicle at a speed of 80 km/h (50 mph). Once the vehicle reaches the desired speed, the water system sprays water in front of the smooth test wheel and then the braking system is engaged. The wheel is kept blocked for around one second and the average SN over that period is recorded (Flintsch et al.,

2012). Texas uses smooth tires given that they are very sensitive to macrotexture, but transportation agencies have also used ribbed tires in the past. Ribbed tires have proven to be more sensitive to microtexture than its smooth counterpart (Hall et al, 2009).



*Figure 1.17* LWT in operation

## 1.2.2.5    Sideway-Force Coefficient Routine Investigation Machine (SCRIM)

The SCRIM is a surface friction tester commonly used in Europe to measure wet-road skidding resistance (**Figure 1.18**). The machine operates by applying a freely rotating fifth wheel at an angle of 20° to the direction of travel on the road surface under a known load. Controlled water jets within the machine wet the pavement surface directly in front of the test wheel to emulate wet weather conditions. The vertical load and sideway force generated by the test wheel's frictional resistance to skidding are measured using transducers, and the output of those forces is then used to calculate an SFC value. The SCRIM can take continuous measurements of the SFC at speeds of 50 km/h (30 mph) (Pms.ie, 2017).

**Figure 1.18** *SCRIM equipment (Pms.ie, 2017)*

### 1.2.2.6 Harmonization of Friction Measurements

Due to the vast variety of friction measuring devices and all the different skid values one can obtain from these tests, making comparisons of skid values across different friction measuring devices is not trivial. For this reason, the Permanent International Association of Road Congresses (PIARC) developed the International Friction Index (IFI), an index that consists of two parameters: the friction number (F60) and the speed constant ($S_p$) to harmonize friction measurements across different friction measuring equipment to a common calibrated index (ASTM E1960-07, 2015; Fuentes and Gunaratne, 2011). This index is generally reported as IFI (F60, $S_p$) and the relationship follows **Equations 1.5** and **1.6** as follows:

$$F60 = A + B * FRS * exp\left[-\frac{(60 - S)}{S_p}\right] + C * MPD \qquad \textbf{(1.5)}$$

$$S_p = a + b * MPD \qquad \textbf{(1.6)}$$

where $FRS$ is the friction measurement obtained from a specific device at slip speed S (km/h); $F60$ is the prediction of calibrated friction number at 60 km/h; $S_p$ is the prediction for the calibrated speed constant; $A, B, C$ are regression parameters specific to a friction-measuring device; and $a, b$ are regression parameters specific to a texture-measuring device used to measure the mean profile depth (MPD). However, it should be noted that the IFI was reviewed and implemented by several highway agencies. There are mixed reviews about the accuracy and efficiency of the IFI to harmonize friction measurements into a single index. Furthermore, a drawback of the IFI is that any friction measuring

devices that did not participate in the international experiment does not have an equation to convert from its output of skid to the IFI (Hall, Smith and Littleton, 2008).

## 1.2.3 Prediction of Skid Resistance Practices

For transportation agencies worldwide, it is of utmost importance that most of the highway network has an adequate skid resistance to reduce the probability of wet-weather crashes. Nevertheless, there are three limitations that affect nearly all currently available skid measuring devices: 1) they are static devices that require traffic control to be used in the field, 2) technology used in the devices is improving but measurement repeatability is not, and the biggest limitation of them all, 3) the in-motion equipment is highly inefficient as it requires significant volumes of water to test a few miles of highway. For instance, to use the GripTester a 200-gallon water tank must first be filled with clean water. Once the tank is filled, surveyors can continuously measure skid resistance in terms of GN for approximately twenty miles before having to refill the tank. As the mileage in a highway network scales it becomes clear that continuous measurements of skid resistance for all roadways is not a sustainable operation, hence agencies must prioritize their major highway links when collecting skid measurements. This is the reason why agencies and research institutions have developed alternative techniques such as mathematical models to predict skid resistance on pavement surfaces.

### 1.2.3.1    Empirical Models

Using statistical analysis to comprehend the relationship between skid resistance and pavement characteristics is a common approach to estimate pavement surface friction. Serigos et al (2014) surveyed a total of 28 in-service flexible pavement sections within the state of Texas with multiple configurations of fine and coarse aggregate macrotexture and smooth and rough microtexture. They measured both pavement macrotexture and microtexture using the LTS device and used a wide array of texture statistics as predictors to estimate low speed skid resistance measured in terms of BPN. Their results showed that using spectral parameters that incorporate microtexture can increase the predictive power of the model from 0.67 to 0.76 in $R^2$. Furthermore, they showed that using spatial parameters, such as MPD, can yield prediction values for BPN that are as good as those obtained using spectral parameters, so long as both microtexture and the type of pavement surface are accounted for.

Zuniga-Garcia (2017) surveyed a total of 36 pavements across Texas including different surface types such as hot-mix asphalt, surface treatments and concrete sidewalks. The friction data was collected using the BPT, the DFT and the Micro-GripTester whereas macro and microtexture measurements were collected using the CTM and the LLS. Furthermore, when characterizing the microtexture only the active area of the profile was considered to compute the

summary statistics. In this study, Zuniga-Garcia tested three different skid prediction models using panel data analysis. One model included only macrotexture information, the second model included only microtexture data, and the final model incorporated both macro and microtexture information. The main findings of this study were as follows: 1) including the surface type of the pavement when modeling friction is important as there is no unique relationship between texture and friction; the relationship between friction and texture is strong but it varies depending on the type of surface, 2) MPD was the most significant parameter at the macro and microtexture levels out of the eight summary statistics that were tested to explain the variance in friction measurements and 3) all skid prediction measurements obtained using the BPT and the DFT were significantly improved once both macro and microtexture data were incorporated into the model, increasing the predictive power in $R^2$ from 0.70 up to 0.80.

Rado and Kane (2014) used the Hilbert-Huang Transform to analyze texture and friction relationships and found a set of parameters calculated from basic functions of the texture profile to be highly correlated with pavement friction. More recently, Rado, Kane and Timmons (2015) expanded on the study performed in 2014 and surveyed a total of eleven pavement surfaces in The French Institute of Science and Technology for Transport, Development and Networks test track to determine how the wavelengths, number and shape of pavement surface asperities affect pavement friction using the empirical mode decomposition of the Hilbert-Huang Transform to decompose the texture. All their texture measurements were collected using the CTM, whereas the friction measurements were collected using the DFT at test speeds of 20, 40 and 60 kph. Once decomposed, the texture's "sharpness" and "density" was quantified and correlated to friction. The study concluded that using solely the texture density in the models can account up to 77% of the variability in the friction measurements of the DFT, texture sharpness alone can account up to 66%, but the product of density and sharpness was able to account up to 85% of the friction measurements. This study further confirmed that accounting for pavement microtexture when predicting friction can increase the predictive power of the model significantly.

Subedi, Wu and Abadie (2016) tested a total of 22 asphalt pavement sections across 15 parishes in the state of Louisiana. They collected friction measurements using the LWT and the DFT and collected texture data on the pavements using the CTM. The pavements they tested consisted of 12.5-mm Superpave, 19-mm Superpave, stone mastic asphalt and open-graded friction course, the most common mixes used in Louisiana. Furthermore, once the researchers knew what aggregates were used in each of the test sections, they obtained a blend PSV, based on the PSV of the aggregates used in the mix. These information plus the design lane ADT, ADT growth factor and other gradation parameters were used to estimate the MPD of the road, SN at 40 km/h using either a smooth (SN40S) or ribbed (SN40R) test tire on the LWT, and the low-

speed skid resistance from the DFT20, which was used as a surrogate for microtexture. The results of their research are as follows: 1) while the prediction values obtained for MPD showed some discrepancies, it is thought that the predictions were only able to capture most of the field macrotexture component, but none of the microtexture, 2) they could estimate DFT20 with an $R^2$ of 0.88 using solely the PSV of the aggregates and traffic information, 3) incorporating macrotexture (predicted MPD) and microtexture (DFT20) into a non-linear prediction model for skid resistance using smooth tires yielded a relationship that can account for 73% of the variability in the SN40S measurements, and 4) by combining the predicted MPD and predicted SN40S, they could properly predict SN40R with an $R^2$ of 0.75. This study showed that incorporating mix design parameters and traffic information into the prediction model can be used as an alternative to avoid taking texture measurements of the network and still provide good enough prediction of pavement skid resistance.

# Chapter 2:   Development and Proposal of Skid Resistance Prediction Method

## 2.1   General Overview of Methodology

This chapter provides a summary of the methodology developed and used to create friction prediction models with a high degree of accuracy based on high-speed measurements of pavement surface profiles. The overall process consists of five major stages:

1. Data collection
2. Data processing
3. Feature engineering
4. Pavement surface prediction
5. Skid prediction modelling


At the data collection stage, the research team used a prototype data measuring and collection system to simultaneously collect friction and profile/texture data, on the same wheel path and at high speeds. During the data processing step, stringent criteria were enforced to ensure both texture and friction data were of the best possible quality before feeding them into the prediction models. At the feature engineering level, the texture statistics were computed and processed to enhance the efficiency of the classification and prediction models. The pavement surface prediction stage is where the processed texture data were used in machine learning models to create the most accurate prediction of the pavement surface at each of the surveyed sites. This step was crucial given that the literature indicates that the best friction prediction models are those that account for the type of pavement surface or mix. The final stage of the process consisted of creating the prediction model that best predicts skid resistance, given field texture data. A general overview of this procedure is provided in **Figure 2.1**, where the main stages are shown with a black background and all processes conducted within each stage are shown underneath with a blue background. Section 2.2 provides detailed specification of the data collection prototype developed by the University of Texas at Austin. An in-depth explanation of each of the stages, shown in **Figure 2.1**, is provided in sections 2.3, 2.4, 2.5, and 2.6. Finally, Section 2.7 describes the data processing performed on all the static data collection devices also used in this project.
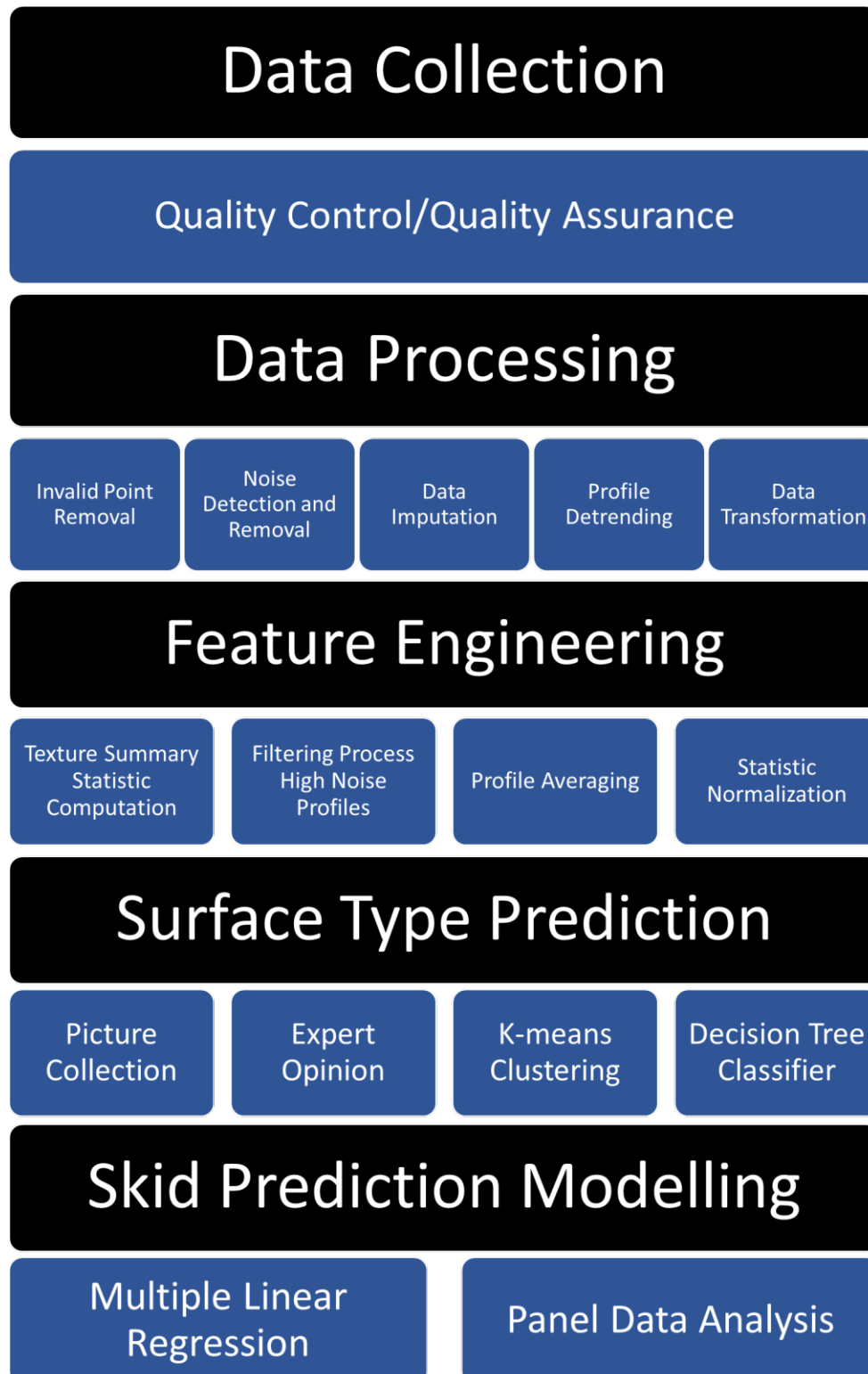
**Figure 2.1** *General overview of methodology from data collection to skid prediction*

## 2.2 Field Data Collection

The research team selected 29 pavement surfaces that cover a wide range of textures and skid numbers encountered in Texas. It was important to cover the most prevalent pavement surfaces in a way that is representative of the distribution of pavement mixes across the state. During this project, the focus was on flexible pavement so rigid pavement were not included. **Table 2.1** shows the breakdown of flexible pavements surveyed in this study.

**Table 2.1 Final selection of pavement surfaces**

| Pavement Type | Pavement Surface | Number ofSamples |
|---|---|---|
| Hot mix asphalt | Dense Coarse Mix (Type C,D) | 4 |
| Hot mix asphalt | Dense Fine Mix (TOM and Type F) | 2 |
| Hot mix asphalt | Stone Matrix Asphalt (SMA) | 3 |
| Hot mix asphalt | Porous Friction Course (PFC) | 7 |
| Surface treatment | Seal coat (Grade 3 and 4) | 8 |
| Surface treatment | Seal coat (Grade 5) | 4 |
| Surface treatment | Micro surfacing | 1 |

All 29 pavement sections were tested dynamically, using continuous measuring equipment moving at highway speeds. This testing included an in-house developed data collection prototype and TxDOT's LWT. In addition, three of these sections received a full battery of static texture and friction tests to validate the measurements obtained by TxDOT and the research team. These three sections were located along SH95, US79, and US290. Details of these tests are given in Section 3.1.2.

## 2.2.1 Testing Equipment

For the static testing, traffic control was coordinated with TxDOT to ensure the safety of both the researchers conducting the tests and the drivers on the road. In terms of texture, the researchers performed two traditional and well-accepted tests: the SPT and the CTM. Additionally, the research team deployed the LLS since it has been proven in previous research studies to be more accurate and efficient than other equipment capable of capturing macro and microtexture. In terms of friction, the researchers ran the DFT as it is one of the most traditional and widely accepted tests. All stationary tests were performed for the sake of comparison and validation of statistics obtained from the dynamic testing devices.

For the dynamic testing, friction data was collected using the conventional methods employed by TxDOT. Skid resistance data were collected using a LWT trailer. The SN measurements from the LWT were used as the ground truth in this research study. The research team also collected skid resistance and

pavement texture using a newly developed data collection prototype that combines a skid measuring trailer (namely, the GripTester) and a line laser sensor mounted on the trailer. The prototype can measure the full spectrum of pavement macrotexture (wavelengths of 50 mm to 0.5 mm) and a portion of microtexture (wavelengths of 0.5 mm to 0.322 mm) at highway speeds while simultaneously collecting skid resistance measurements on the same spot the laser is scanning.

## 2.2.2 Prototype Equipment Specifications

The GripTester was selected for measuring skid resistance due to its wide range of testing speeds (5 to 130 km/h), good repeatability, reproducibility, and its ability to grant the operator full control of the water flow used to achieve a given water thickness between the test tire and the pavement surface. In compliance with ASTM E2340, the device uses a smooth thread measuring wheel of 25.4 cm (10 in.) diameter that, when in motion, simulates a fixed wheel with 15% continuous slippage. The measurement tire is equipped with an automatic watering system that provides enough water to create a precise water thickness set by the operator. The amount of water that flows to the wheel self-adjusts depending on the traveling speed. The device was retrofitted with a laser sensor to capture texture profiles that are in sync with the GripTester's built-in encoder. The specificationsof the laser sensor are shown in **Table 2.2**. The laser used had a vertical accuracy of 2.6 microns.

**Table 2.2 Laser sensor specifications**

| Characteristics | | Specifications |
|---|---|---|
| Mounting conditions | | Diffuse reflection |
| Working distance | | 400 mm |
| Z-Range (+/-) | | 150 mm |
| Light source | Wavelength | 660 nm |
| | Laser class | Class 3B |
| | Output | 130 mW |
| Points per profile | | 2,048 |
| Resolution lateral | | 0. 161 mm |
| Sampling cycle (max) | | 25,000 profiles/s |
| Repeatability | | 2.6 µm |
| Linearity (% of Z-Range) | | ±0.01 |
| Environmental resistance | Enclosure rating | IP67 |
| | Ambient temperature | 0-50 C° (non-condensing) |
| | Vibration resistance | 2 g, 20–500 Hz ±0.01 (IEC 60068-2-6) |
| | Shock resistance | 15 g (IEC 60068-2-27) |

In the transverse direction, the laser has a resolution of 0.161 mm, meaning the spacing in betweeneach point within the laser line is on average 0.161 mm, with a total distance of 330 mm for a single profile. In the longitudinal direction, or the direction of traffic, a profile was obtained every 40 mm so as to obtain 25 texture reading for each grip number value. Lastly, the resolution in the vertical direction of the sensor is 5.0 μm. **Figure 2.2** shows the axis/direction convention for the line laser sensor being used.
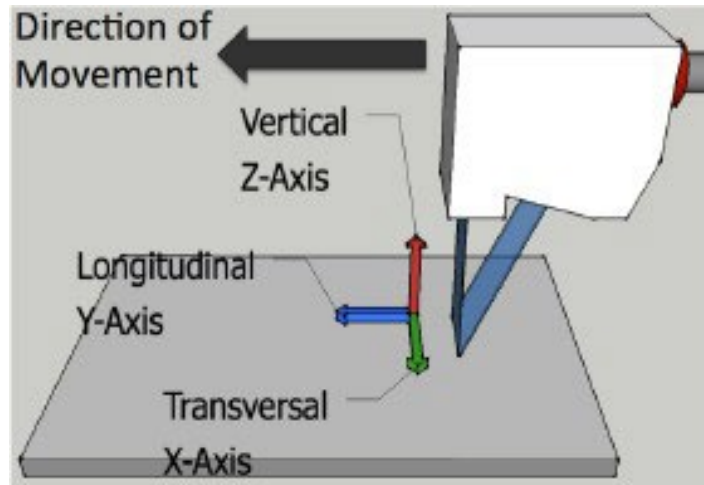


***Figure 2.2*** *Axis convention and direction of movement (Zuniga-Garcia, 2017)*

As indicated earlier, the GripTester was used for measuring skid resistance at a wide range of testing speeds. The combination of transverse profiles allows the 3D modeling of the surface without the need of adding longitudinal profiles. The laser sensor is synchronized with the GripTester and centered in front of the measuring tire and the water outlet. The laser sensor can measure a texture profile that is 330 mm in width on the transverse direction, enabling the researchers to capture the tire's contact area with the pavement which is roughly 50 mm (2 in.) wide. The two systems work together as they are both simultaneously triggered to collect data. For the GripTester, the trigger is converted to distance, and, for every meter of travel, the drag and load force are averaged and saved. For the laser sensor, the trigger is used to capture a single profile of height values. When the tires are inflated to 20 psi, the diameter is 254 mm, resulting in profile spacing of approximately 40 mm, subject to small fluctuations as the tire expands and contracts. More importantly, the trigger sends a signal to both systems to initiate data collection, keeping both data streams synchronized. **Figure 2.3** illustrates the data collection prototype.

**Figure 2.3** *Data collection prototype*

## 2.2.3 Data Collection Protocol Using the Prototype

The test starts when the survey vehicle reaches the test section that has been marked and pre- programmed into a GPS device. Near the test site, the system is connected to the test vehicle. The prototype has only two cables for data communication with the PC and is operated from inside the vehicle. A minimum of two individuals are needed: one for driving the vehicle and one for operating the software. With the vehicle stationary, the controlling computer awaits the trigger to initiate data collection. When the vehicle starts to move and reaches testing speed (50 mph), the user can monitor real-time data from the laser sensor (profiles, MPD, exposure of camera, and threshold of laser brightness) and real-time data from the GripTester (GN, target water flow, actual water flow, and vehicle speed). Furthermore, as data are collected, the operator can make notes that are saved with the data and stamped with the corresponding location. This is important when there is a specific start or stop in the test section or for the operator to denote changes in pavement. The software operator can check the real-time data and monitor the data collection system in a rear-view camera for proper operation. After completion of the test, the system is stored inside the vehicle to reduce wear on the test tire used to measure skid.

## 2.3   Prototype Texture Data Processing

This section explains how the raw data measured by the data collection prototype were processed before computing statistics or running prediction models.

## 2.3.1 Data Quality Control

Before processing the raw data, meticulous inspections were conducted to remove any faulty or invalid raw measurements. In terms of the measured skid, the GripTester provides a file for each survey performed, summarizing the distance travelled, GN measurements at every meter, load on the device, measuring speed, and water flow. Based on all the preliminary testing done on the prototype, the research team agreed upon certain filtering criteria to isolate valid GNs from invalid ones. A GN is considered valid under these conditions:

- the load on the GripTester device is between 100 and 400 Newtons,
- the water flow to the wheel is ± 5 liters per meter from the mode, and
- the speed of the surveying vehicle is higher than or equal to 47 mph.

The first filter was implemented to omit measurements taken when the GripTester went over a pothole, debris, or some other pavement distress that might make the device bounce and the wheel load fluctuate out of range. The second filter avoids measurements where the water flow to the wheel is not sufficient to provide a water thickness of about 0.5 mm. Finally, the last criterion eliminates measurements taken before the survey vehicle reaches highway speeds. Typically, during preliminary testing, this speed would be at least 80 kph (47 mph). **Figure 2.4** illustrates one of the quality control graphs used to isolate good measurements from invalid ones. The top part of the graph shows GN measurements that met all the criteria, highlighted in orange.
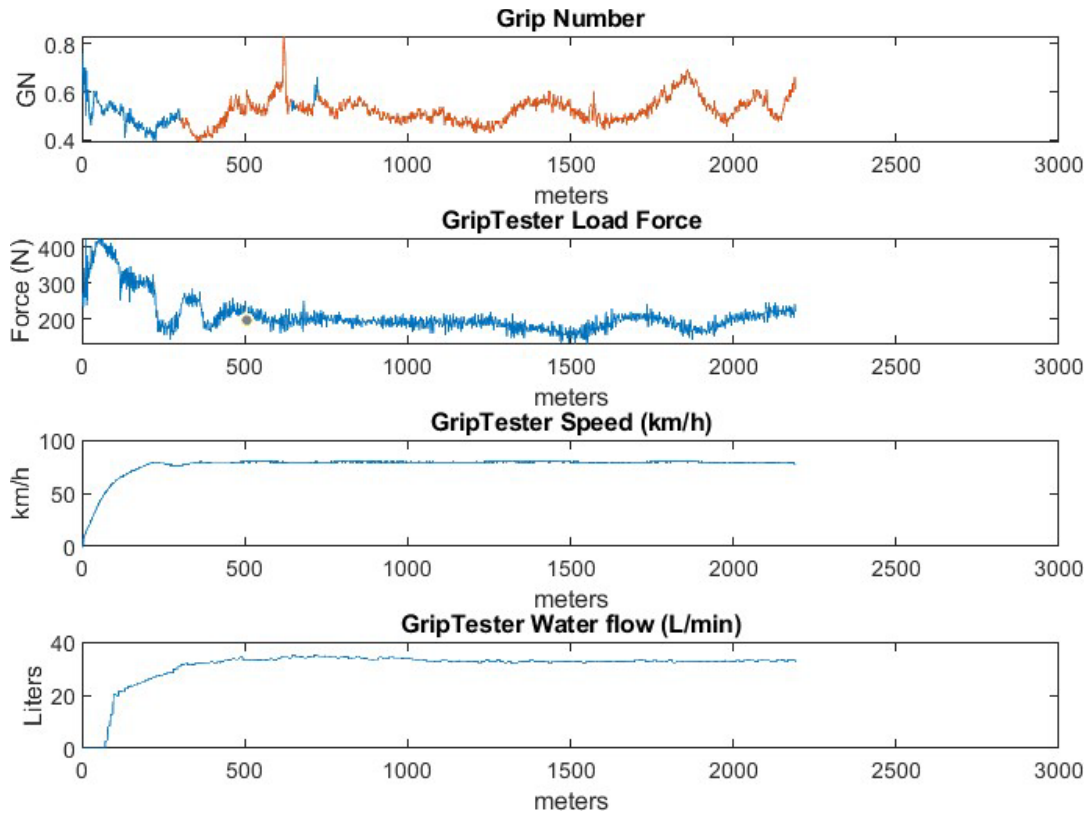
**Figure 2.4** *Skid resistance quality control chart: (top) GN measurements, (second) load force on GripTester, (third) vehicle speed, (bottom) water flow*

The texture data collected with the laser sensor mounted on the GripTester were first filtered to keep only data for which there was valid GN information. In other words, if the friction data for a given portion of the pavement section were invalid and filtered out, then all the texture data corresponding to that interval of length were also filtered out. This filtering process enabled the research team to work with valid measurements for skid and texture for the same locations along the pavement. The next step consists of trimming the scan area to isolate the 100 mm that correspond to the wheel path where the GripTester's wheel is measuring skid. In terms of length, this trimming process removes the leftmost and rightmost 114 mm of the cross-sectional profile.

## 2.3.2 Texture Data Processing

The above-mentioned preliminary filtering ensured every pavement cross-sectional profile had a corresponding valid skid number. The last thing that remains is to process the raw texture data from the sensor. Texture data were processed using a series of steps (shown in **Figure 2.5**) to ensure the data were of good quality before computing texture statistics.

These five steps are the foundation of texture data processing to ensure a high degree of quality in the final predictions. The research team performed extensive

32

research in each of those areas and developed robust algorithms capable of performing all these tasks. The first step is critical: to separate dead pixels (invalid data) from actual measurements. This is known as invalid point detection. The next step requires having an algorithm that can consistently and reliably detects and removes noise from profiles to prevent outliers from skewing or biasing the texture statistics. A robust imputation algorithm allowed the research team to work with complete datasets and remove any uncertainty and bias potentially introduced by missing data, i.e., the noise that was removed at the previous step. Detrending might be considered the simplest out of all the steps, but it is important to have a consensus on what is the best method to remove polynomial trends from a profile and what metric to use when removing an offset in the data. Finally, data transformation is a process that allows the user to assess the same texture data from a different point of view. For instance, by applying the Fourier transform, the data are transformed from the spatial domain into the spectral/frequency domain, where metrics such as the power spectral density (PSD) of the signal can be quantified. Examples of other transformations that have been used in pavement analysis include the Laplace transform, the Hilbert-Huang transform, and the wavelet transform.
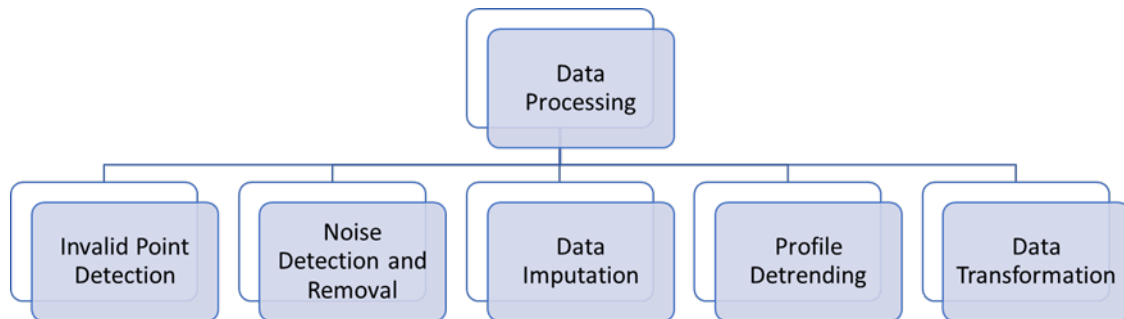


**Figure 2.5** *Texture data processing steps*

## 2.3.2.1    Invalid Point Detection and Removal

From this point on, invalid points are referred to as dropouts to avoid any confusion between dropout values and values that are just noise within the data. The research team defined dropouts as invalid readings at the edges of the profile. These dropouts are generated by a width correction algorithm in the sensor, whose purpose is to keep the distance between points at a constant interval in case the sensor's elevation changes. The camera captures less information across the x-axis the closer the sensor is to the scanning surface; thus, dropouts are imputed at the edges of the profiles to correct for the distortion of distance spacing. The left side of **Figure 2.6** illustrates this fact, where on the near side (the height where the sensor is closest to the surface), the number of dropouts at the edges of the profile is significant but decreases as the laser sensor is moved closer to the far side. When collecting data, the sensor must be placed at the reference distance, so it has room to oscillate between the near and far side as it collects data. The right side of **Figure 2.6** portrays an example where dropout values are shown as negative elevations with a high magnitude. The

valid measurements typically occur in the middle section of the profile, in this case, in places where the elevation is around 17 mm.
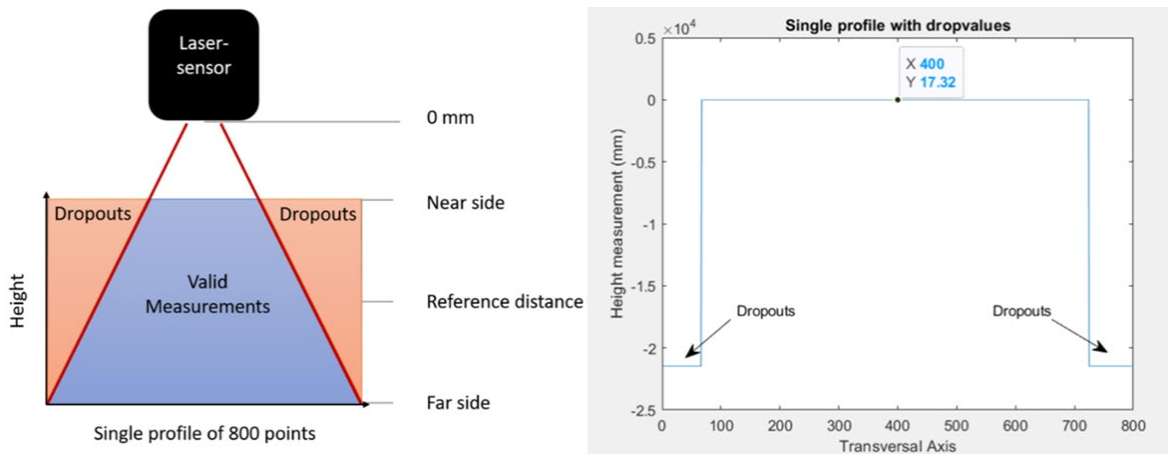


**Figure 2.6** *Schematic portraying how the number of dropouts reduces as the laser line approaches the far side (left); 2D view of data dropouts in a pavement profile (right)*

At this stage, profiles are free from dropouts because of the trimming performed at the quality control stage. However, the sensor's software outputs a value of -97.4 mm whenever the laser goes out of range or there is extreme light interference such that the camera is unable to capture the true surface elevation. This phenomenon simplifies identification of these other invalid points, as it implies that any value that is equal to -97.4 mm. is an invalid point and must be removed from the data. However, these types of points were removed at the noise removal stage.

## 2.3.2.2    Noise Detection and Removal

In signal processing, noise is broadly defined as anything that affects the signal that is being measured. Noise can arise from a variety of sources, related to the physics, sensors, data acquisition, or transmission. Some examples include thermal noise, electrical noise, electromagnetic noise, or even the effect of unmodelled physical effects. For the application of pavement surface scanning, often field conditions are not optimal when scanning a pavement surface, which leads to the introduction of noise within the signal. The most common instances of noise found in a profile are white noise, spikes, and flat signals.

### 2.3.2.2.1    White Noise

White noise is a random signal having equal intensity at different frequencies, giving it a constant PSD. This type of noise is inevitable and can even masquerade as microtexture within the profile. For this reason, it is important to note the resolution of the laser in the vertical direction before assuming that the laser has accurately captured the microtexture component. **Figure 2.7** shows an

34

example of this phenomenon, where white noise is added to a sine wave. To interpret the figure, the reader should assume that the sine wave at the top of **Figure 2.7** was a representation of a true pavement profile. The middle part was white noise generated by a sensor used to measure the profile (notice the scales are different). The true profile of the surface was smooth and had no microtexture; nonetheless the sensor introduced this white noise as it scanned the pavement. The output of the scan is given by the bottom graph in **Figure 2.7**. The white noise added by the sensor resembles micro-asperities that do not exist in the true profile shown on the top. To mitigate the influence of induced microtexture due to sensor white noise, low-pass filters could be used to remove wavelengths smaller than the vertical resolution of the sensor; however, in this project the implementation of such a filter was not necessary.
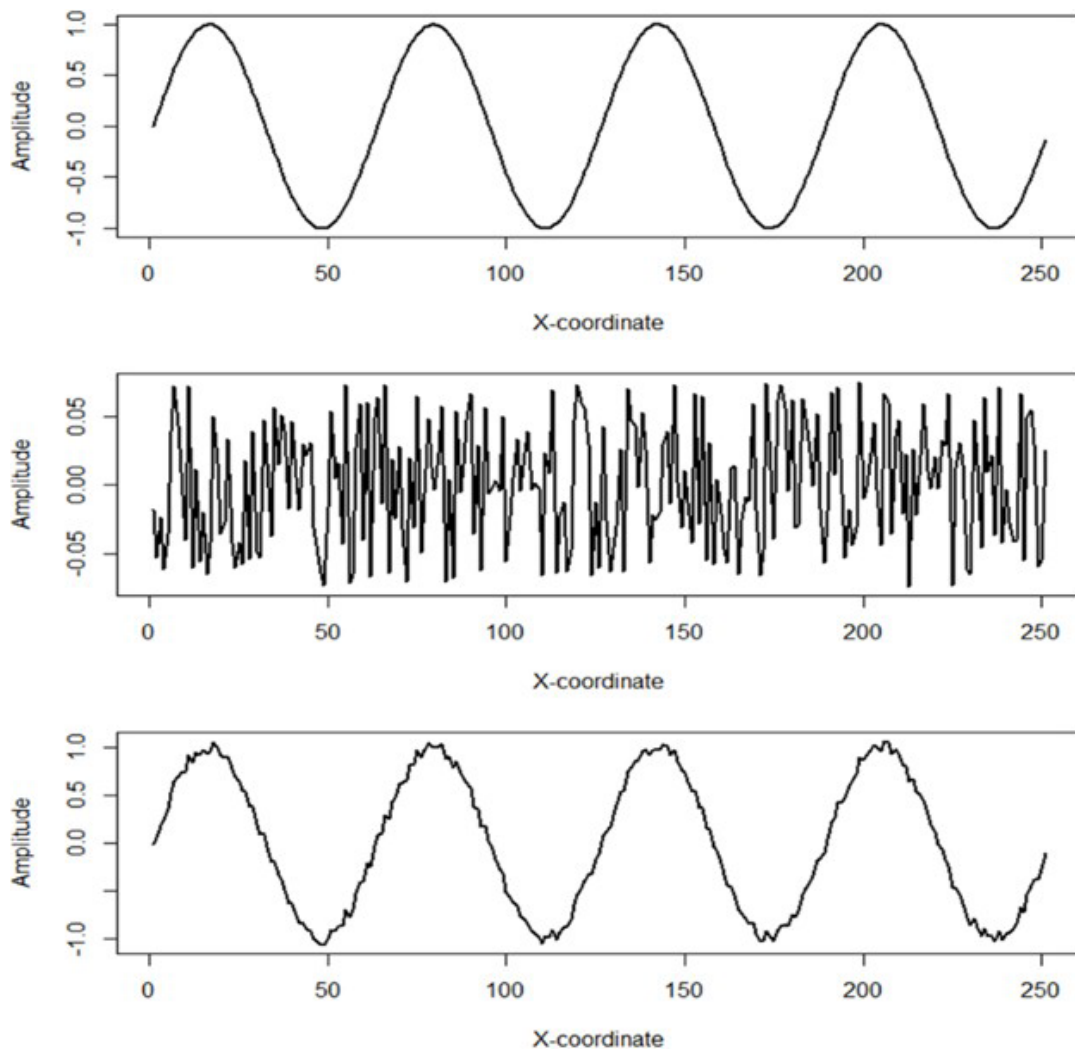


***Figure 2.7*** *Example of how white noise can be mistaken for microtexture: sine wave (top), white noise (middle), signal and noise (bottom)*

## 2.3.2.2.2 Spike Noise

Spikes are defined as any data point that shows as a short-duration, drastic elevation change. Spikes are usually due to the laser light reflecting on a shiny surface or not being captured by the camera. These points break the trend of the pavement profile and can be identified by visual inspection. Some spikes are extreme outliers, and their detection and removal can be automated with ease. However, there are also mild outliers that still break the trend of the profile, but their detection and removal process is not as straightforward and requires careful consideration. An easy way to distinguish between a mild and extreme outlier is that extreme outliers are usually the maximum or minimum points of the profile. Mild outliers, on the other hand, are not the extreme points of the profile, but they still clearly break the trend of the data. **Figure 2.8** illustrates examples of both types of spikes. It should be noticed that there is an argument that downward spikes could be the results of cracks or joints in the pavement and not necessarily noise. The validity of that argument depends on the spacing of points along the profile. The sensor being used has a spacing of 0.161 mm between points. According to TxDOT construction specifications for surface treatments, TxDOT seals cracks with a width in the range of 1/16" (1.5 mm) to 1/2" (13 mm). This means that the laser should be able to capture at least nine points for the smallest crack width that TxDOT determines to be problematic enough to require sealing. Recall that a spike is a single data point. This argument is made to guarantee that the mild or extreme downward spikes in these profiles are not joints or cracks on the pavement.
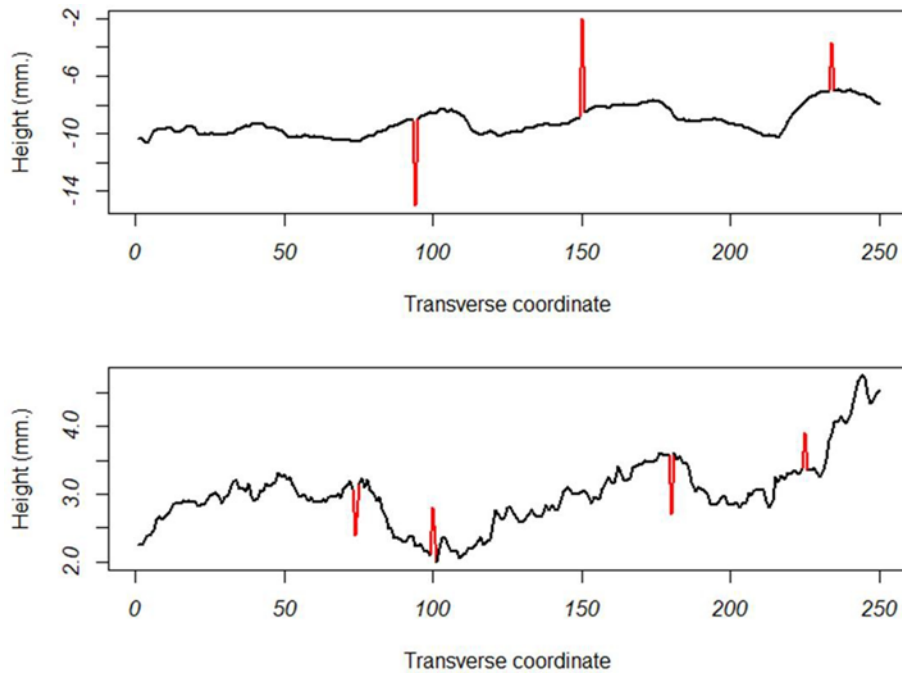


**Figure 2.8** *Different types of spikes: extreme outlier (top), mild outlier (bottom)*

### 2.3.2.2.3 Flat Signal Noise

Flat signals are the result of the combination of a low exposure time for the camera and a very dark pavement surface. In this situation, the sensor blurs the measured information and outputs a flat line where the elevation at multiple locations is the same as the last "good" point measured by the sensor. It should also be mentioned that a more powerful laser and corresponding filters could help in minimizing flat signals. **Figure 2.9** shows an example of flat signals within a profile.
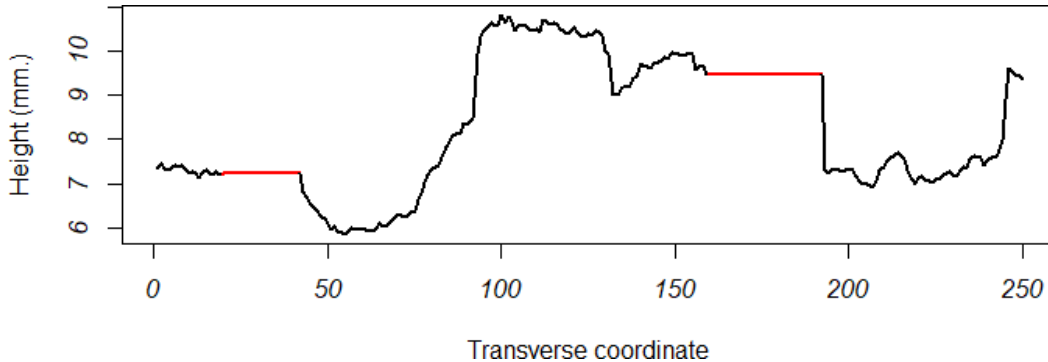


**Figure 2.9** *Example of flat signals*

The next subsection specifies the algorithm used to detect and remove spikes and flat signal noise in the collected profiles.

### 2.3.2.2.4 Sabillon-Orellana Filtering Algorithm (SOFA)

The filtering algorithm developed by the research team to deal with these instances of noise is known as the *SOFA*, which stands for Sabillon-Orellana Filtering Algorithm. This algorithm uses boxplots and the difference between consecutive points to consistently detect and remove all instances of spikes and flatlines along the profiles in a timely manner. The SOFA consists of a calibration phase and eight filtering stages:

1) Pre-processing
3) Flag signal removal
5) Spiked flatline removal
7) Mid-flatline spike removal

2) Boxplot outlier removal
4) Difference removal
6) Fine-tuned spiked removal
8) Endpoint pre-imputation

In the calibration phase the algorithm processes at least 2,000 profiles collected with the laser sensor used for field data collection. This allows the SOFA to adjust to the specifications of any sensor that is chosen. The calibration phase is used to determine five metrics: 1) a lower bound for what would be considered an extreme difference between two points (usually the 5th percentile), 2) an upper bound for that same extreme difference (usually the 95th percentile), 3) a fine-tuning parameter to remove a specific type of spike from the profile (usually the

98th percentile of extreme differences), 4) an absolute lower bound for which any point that has an elevation lower than it, is an extreme outlier and, 5) an absolute upper bound for which any point that has an elevation higher than it, is an extreme outlier.

Once the calibration phase is over, those five metrics are used as threshold inputs in the SOFA for the eight filtering stages. To visualize what SOFA does, a sample profile was selected from the data. This profile shows most instances of noise that are removed at every stage of the algorithm. As this section discusses each of the subsequent stages of SOFA, a picture of this profile will be shown with the output of the algorithm. The sample profile can be observed in **Figure 2.10.**
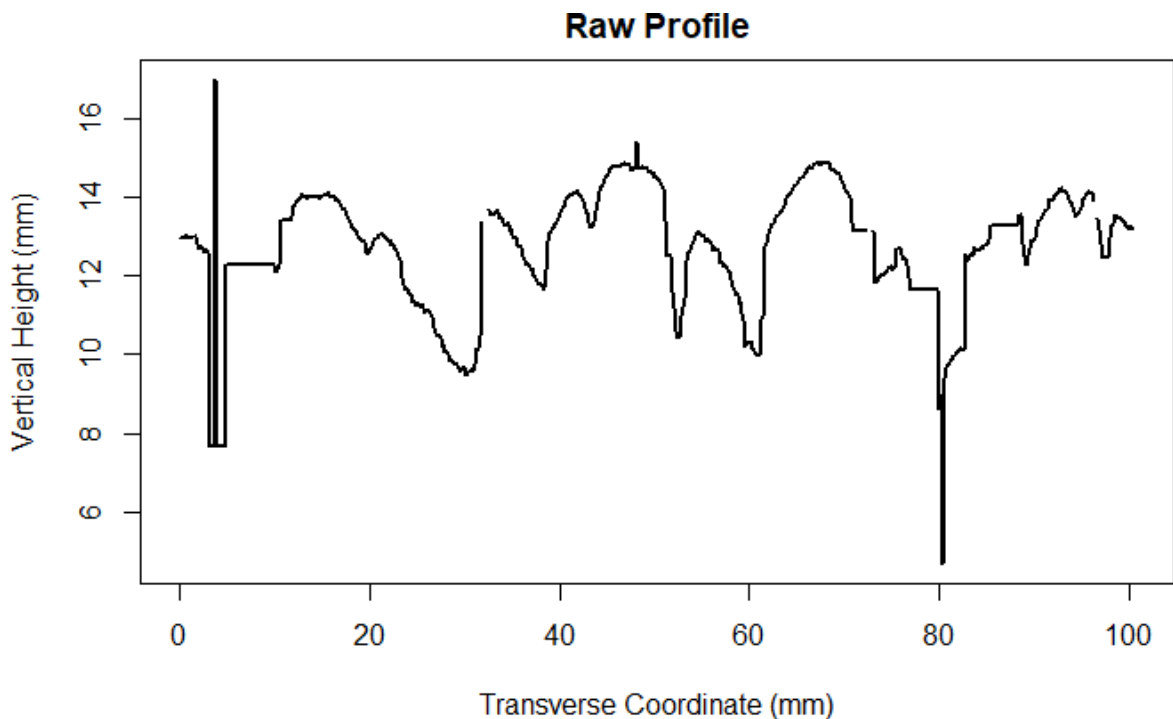


**Figure 2.10** *Sample raw profile*

The pre-processing stage consists of three steps: pre-imputation, offset suppression and difference computation. At the pre-imputation step, the algorithm imputes the value of -97.4 anywhere in the profile that might have missing data. This is to ensure that the dataset is complete as future stages in the algorithm do not work if there are missing data. The offset suppression step's goal is to center the profile around 0.0 mm in the vertical direction. To do this, the median of the profile is computed and subtracted from the whole profile. **Figure 2.11** illustrates the pre-imputation and offset suppression stage on the sample profile.
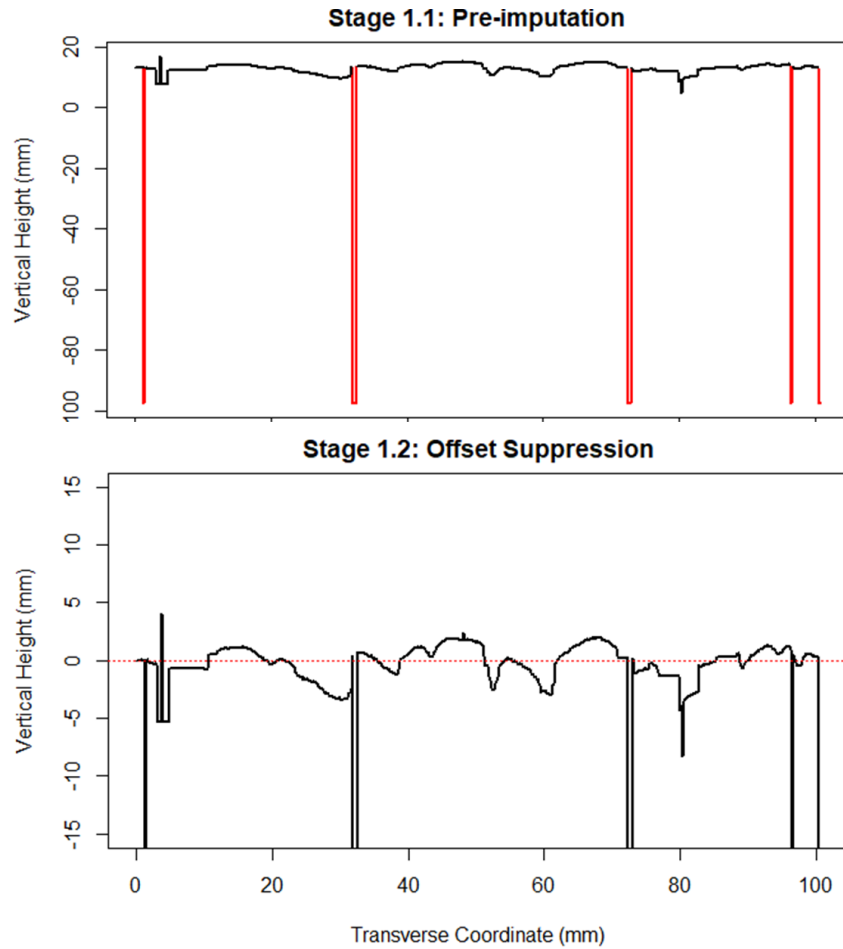
**Figure 2.11** *Pre-imputation step with imputed values highlighted in red (top) and offset suppression step with a highlighted horizontal line at 0.0 mm (bottom)*

Lastly, at the difference computation step the algorithm computes two vectors:

1) The Backward Difference (BD): This vector considers a point, $p_i$, within the profile and the point immediately behind it, $p_{i-1}$, and takes the difference of the two as follows:

$$BD_i = p_i - p_{i-1}$$

2) The Forward Difference (FD): This vector considers a point, $p_i$, within the profile and the point immediately in front of it, $p_{i+1}$, and takes the difference of the two as follows:

$$FD_i = p_i - p_{i+1}$$

Because of the way the BD vector is defined, there is a problem when the first point in the profile is analyzed since there is no point immediately behind it. FD suffers the same limitation when analyzing the last point. To accommodate for this issue, the first and last two points in the profile are used to compute these vectors but they are not a part of the final denoised profile. That is, once the filtering process is completed, the first two points and last two points are trimmed away.

The second stage involves using boxplots to remove any extreme outliers from the profile. Using the fourth (Q1) and fifth (Q3) metrics from the calibration, the average interquartile range (IQR) of the profile is computed as the difference between Q3 and Q1. In this dataset, these statistics were determined to be: Q1= -3.74 mm,Q3 =3 .42 mm and IQR = 0.94 mm. The boxplot filter is then defined as any value that is more extreme than either of these two quartiles by more than three times the interquartile range as shown below.

$$\begin{cases} X < Q1 - 3 * IQR \\ X > Q3 + 3 * IQR \end{cases}$$

where X is the elevation at any point along the profile. **Figure 2.12** shows the output of the boxplot filter. Using the values stated above, the threshold values for the boxplot filter are as follows:

- If $X < -6.58\ mm$, then remove the point
- If $X > 6.26\ mm$, then remove the point
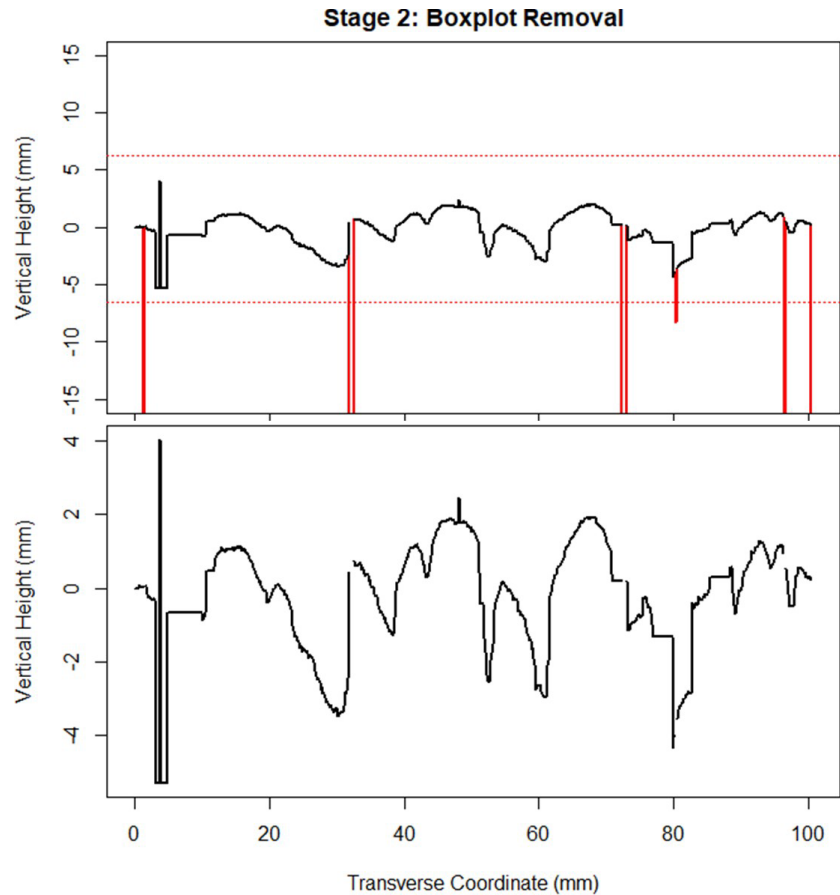
**Figure 2.12** *Boxplot filter with threshold shown as red horizontal dashed lines and removed data points highlighted in red (top) and profile after boxplot filter has been applied (bottom).*

The third step of the SOFA removes flat signals from the profile. As noted in the discussion above, flat signals blur the measured information and output a flat line where the elevation at multiple locations is the same as the last "good" point measured by the sensor. This implies that the first point in the flat signal is valid, but all the others are not. Hence, this step removes from the profile any point that an entry in the *BD* vector where *BD* = 0. **Figure 2.13** shows the output of the flat signal removal.
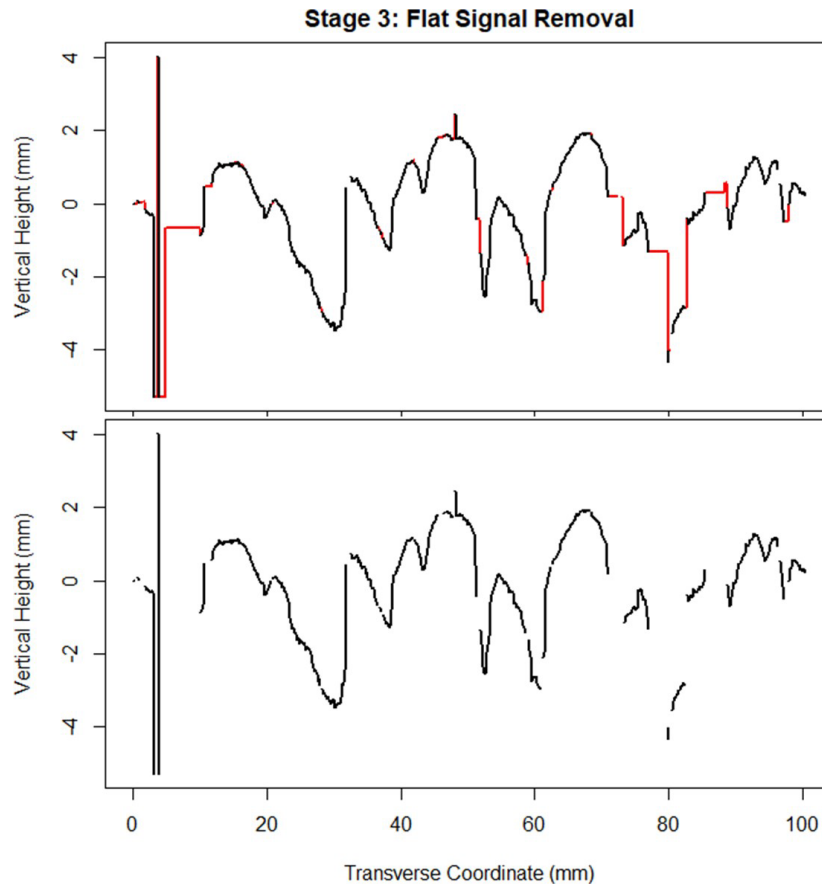
**Figure 2.13** *Profile with removed data points highlighted in red (top) and profile after all flat signals have been removed (bottom).*

The fourth stage removes mild spikes from the profile. Here the first and second calibration metrics (T1 and T2, respectively) from the calibration stage are used to remove all mild spikes from the profile. For the dataset that was used in this study, it was determined that T1 and T2 were -0.21 and 0.21 mm., respectively. The research team acknowledges that there is a small probability that there could be valid data points that meet this criterion, however, the proportion of such points is minuscule when compared to the data points that meet this criterion but are indeed spikes. For this reason, this is a tradeoff that the research team is willing to take. Thus, 0.21 mm was the threshold value used to differentiate a mild outlier from the rest of the data. The detection and removal criteria are as follows:

- If ($BD_i > 0.21$ AND $FD_i > 0.21$), then remove the point
- If ($BD_i < -0.21$ AND $FD_i < -0.21$), then remove the point

**Figure 2.15** shows the output of the difference removal.
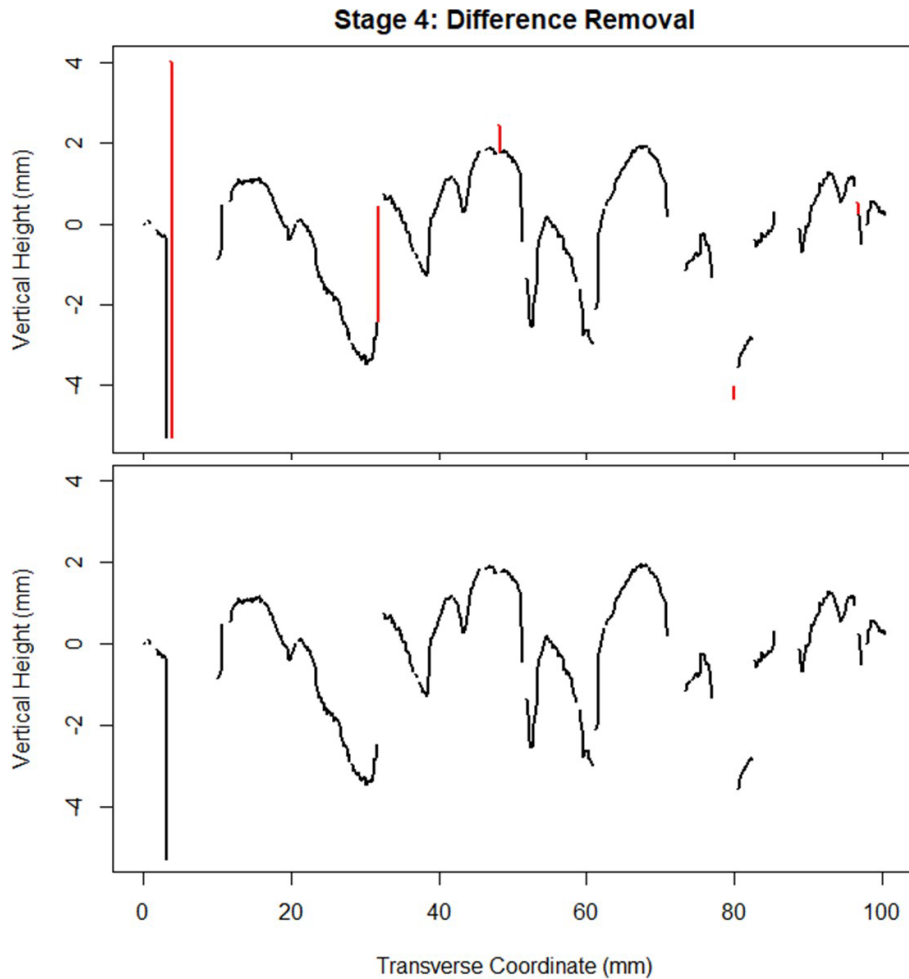
**Figure 2.14** *Profile with removed data points highlighted in red (top) and profile after mild spikes have been removed (bottom).*

These last three steps combined can detect and remove about 88% of noisy data points based on a visual inspection of a sample of 250 profiles coming from different pavement surfaces. All other stages fine- tune the algorithm to get that percentage of detection and removal as close as possible to 100%. The fifth stage of the algorithm consists of removing the first point in a flatline, whenever that first point was a spike. However, in this case, the threshold for the difference in elevation to identify this spike has been increased from 0.21 to 2 mm in magnitude. 2 mm is the value obtained when the IQR multiplied by 2 is rounded up to the nearest integer. This value was arbitrarily selected and carries no statistical significance, but empirically it is able to remove the spikes that still remain in the data. This empirical value is used instead of 0.21 mm because the trend of the data proceeding the first point in a flat signa is unknown. **Figure 2.15** shows the output of the spiked flatline removal.

43
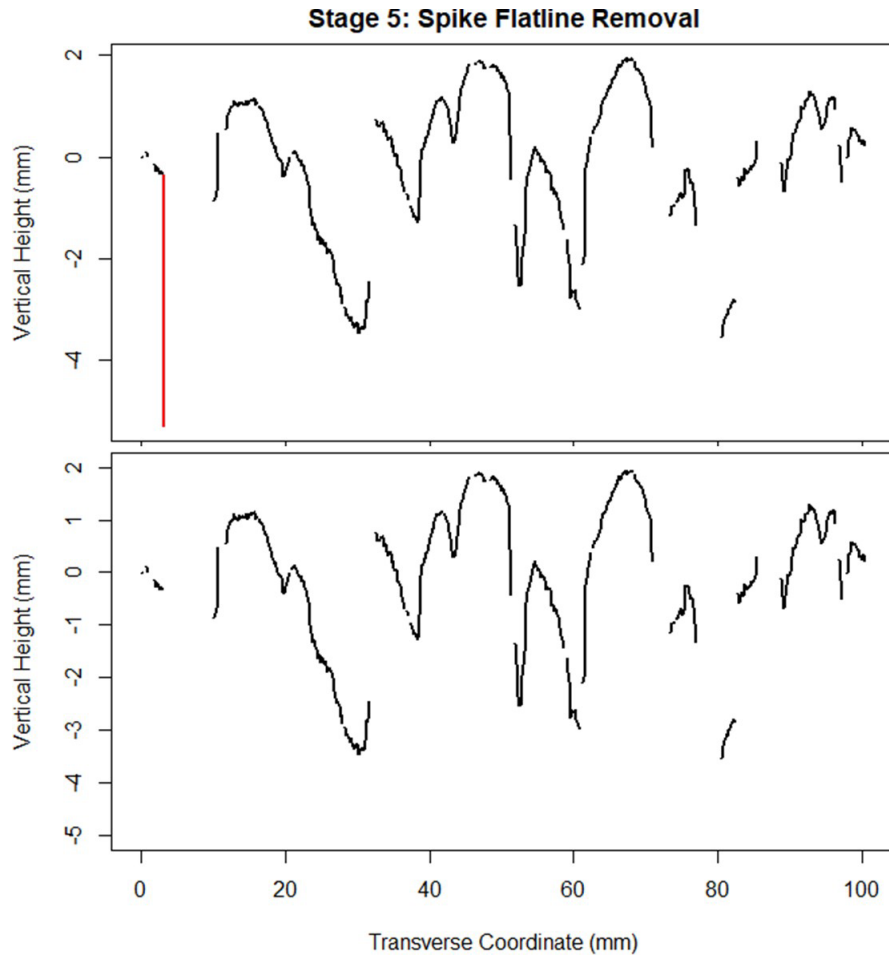
**Figure 2.15** : *Profile with removed data points highlighted in red (top) and profile after spiked flatline removal has been applied (bottom).*

The sixth stage is a fine-tuning of spike detection that captures mild spikes that were not removed in the second or fourth stages. The threshold used at this stage is the third metric computed in the calibration algorithm. For the dataset being used, this threshold was equal to 0.90 mm. This implementation works as follows.

- If ($BD_{i+1} > 0.9$  AND $FD_i < -0.9$), then remove the point
- If ($BD_i < -0.9$ AND $FD_{i+1} > 0.9$), then remove the point
- If ($BD_i > 0.9$  AND $FD_{i+1} < -0.9$), then remove the point

**Figure 2.16** shows the output of the fine-tuned spike removal.
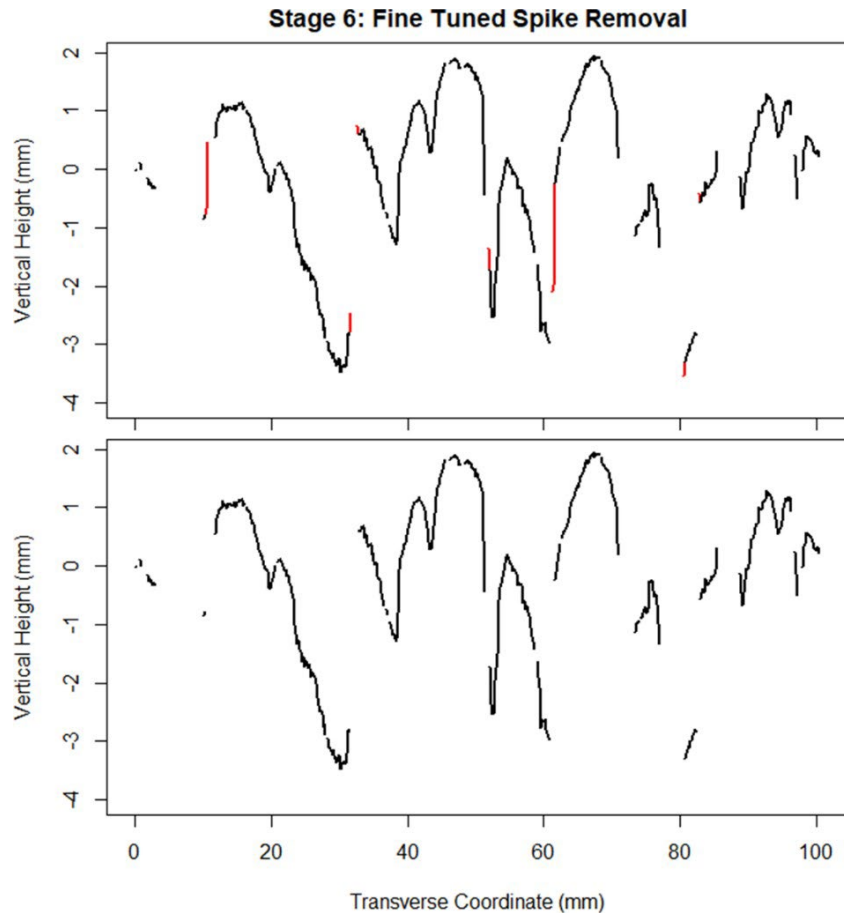
**Figure 2.16** *Profile with removed data points highlighted in red (top) and profile after spiked flatline removal has been applied (bottom).*

The seventh step removes limited cases where a single spike occurs in the middle of two flatlines. These spikes are not removed at stage two or four, but these instances were determined to be spikes as they occurred in the middle of two flatlines. The implementation is as follows:

- If $p_i$ = NULL, then skip this value
- If ($p_i \neq NULL$) AND ($p_{i+1}$ = NULL) AND ($p_{i-1}$ = NULL), then remove the point

At this stage, it is hard to visualize the noisy data points being removed since they are single isolated points along the profile; therefore, **Figure 2.17** shows a zoomed-in plot of the left side of the profile where the output of the mid-flatline spike removal can be observed.
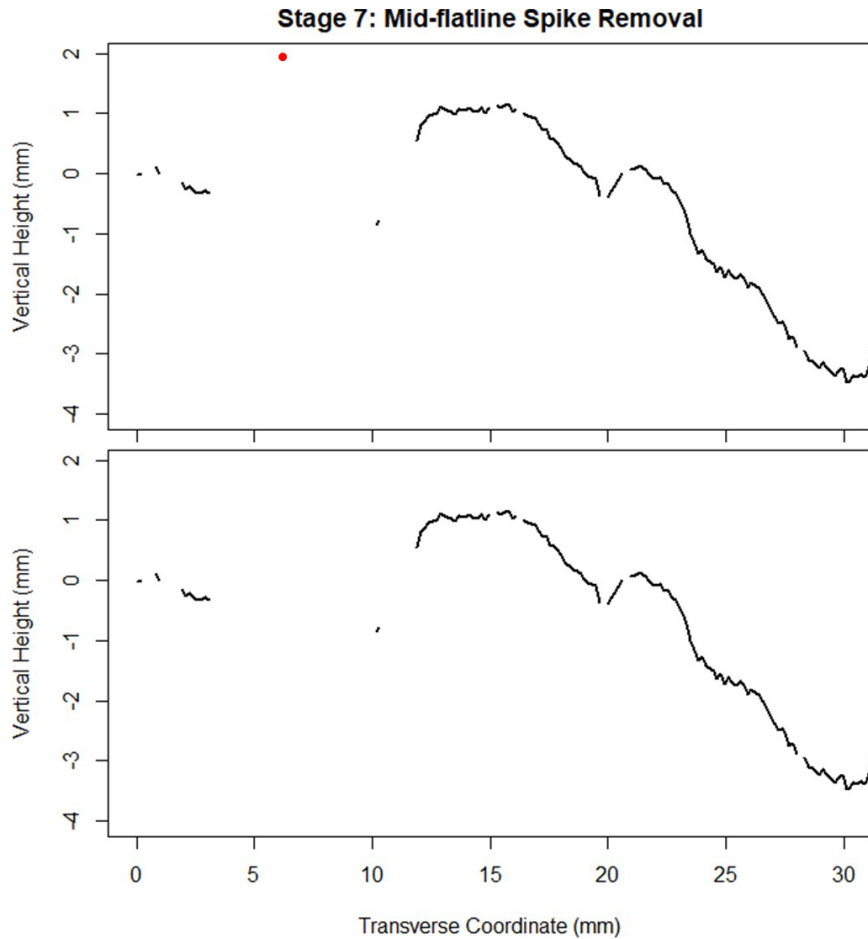
**Figure 2.17** *Profile with removed data points highlighted in red (top) and profile after mid-flatline spike removal has been applied (bottom).*

The eighth and final step deals with the rare occasion where the endpoints of the profile are part of a flatline. While they do get removed at stage one, this action complicates the imputation and detrending methods later because it is hard to impute data that occurs at the endpoints. This stage does a "pre-imputation" to deal with the problem of missing data at the endpoints. To do so, the algorithm verifies whether the endpoints and the points adjacent to the endpoints have been removed at previous stages. If the endpoints have been removed, then SOFA imputes the first or last point with the median value of the profile height. This type of imputation is known as *mean/median imputation*. Typically, researchers abstain from using this imputation method for multiple instances of missing data because it tends to underestimate the variance, but the approach is safe to use if only a few points are being imputed. In this case "few" refers to one or two data points out of 622. **Figure 2.18** shows the output of endpoint pre-imputation.

46
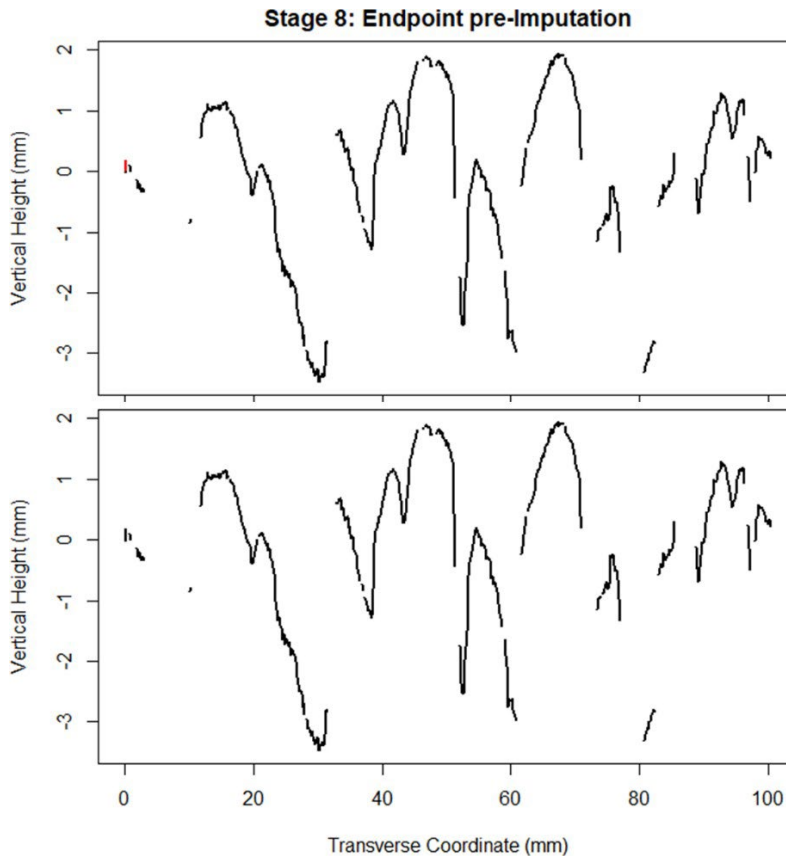
**Figure 2.18** *Profile with pre-imputed point highlighted in red (top) and profile after end pointpre-imputation has been applied (bottom).*

### 2.3.2.3 Data Imputation

Data imputation is the process of replacing missing data with substituted values. There is some criticism of imputing data on the grounds that imputation is essentially coming up with artificial data to fill in any gaps; often researchers might discourage the use of artificial data in favor of using only real data. Depending on the specific application, this kind of criticism is unfounded for a couple of reasons. First, the idea of imputation is not a tool used to generate valid estimates of specific case values but rather a tool for calculating relationships between variables. Whether the estimates for individual case values are correct is irrelevant if the correlations and other statistical associations are right. Second, it has been proven to be consistent and produce better results than simply using whatever data is complete and deleting those cases that are not complete. In fact, the latter practice could even lead to biased results (Rubin, 1976; Sabillon-Orellana, 2020).

### 2.3.2.3.1 Missing Data

Missing data problems can be classified into three main categories: missing completely at random (MCAR), missing at random (MAR), and missing not at

random (MNAR). The theory of missing data that governs these probabilities is called the missing data mechanism or response mechanism. If the reason for missing data points is random, meaning that the pattern of missing values is uncorrelated with the structure of the data, then the data are said to be missing completely at random (MCAR). This effectively implies that the causes for data being missing are unrelated to the data (Rubin, 1976; Kang, 2013). An example of MCAR is a weighing scale that ran out of batteries. Some of the data are missing simply because of bad luck.

If the probability of being missing is the same only within groups defined by the observed data, then the data are missing at random (MAR). MAR is a much broader class than MCAR (Rubin, 1976; Kang, 2013). For example, when placed on a soft surface, a weighing scale may produce more missing values than when placed on a hard surface. Such data are thus not MCAR. If, however, we know the surface type and if we can assume MCAR within the type of surface, then the data are MAR.

Lastly, the data is said to be missing not at random (MNAR) if neither MCAR nor MAR hold. MNAR means that the probability of missingness varies for unknown reasons, but the propensity of being missing depends on the observed data, not the missing data. For instance, if a survey is conducted on college students asking for their current GPA, students with a low GPA might decide not to answer because their GPA is low. In this case, the value of the data is the reason why it is missing, but one can never know if that is indeed the correct reason for its missingness. MNAR is the most complex case. Strategies to handle MNAR are to find more data about the causes for the missingness, or to perform what-if analyses to see how sensitive the results are under various scenarios (Rubin, 1976; Kang, 2013).

Most modern imputation techniques start with the MAR assumption. While MCAR is desirable, in practice, it is unrealistic. Thus, one must assume that missing values can be replaced by predictions derived by the observable portion of the dataset. This is a fundamental assumption to make; otherwise, it would be impossible to predict plausible values of missing data points from the observed data (Rubin, 1976; Kang, 2013).

### 2.3.2.3.2    *Imputation in Pavement Texture Data Processing*

The field of data imputation within statistics has made tremendous progress over the years across multiple fields of science. However, there is little to no documentation that specifies which techniques are the most ideal when attempting to impute a cross-sectional profile of pavement texture. Standards for processing texture data, like ISO 13473, recommend the use of linear interpolation or multiple imputation to deal with the missing data, but no testing

has been done on whether these imputation methods are still valid when long gaps of missing data are present within the profile. Some research studies have even decided not to impute data and do their analysis with incomplete datasets.

In this project, the research team designed a thorough and meticulous experiment aimed at bridging this gap in the literature. The research team studied the process of data imputation to determine the best imputation method based on their accuracy and computation time. The case study explored ten popular imputation methods, explained how they work, tested each by means of Monte Carlo simulation, and ranked their efficiency using the analytic hierarchical process. A two-tailed hypothesis test was used to make the final decision and determine whether the gain in imputation accuracy (if any) was statistically significant compared to the same statistic computed with missing data.

### 2.3.2.3.3     Imputation Experimental Design

A pavement profile with no significant noise was manually selected from the field data and detrended to test all the imputation methods (**Figure 2.19**). Monte Carlo simulation was then used by means of a noise-generating function to create missing data within the profile. The objective of the noise-generating function was to simulate the effect of the noise detection and removal algorithm on the signal. The process aimed at identifying noise and removing those points from the profile.
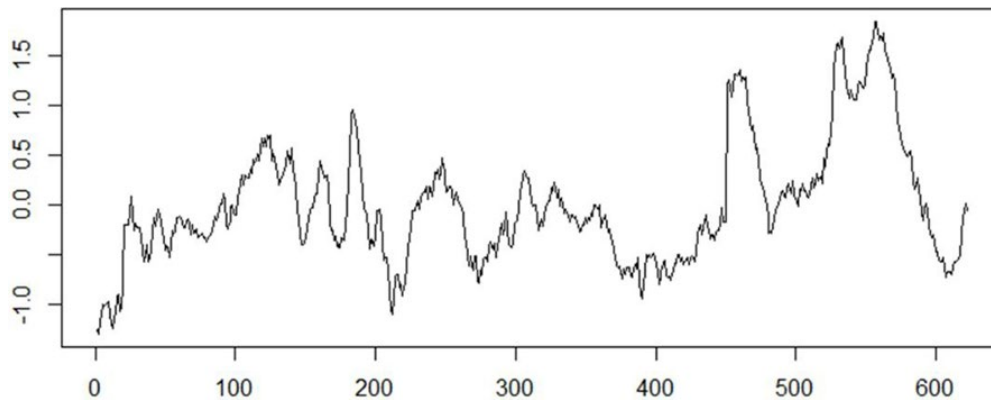


**Figure 2.19** *Original profile after detrending to be subjected to Monte Carlo simulation*

Noise can be generated as a single point, multiple single points, a string of points (gap of size n), or multiple strings of points. **Figure 2.20** shows examples of how the noise-generating function removes these points. All points in the profile have a uniform probability of being removed by the algorithm and the location of the missing data along the profile changes at every iteration. However, the amount of noise within the profile was set not to exceed 10% of the total number of data points. This threshold was established based on ISO standard 13473.
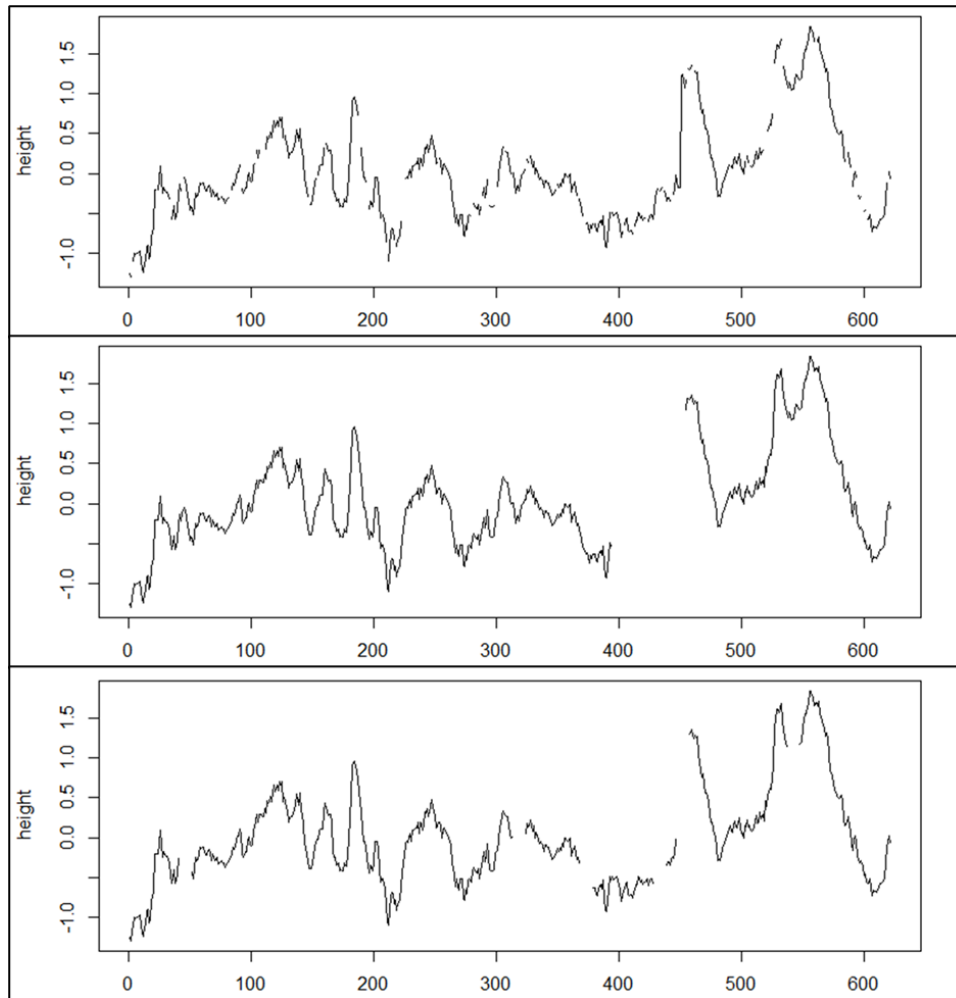
**Figure 2.20** *Profile after noise was removed: 62 single points (top), a gap of size 50 (middle) and 6 gaps of size 10 (bottom)*

The protocol used to simulate missing data creates the following scenarios:

- Scenario 1: the protocol removes 62 single points (10% of the data) from the profile to simulate the worst-case scenario for maximum number of single data points missing. In this case the gap size is one.

- Scenario 2: the protocol removes a single gap of length $n$, from $n = 2$ to $n = 62$.

Each imputation method was implemented after the noise was generated and its output was compared to the original profile. This process was performed 5,000 times to ensure that every possible scenario of noise was captured while not exceeding 10% of the total number of data points. For these data, the texture profile had a total of 622 data points; therefore, the maximum allowable number of missing data were 62 points. Recall that if a profile has more than 10% noise, the profile was discarded.

To determine which imputation method is the best when processing pavement texture data, three tests were conducted. First, the accuracy of the imputation method was tested in terms of how well the imputed data replicated the true shape of the original pavement profile. This accuracy was quantified using the sum of square errors (SSE). Since there are 5,000 iterations for every gap size, the mean and standard deviation of the 5,000 SSE values for every gap size were recorded. Second, the average computation time necessary to impute a profile over 5,000 different scenarios was also recorded. This is an important metric given that, during field data collection, the number of profiles to be processed can easily exceed 10,000. Hence, algorithms that are quick at imputing data are preferable. The last test was probably the most important. This test aimed at quantifying whether it was worth running an imputation algorithm or better to work with profiles with missing data. This was tested by computing a statistic using the original true profile, setting that as the ground truth. Then, the same statistic was computed once the profile had missing data, i.e., after the noise had been generated and removed, and after the profile had been imputed.

If the statistic computed with the imputed data is closer to the ground truth than the statistic computed with missing data, then the imputation method is efficient. To achieve this, the percent error for the missing and imputed were computed. Then, if an improvement in the accuracy of the statistic was observed, a two-tail t-test was performed on the percent errors to determine whether they were statistically different from one another. For this experiment, two statistics were considered: the fourth sample standardized moment ($M4$), i.e., the kurtosis; and the MPD of the profile. $M4$ was chosen because of its high sensitivity to changes in the elevation values of the profile, particularly those that are the largest in magnitude. The MPD was chosen because it is the most commonly used metric by transportation agencies to quantify pavement texture. Finally, the analytic hierarchical process was used to make an objective decision of which imputation algorithm was the best, given all the tests above.

This study provided valuable information, as it proved that data imputation for texture data processing significantly increased the accuracy of estimates of texture statistics when the right imputation method was implemented. This study found that linear interpolation imputation was the best imputation technique, not only because of its robustness and efficiency but also because of its simplicity and ease of implementation. However, it was also proven that using poor imputation techniques—such as spline interpolation for gaps of missing data that are greater than ten data points—can potentially yield biased estimation of pavement texture statistics that are significantly worse than simply computing those statistics using the data with missing entries. **Table 2.3** provides a summary of the ranking for the ten imputation methods tested in this case study; the higher the value in the "Overall Relative Weight" column, the more desirable that implementation is.

**Table 2.3 Ranking of imputation methods based on the analytic hierarchical process**

| Rank | Method | Overall Relative Weight |
|---|---|---|
| 1. | Linear Interpolation | 0.138 |
| 2. | Seasonally Decomposed Missing Value | 0.136 |
| 3. | Simple Moving Average | 0.112 |
| 4. | Exponential Moving Average | 0.112 |
| 5. | Autoregressive Integrated Moving Average | 0.099 |
| 6. | Stineman Interpolation | 0.092 |
| 7. | Stochastic Regression | 0.091 |
| 8. | Mean Imputation | 0.086 |
| 9. | Deterministic Regression | 0.086 |
| 10. | Spline Interpolation | 0.048 |

### 2.3.2.3.4    *Linear Interpolation Imputation*

This method is by far the most popular imputation method for pavement texture data, and it is usually the one recommended by pavement profile processing standards (ISO, 2008). Linear interpolation is an imputation technique that assumes a linear relationship between data points and utilizes the available values from adjacent data points to compute a value for the missing cases. An implementation of linear interpolation imputation is shown in **Figure 2.21.** In **Figure 2.21**, the black points represent the original data, while the grey points are the data the was intentionally removed and represent missing data. The orange lines represent the linear interpolation that is used to replace the missing readings.



Delta Airlines Closing Stock Market Price:
Linear Interpolation

Additionally, **Figure 2.22** presents the profile that was shown in the noise detection and removal subsection after linear interpolation was applied. The red lines represent the portion of data that was removed as noise and then imputed by means of linear interpolation.
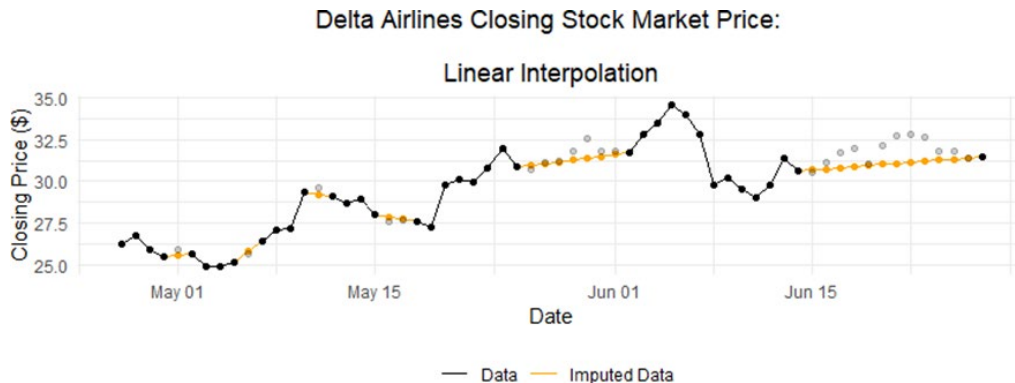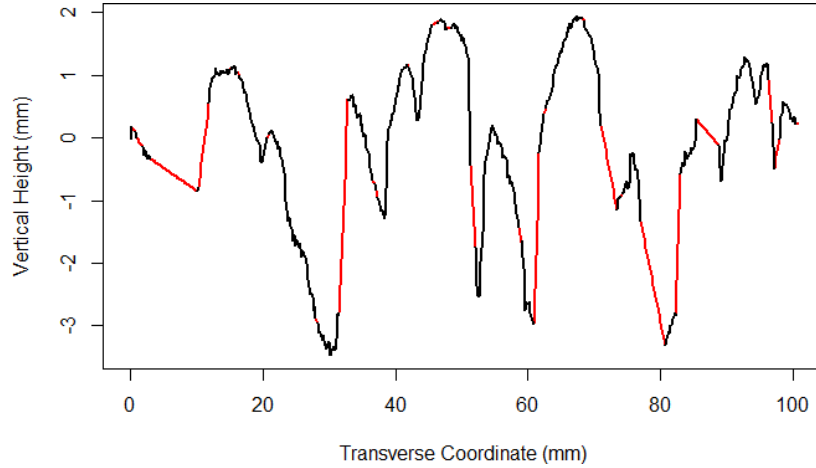


**Figure 2.22** *Linear interpolation method applied onto denoised texture profile*

## 2.3.2.4     Profile Detrending

After processing the profiles for noise and imputing all missing data points, further detrending was performed such that all pavement profiles were centered around a flat horizontal plane at the origin. This is also a required step if one seeks to transform the data from the spatial domain to the spectral domain. During this project and to be consistent with the MPD standard, the middle 100 m of the signal were selected to also correspond to the GripTester wheel path. There are two ways to remove a linear or polynomial trend within time series data: integration and regression detrending. This section addresses only regression detrending, given that this is the method used on the denoised profiles. Regression detrending involves using linear or polynomial regression and subtracting the regression line from the data to achieve an approximately stationary time series, as shown in **Equations 2.1** and **2.2**.

$$\hat{y}(t) = \beta_0 + \sum_{i=i}^{n} x_i \beta_i \qquad\qquad (2.1)$$

$$z(t) = y(t) - \hat{y}(t) \qquad\qquad (2.2)$$

where $\hat{y}(t)$ is the regression line that fits the profile, $\beta_i$ are regression coefficients, $x$ is the transverse coordinate, $z(t)$ is the detrended profile, and $y(t)$ is the original profile. **Figure 2.23** shows a time series with a linearly

increasing trend. In the middle of the figure, the best-fit line is estimated using linear regression and highlighted in red. The regression line is then subtracted from the data and the result is an approximately stationary time series. The resulting time series after using regression detrending is still not fully stationary because there is still seasonality within the cross-sectional profile. Seasonality is a characteristic of a time series in which the data experiences regular and predictable changes that recur after a given time period or, in this case, distance. The seasonality within a pavement profile is due to the aggregate gradation of the mix and that seasonality must not be removed as it is a characteristic of pavement texture.
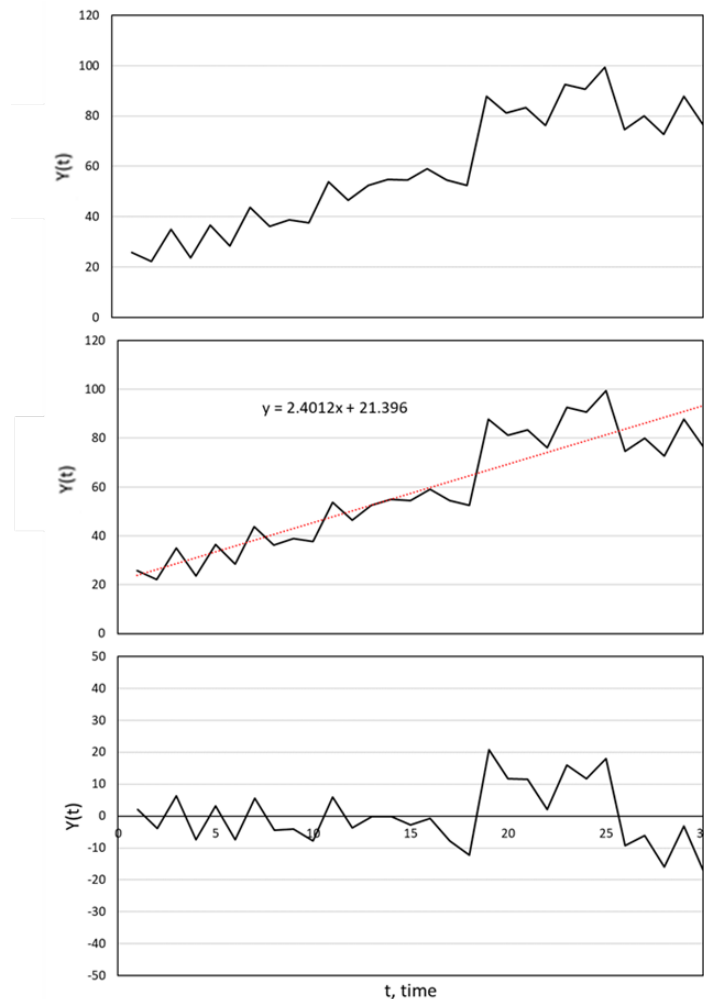


**Figure 2.23** *Data with linear trend removed by means of regression detrending*

**Figure 2.24** shows a comparison between the raw texture profile collected by the prototype and the finalized processed profile after regression detrending has been applied.
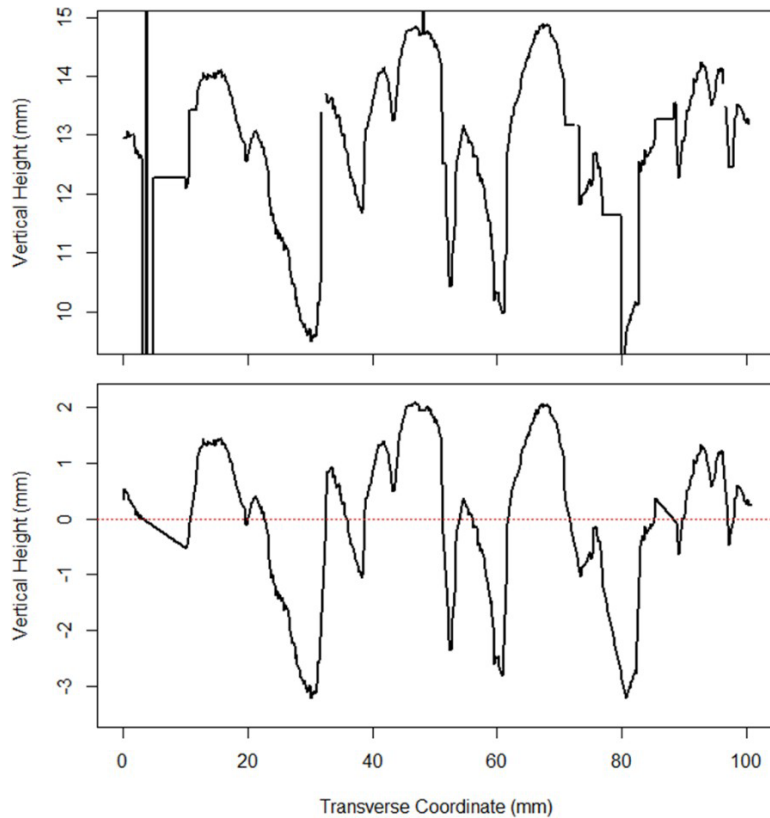
**Figure 2.24** *Comparison between (top) and (bottom) the processed profile after denoising, imputation, and detrending*

## 2.3.2.5    Data Transformation

The last step of the data processing involves transforming the data from the spatial domain to the frequency domain. This step is only required if one seeks to characterize the pavement profile using metrics such as the PSD, or one seeks to isolate a particular component of the texture spectrum such as the macrotexture of the profile by using band-pass filters. The research team decided to use the Discrete Fourier Transform (DFT) as previous research studies have shown promising results when correlating texture with friction.

Before transforming the texture data to the spectral domain, the profile is subjected to a windowing algorithm (**Figure 2.25**) to reduce the amplitude of the signal to zero at the edges of the profile and avoid leakage. Spectral leakage occurs when a signal is transformed into the spectral domain, but with the wrong frequencies being amplified. This occurs because the Fourier transformation assumes that the period of the signal being sampled is representative of the original signal. This means that, if one were to infinitely reproduce the sampled signal to the left and right, the original signal should be recreated. However, on some occasions, the signal may not have a smooth transition at the endpoints, and hence if the signal is reproduced sharp edges develop at the junctions. These sharp edges are the ones responsible for amplifying the wrong frequencies when the signal is transformed to the frequency domain. Spectral leakage can be

minimized by increasing the window size of the sampling period: the longer the signal is sampled, the less impactful the errors associated to leakage. In pavement profiles, this sampling period refers to the length of the scan. As the length of the scan increases, the bandwidth of the spectrum of the window becomes narrower and hence the effects of spectral leakage are minimized. However, given that the length of the measured profile is less than one meter, a Split Cosine Bell Window (SCBW) was applied as per **Equation 2.3**.
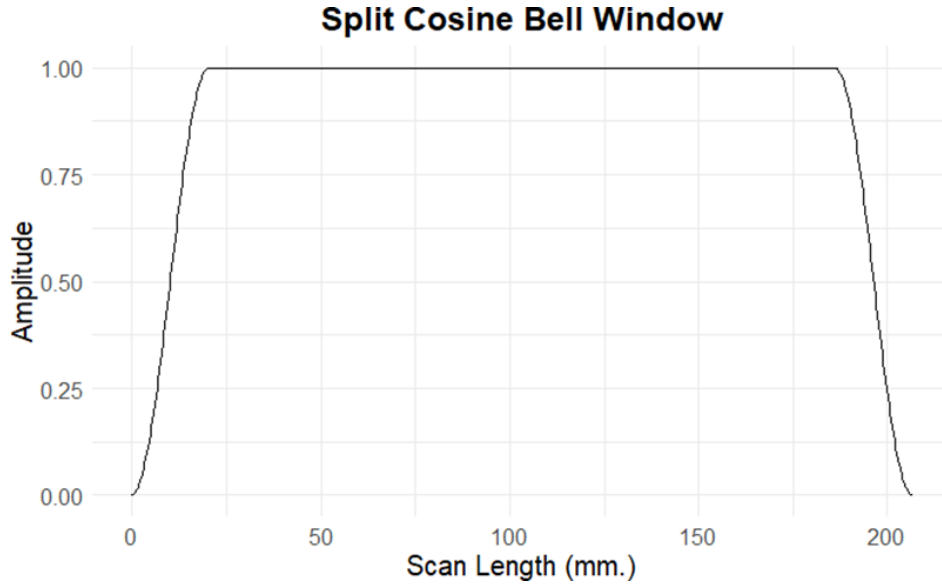


**Figure 2.25** *Response on the SCBW*

$$w_{i,C} = \begin{cases} \cos^2\left(\dfrac{5\pi i}{N} - \dfrac{\pi}{2}\right) & for\ 0 \le i < \dfrac{N}{10} \\ 1 & for\ \dfrac{N}{10} \le i < \dfrac{9N}{10} \\ \cos^2\left(\dfrac{5\pi i}{N} - \dfrac{9\pi}{2}\right) & for\ \dfrac{9N}{10} \le i < N \end{cases} \quad (2.3)$$

where $w_{i,C}$ is the window coefficient, $N$ is the number of data points, and $i$ is the sample number. The window coefficient was multiplied by the signal and later normalized by the integral of the window to prevent attenuation of the signal as per **Equation 2.4**.

$$Z_{i,win} = \frac{w_{i,C} * Z_i}{0.9354} \quad for\ i = 0, \dots, N - 1 \quad (2.4)$$

where $Z_{i,win}$ is the windowed profile height at point $i$ (mm). A detrended profile can be seen before and after being subjected to the SCBW in **Figure 2.26.** Notice

that only 100 mm of the profile are subjected to SCBW and detrended to be consistent with the MPD standard.

### Cross-Sectional Profile Before SCBW



### Cross-Sectional Profile After SCBW
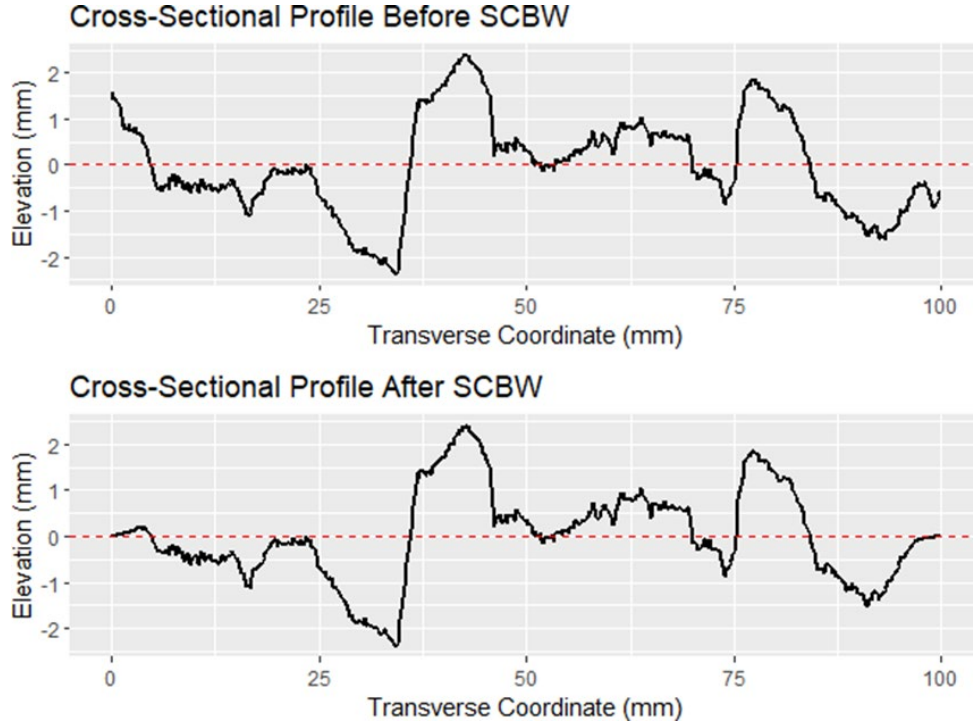


**Figure 2.26** *Detrended profile (top) and same profile after being subjected to the SCBW (bottom)*

DFT is applied to the windowed profile as defined by **Equation 2.5** to transform the texture data from the spatial time domain into the spatial frequency domain.

$$Z_k = \frac{1}{N} \sum_{i=0}^{N-1} Z_{i,win} * e^{-j\left(\frac{2\pi k}{N}\right)i} \quad for \; k = 0, \dots, N-1 \tag{2.5}$$

where $Z_k$ is the DFT of the windowed profile, and $j$ stands for the imaginary unit ($j^2 = -1$). The result of the DFT is a constant bandwidth narrow band spectrum with complex values. The bandwidth is a function of the evaluation length defined by **Equation 2.6.**

$$\Delta f_{sp} = \frac{1}{l} \tag{2.6}$$

where $\Delta f_{sp}$ is the frequency interval (cycle/meter) and $l$ is the evaluation length (m). An important property of DFT is that it obeys the Shannon Sampling Theorem, which states that the sampling frequency should be at least twice the

highest frequency contained in the original signal. An alternate way to interpret this statement is that the shortest wavelength that can be obtained from a discrete signal is twice the sample spacing. The sensor used on the prototype is capable of sampling two points with a spacing of 0.161 mm in the transverse direction. Thus, the shortest wavelength that can be analyzed using the DFT is 0.322 mm. This implies that the DFT can capture all the wavelengths at the macrotexture level and a few wavelengths within the first decade of microtexture.

The results of the DFT are later converted into a PSD by means of **Equation 2.7**. The PSD is then plotted on a log-log scale against the wavelength. **Figure 2.27** shows a sample PSD plot using the center 100 mm for consistency.

$$Z_{PSD} = \frac{2|Z_k|^2}{\Delta f_{sp}} \quad for\ k = 0, \dots, \left(\frac{N}{2} - 1\right) \tag{2.7}$$

where $Z_{PSD}$ is the PSD.
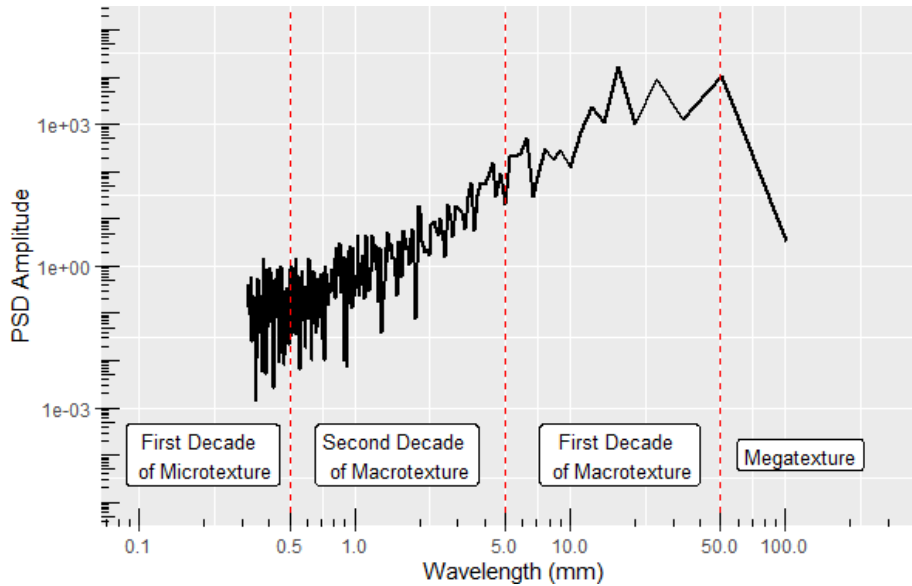


**Figure 2.27** *PSD plot with breaks for texture components*

## 2.4   Feature Engineering

This section addresses how texture statistics were computed and explains subsequent processing on the statistics before using them in the skid prediction models.

### 2.4.1 Texture statistics

As mentioned in Section 1.1.2, summary statistics used to characterize texture can be broken down into two main categories: spatial and spectral. Spatial

texture statistics are divided into four groups: amplitude, spacing, hybrid, and functional parameters.

## 2.4.1.1　　　Spatial Amplitude Statistics

Amplitude statistics are the most important metrics to characterize the pavement surface topography. They are used to measure the vertical characteristics of the surface deviations. The amplitude statistics used in this study are briefly described in this section and their equations are shown in **Table 2.4**

**Table 2.4 Summary of spatial amplitude statistics**

| Statistic | Equation |
|---|---|
| Maximum Height ($R_z$) | $R_z = \max(h_i) - \min(h_i), i = 1,2,\dots,N$ |
| Absolute Height Average ($R_a$) | $R_a = \dfrac{1}{N}\sum_{i=1}^{N} |h_i|$ |
| Height Variance ($R_v$) | $R_v = \dfrac{1}{n-1}\sum_{i=1}^{n}\left(h_i - \bar{h}_i\right)^2$ |
| Root Mean Square ($RMS$) | $RMS = \sqrt{R_v}$ |
| Skewness ($R_s$) | $R_s = \dfrac{n}{(n-1)(n-2)}\sum_{i=1}^{n}\dfrac{\left(h_i - \bar{h}_i\right)^3}{RMS^3}$ |
| Kurtosis ($R_k$) | $R_k = \dfrac{n(n+1)}{(n-1)(n-2)(n-3)}\sum_{i=1}^{n}\dfrac{\left(h_i - \bar{h}_i\right)^4}{RMS^4} - \dfrac{3(n-1)^2}{(n-2)(n-3)}$ |
| Ten Point Mean Roughness ($R_t$) | $R_t = \dfrac{1}{5}\sum_{j=1}^{5}(h_{pj} - h_{vj})$ |
| Mean Profile Depth ($MPD$) | $MPD = \dfrac{1}{2}\left[\max\left(h_1,\dots,h_{N/2}\right) + \max\left(h_{N/2},\dots,h_N\right)\right]$ |
| Solidity Factor ($R_r$) | $R_r = \dfrac{\min(h_i)}{\max(h_i)}$ |

where $h_i$ is the elevation at point $i$, $\bar{h}$ is the mean elevation, $n$ is the number of datapoints, $h_{pj}$ is the $j^{th}$ highest peak in the profile, $h_{vj}$ is the $j^{th}$ lowest valley in the profile, $h_{m/2}$ is the elevation value midway through segment, and $h_m$ is the elevation value at the end of segment

### 2.4.1.1.1 Maximum Height ($R_z$)

The maximum height of the profile indicates the absolute vertical distance between the maximum profile peak height and the maximum profile valley depth along the sampling length. When dealing with roughness profile, $R_z$ is commonly referred to as the *maximum roughness*. **Figure 2.28** depicts the $R_z$ statistic in texture profile. **Figure 2.29** shows a comparison between a profile with a high $R_z$ a low $R_z$.
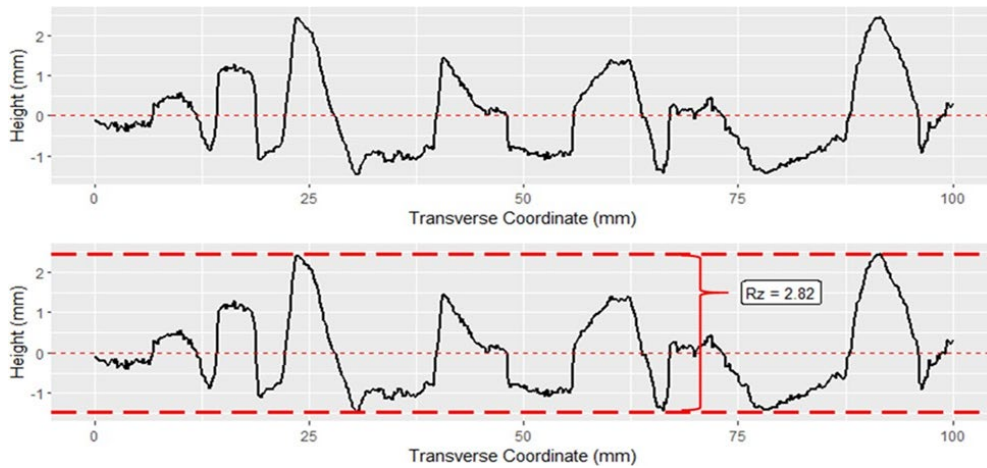
**Figure 2.28** *Sample profile (top), visualization of the computation of $R_z$ (bottom)*
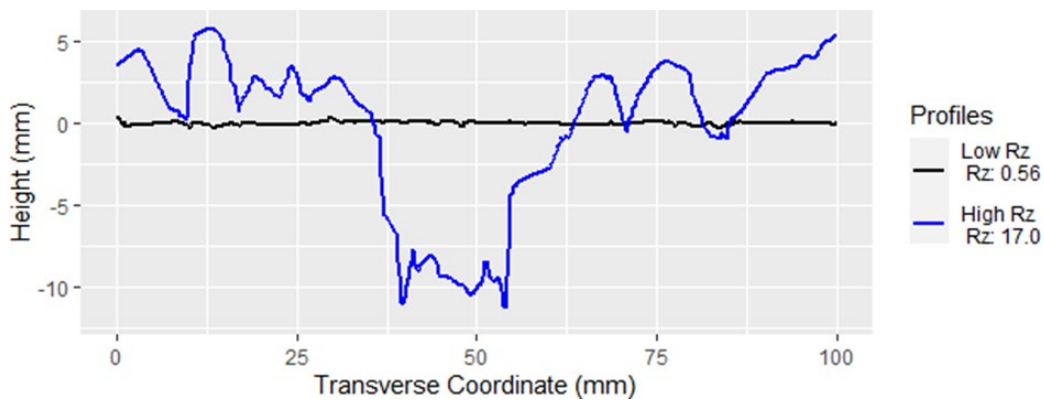


**Figure 2.29** *Profile with high $R_z$ (blue) and one with low $R_z$ (black)*

### 2.4.1.1.2    Absolute Height Average ($R_a$)

The absolute height average of the profile is a substitute for the first moment or mean height of the average profile. All profiles have been detrended which implies the mean elevation of the pavement profile is centered around zero. Thus, computing the mean height becomes trivial. Instead, this statistic quantifies the average height for the absolute value of elevations along the sampling length. **Figure 2.30** shows the $R_a$ statistic in texture profile. **Figure 2.31** shows a comparison between a profile with a high $R_a$ and a low $R_a$.
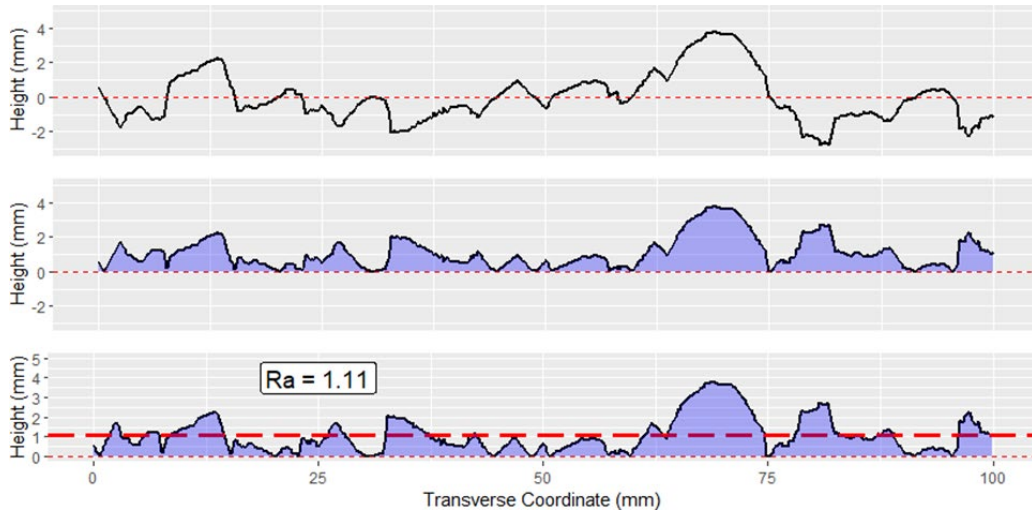
**Figure 2.30** *Sample profile (top), absolute value elevation (middle) and $R_a$ (bottom)*
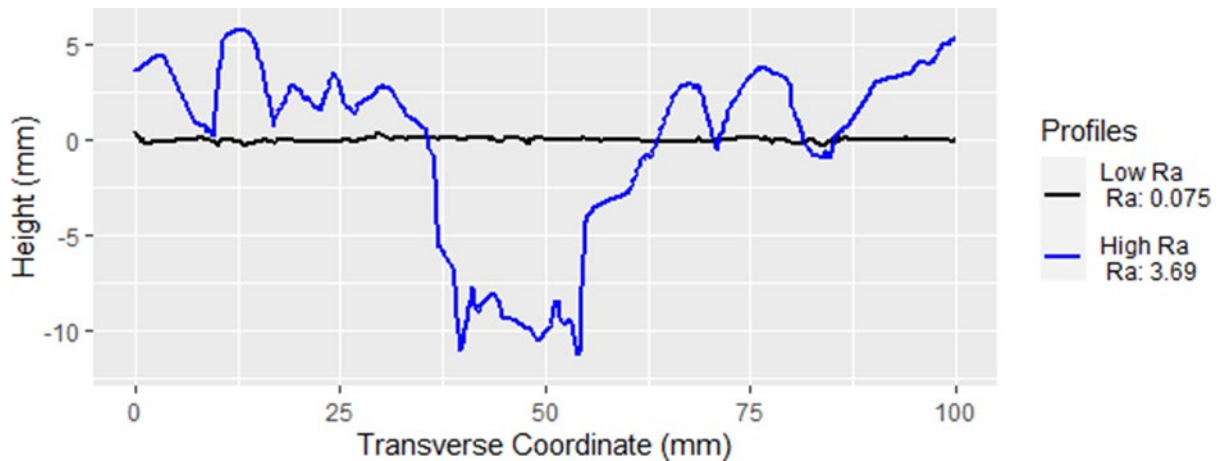


**Figure 2.31** *Profile with high $R_a$ (blue) and one with low $R_a$ (black)*

### 2.4.1.1.3    Height Variance ($R_v$)

The height variance quantifies how the distribution of heights is spread along the profile. Low values of $R_v$ indicate the presence of pavements that are predominantly fine mixes or low macrotexture; whereas high values are generally indicators of coarser mixes or chip seals, or other mixes that have high macrotexture. Moreover, spikes in this statistic could also indicate the presence of joints, open pores, or cracking on the road as all these phenomena drastically increase the range of heights in the profile. **Figure 2.32** shows a comparison between a profile with a high $R_v$ and a low $R_v$.
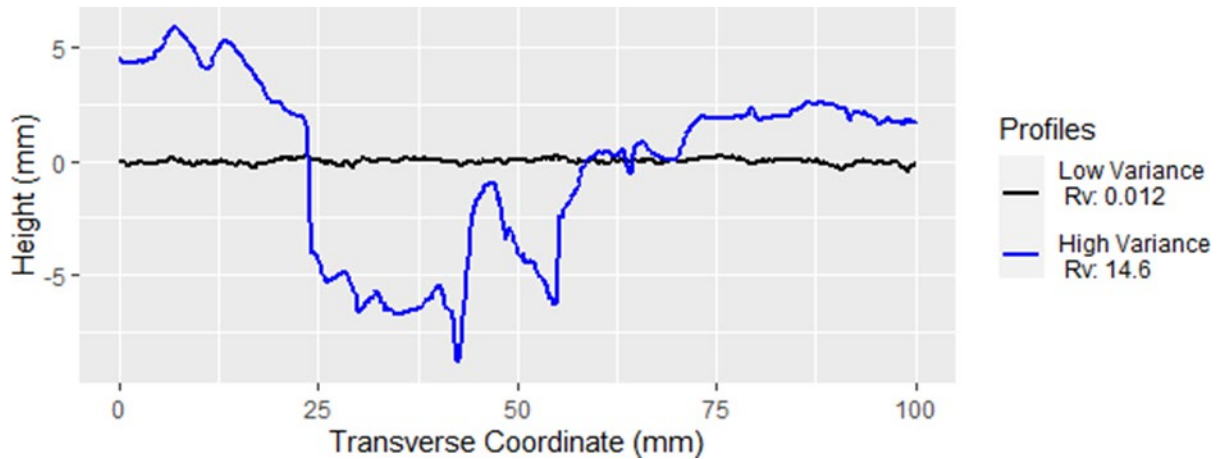
**Figure 2.32** *Profile with high $R_v$ (blue) and one with low $R_v$ (black)*

### 2.4.1.1.4    Root Mean Square (RMS))

The *RMS* is the standard deviation of the elevation within the profile. It measures how much the measured profile deviates on average from the horizontal flat plane. One of its main applications is to provide a more accurate measurement of the surface roughness. It is also typically used in conjunction with the MPD to identify whether the surface has a negative or positive texture. For example, in **Figure 2.33**, both profiles have an identical variation, hence they have the same RMS. But one can determine whether if the texture is negative or positive based on the MPD. The profile with the larger MPD will have a positive texture. RMS captures the same elevation characteristics of the profile that the variance captures.
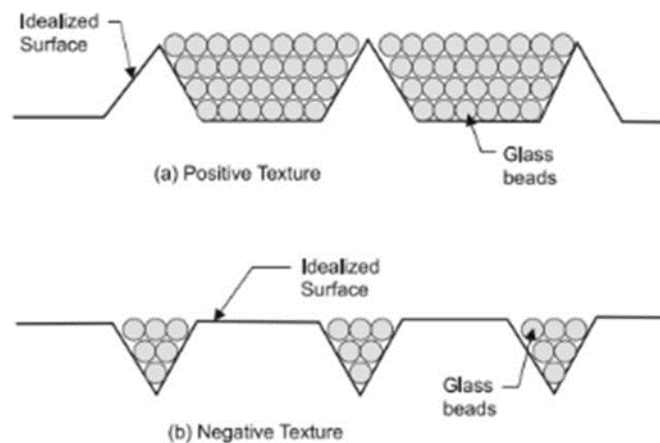


**Figure 2.33** *: Positive and negative texture (McGhee and Flintsch, 2003)*

### 2.4.1.1.5    Height Skewness ($R_s$)

The skewness is a measure of the size of the two tails of the distribution. For pavement texture profiles, it determines the degree of asymmetry of the profile about the horizontal plane. A positive value for $R_s$ indicates the predominance

63

of peaks along the profile; negative values indicate the predominance of valleys; values close to zero indicate a balanced presence of the two. Skewness is a metric of interest because when applied to pavement texture profiles, it can help to distinguish between positive- and negative-oriented texture based on the sign of the statistic (**Figure 2.34**). **Figure 2.35** shows a comparison between a profile with a positive, neutral, and negative $R_s$.
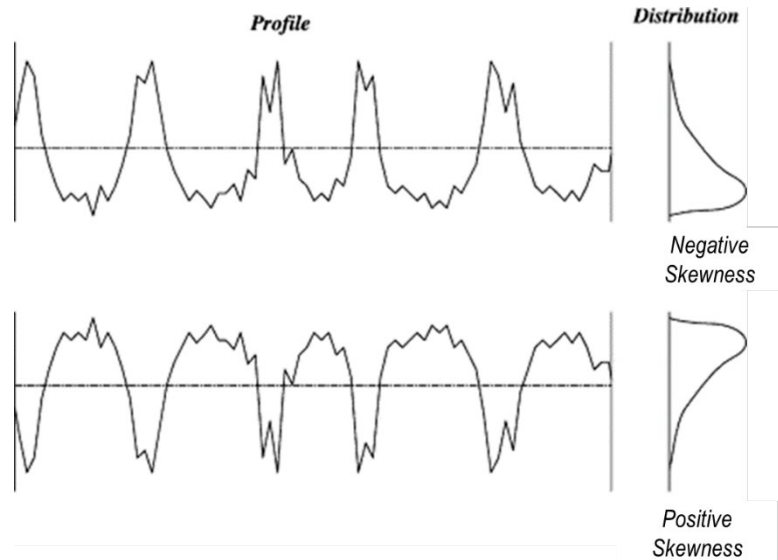


**Figure 2.34** : Idealized profiles showing the difference between (top) negative texture and positive texture (bottom) based on their skewness (Gadelmawla et al. 2002)
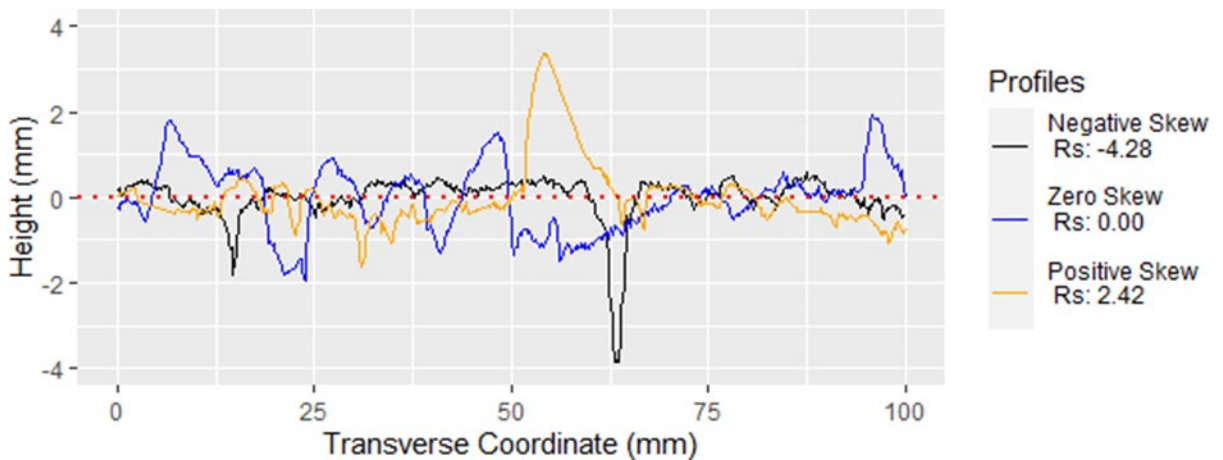


**Figure 2.35** : Profiles with positive $R_s$ (yellow), neutral $R_s$ (blue), and negative $R_s$ (black)

### 2.4.1.1.6    Height Kurtosis ($R_k$)

Kurtosis is a measure of the combined size of the tails relative to whole distribution. When $R_k$ is positive, it indicates the presence of extremely high peaks or deep valleys. When it is negative, it indicates a lack of extreme peaks or values. Lastly, if the value of kurtosis is close to zero, it means that the

distribution of height is about normal, with very few high peaks or deep valleys. **Figure 2.36** shows a comparison between a profile with a positive, neutral, and negative $R_k$.
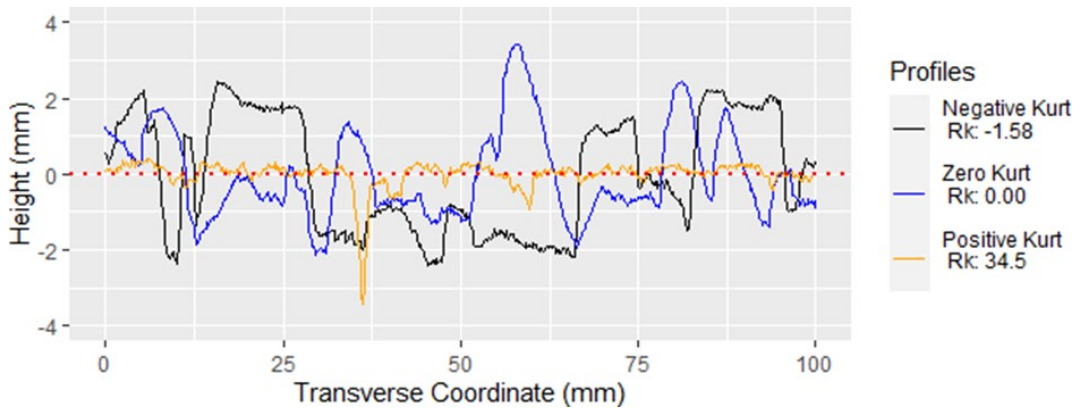


**Figure 2.36** *Profiles with positive $R_k$ (yellow), neutral $R_k$ (blue), and negative $R_k$ (black)*

### 2.4.1.1.7 Ten Point Mean Roughness ($R_t$)

The $R_t$ is the difference between the highest peak and the lowest valley, the difference between the second highest peak and the second lowest valley, and so on, until the five most extreme differences in data points within the profile have been acquired and averaged. **Figure 2.37** shows a comparison between a profile with a high $R_t$ and a low $R_t$.
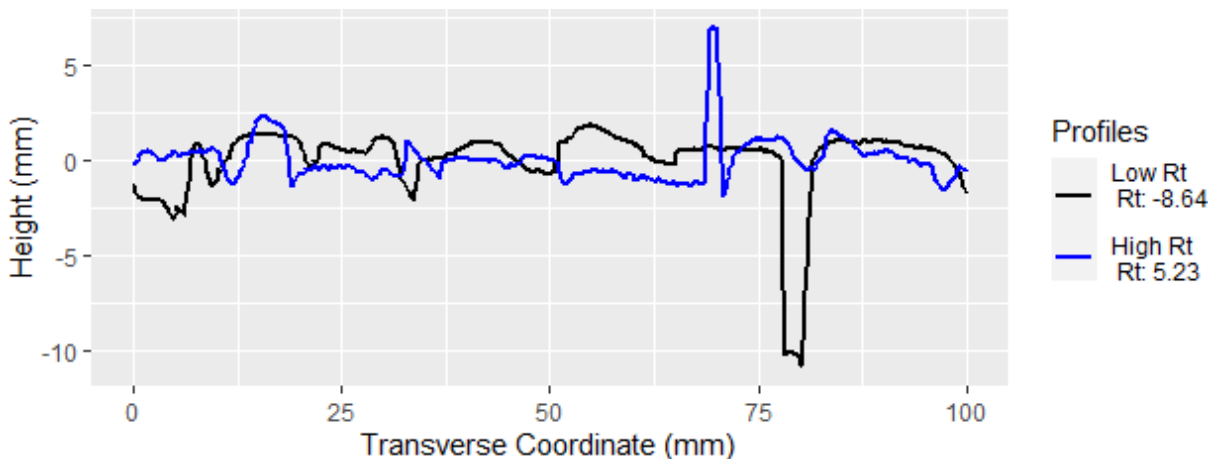


**Figure 2.37** *Profile with high $R_t$ (blue) and one with low $R_t$ (black)*

### 2.4.1.1.8 Solidity Factor ($R_r$)

The solidity factor is the ratio between the maximum depth of valleys and the maximum height of the profile. This statistic is one of the simplest to compute and yet it appears to have a strong predictive power for distinguishing between different pavement surfaces. An image for $R_r$ is not shown as visually, it captures properties similar to the ten-point mean roughness. Profiles with a negative $R_r$

and high in magnitude are similar to those with a low $R_t$, whereas profiles with negative $R_r$ and small in magnitude look similar to profiles with a high $R_t$.

### 2.4.1.1.9 Mean Profile Depth (MPD)

MPD is purely a geometric indicator that relies on the ratio between the surface area and the length and usually refers to the macrotexture domain. The MPD is estimated by diving the texture profile into segments of 100 mm in length. The profile needs to be fully detrended to provide a zero-mean profile segment. The segment is then subdivided into two halves, and the height of the highest peak within each half is determined. The average of these two peaks is referred to as the mean segment depth, as shown in **Figure 2.37**. The average value of the mean segment depth of all the measured profiles is the MPD (ASTM E 1845, 2009). **Figure 2.38** shows the MPD statistic in texture profile. **Figure 2.39** shows a comparison between a profile with a high MPD and a low MPD.
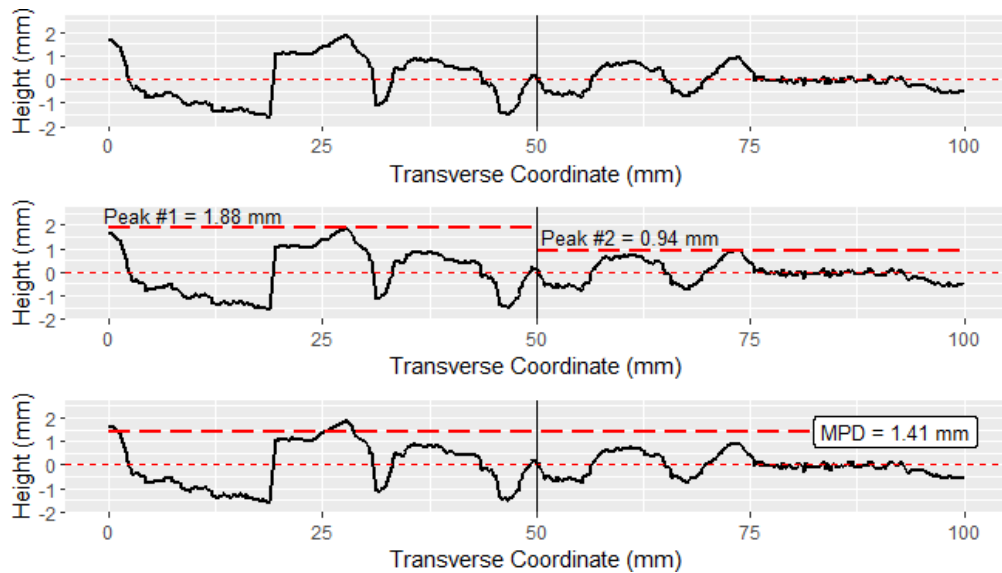


**Figure 2.38** : *Sample profile divided into two 50mm segments (top), finding the peaks of each segment (middle), computation of the MPD (bottom).*
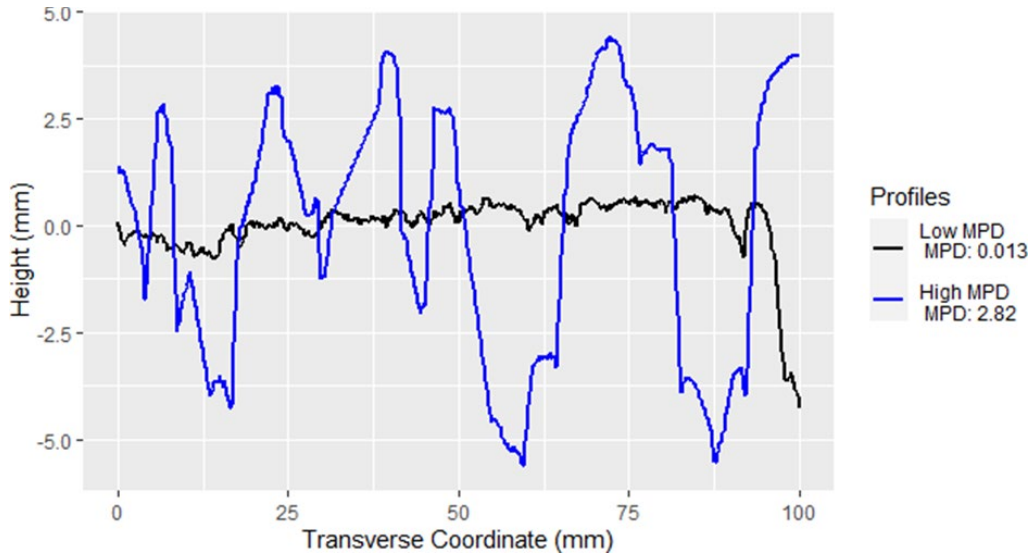
**Figure 2.39** : *Profile with high $MPD$ (blue) and one with low $MPD$ (black)*

## 2.4.1.2 Spatial Spacing Statistics

Spacing parameters are those that measure the horizontal characteristics of the surface deviations. The spacing parameters are very important in fields like manufacturing, such as when pressing sheet steel. In this case, evaluating the spacing parameters is necessary to obtain consistent lubrication when pressing the sheets to avoid scoring and to prevent the appearance of surface texture on the final product (Gadelmawla et al, 2002). The spacing statistics used in this project are briefly described in this section and their equations are shown in **Table 2.5**. The equations in **Table 2.5** are similar to those in **Table 2.4**, the only difference is that instead of using elevations ($h_i$), these equations use horizontal spacing ($x_i$) is measured in mm.

**Table 2.5 Summary of spacing summary statistics**

| Statistic | Equation |
|---|---|
| Mean Cross Width ($C_m$) | $C_m = \dfrac{1}{n}\sum_{i=1}^{n} x_i$ |
| Cross Width Variance ($C_v$) | $C_v = \dfrac{1}{n-1}\sum_{i=1}^{n} (x_i - \bar{x}_i)^2$ |
| Cross Width Skewness ($C_s$) | $C_s = \dfrac{n}{(n-1)(n-2)}\sum_{i=1}^{n} \dfrac{(x_i - \bar{x}_i)^3}{RMS^3}$ |

### 2.4.1.2.1    Cross Width

The cross width measures the horizontal distance between points inflection points along the profile. That is, the distance between two consecutive points that cross the zero elevation line. Unlike some of the amplitude statistics, this spacing parameter is always strictly positive. Thus, the research team computed its mean ($Cm$), variance ($Cv$), and skewness ($Cs$) to characterize the distribution of spacing across the profile. **Figure 2.40** shows a comparison between a profile with a high $Cm$ and a low $Cm$. The other two spacing statistics are not presented as they capture similar spacing characteristics to those of $Cm$. It should also be noted that it is impossible to compute the kurtosis of spacing for all the profiles, given that some profiles cross the baseline only twice, meaning there are not enough data points to compute the correction factor in the kurtosis equation. The kurtosis equation requires at least four data points.
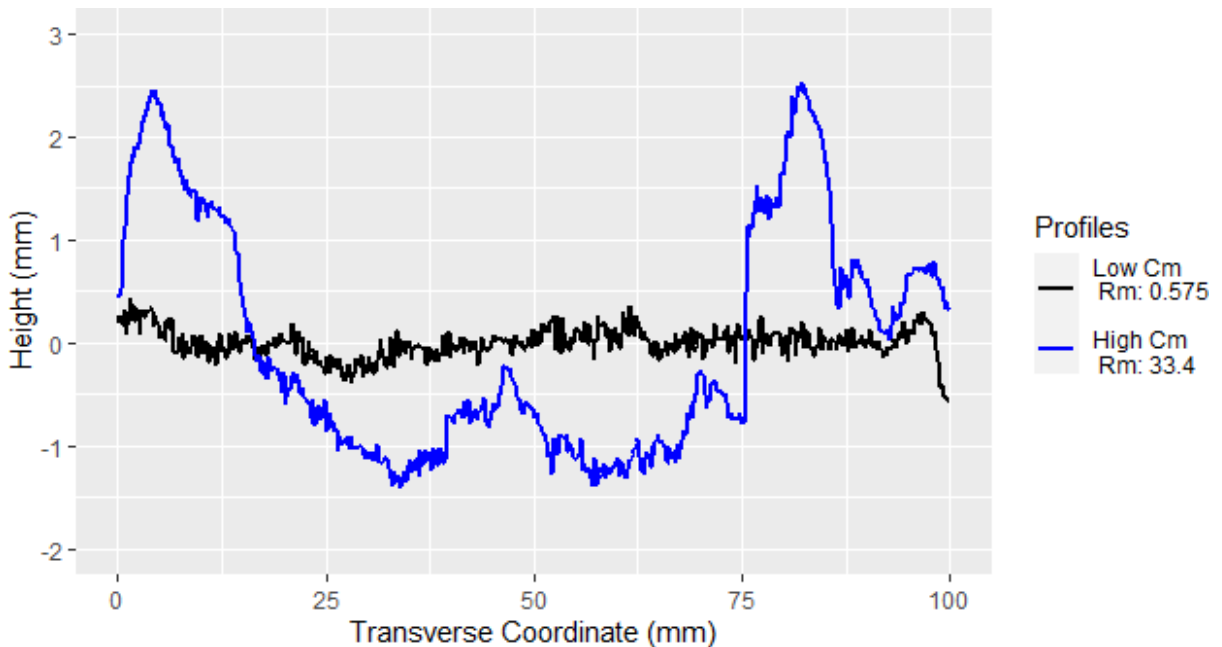


**Figure 2.40** : *Profile with high $C_m$ (blue) and one with low $C_m$ (black)*

## 2.4.1.3    Spatial Hybrid Statistics

The hybrid statistics are a combination of amplitude and spacing. Any changes that occur in either amplitude or spacing may have effects on the hybrid properties. In tribology analysis, surface slope, surface curvature, and developed interfacial area are important factors, which influence the tribological properties of surfaces. The tribology refers to all of the characteristics relating to interacting surfaces in relative motion, including friction, wear, and lubrication (Gadelmawla et al. 2002). The hybrid statistics used in this study are briefly described in this section and their equations are shown in **Table 2.6.**

**Table 2.6 Summary of hybrid summary statistics**

| Statistic | Equation |
|---|---|
| Two-Point Slope Variance (*SV*2) | $$SV_2 = \sqrt{\frac{1}{N}\sum_{i=1}^{N}\left(\frac{h_i - h_{i+1}}{\Delta x}\right)^2}$$ |
| Six-Point Slope Variance (*SV*6) | $$SV_6 = \sqrt{\frac{1}{N}\sum_{i=1}^{N}\left(\frac{h_{i+3} - 9h_{i+2} + 45h_{i+1} - 45h_{i-1} + 9h_{i-2} - h_{i-3}}{60\Delta x}\right)^2}$$ |

where $\Delta x$ is the pacing between two adjacent points.

### 2.4.1.3.1    Two-Point Slope Variance (*SV2*)

The two-point slope variance (SV2) measures the slopes between two consecutive points as the difference in height between two consecutive coordinates, divided by the horizontal distance between them. **Figure 2.41** shows a comparison between a profile with a high SV2 and a low SV2.
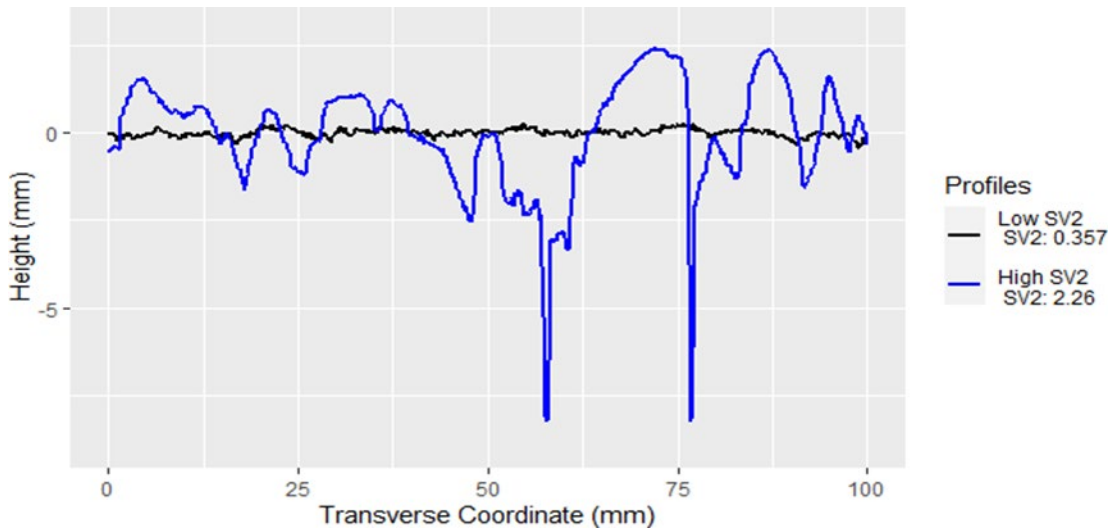


**Figure 2.41** *: Comparison between a profile with high SV2 (blue) and one with low SV2 (black)*

### 2.4.1.3.2    Six-Point Slope Variance (SV6)

The second parameter, *SV6*, calculates the slopes using a weighted sum of the height values of six coordinates divided by the horizontal distance between them. At this scale, a high *SV6* is indicative of aggregate angularity, which can be related to high macro and microtexture. **Figure 2.42** shows a comparison between a profile with a high *SV6* and a low *SV6*.

69
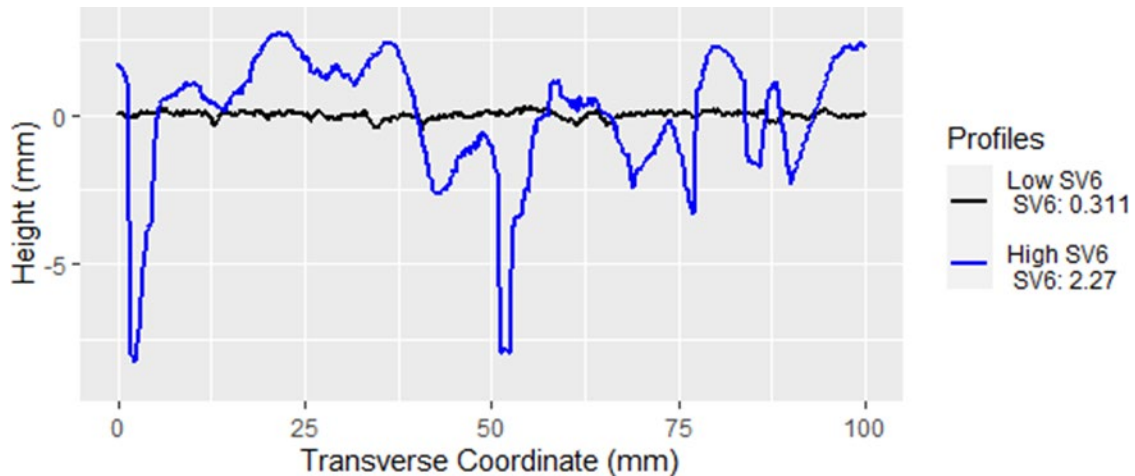
**Figure 2.42** *Comparison between a profile with high SV6 (blue) and one with low SV6 (black)*

## 2.4.1.4 Spectral Statistics

Spectral parameters are calculated in the frequency domain and considered to be scale independent, given that they are estimated along a wide range of texture wavelengths covering multiple texture components (Serigos et al., 2016). Obtaining spectral parameters requires the use of Fourier analysis to examine the surface texture profile. In this project, two spectral statistics were used to characterize the PSD of the pavement profiles.

### 2.4.1.4.1 Power Spectral Density (PSD)

The PSD is a description of how the energy of a pavement texture profile is distributed over the different frequencies. The PSD of a roadway is obtained by applying a DFT to the linear profile of a pavement surface to decompose it into a series of sinusoidal functions with discrete frequencies. Because so many sinusoids must be added together to build complex road profiles, individual amplitudes are almost always small. Hence, the Fourier Transform is adjusted to show how the variance of the profiles is distributed over a set of sinusoids. This adjustment is known as the PSD (Sayers and Karamihas, 1998). Serigos et al. (2016) used the slope and intercept of the linearized PSD curve to characterize the surface macro and microtexture. The method of least squares is used to compute the regression line that best fits the PSD curve and extract its slope and intercept. Furthermore, the logarithm is computed given that the values can be orders of magnitude different from one another. By taking the logarithm, the scale of this statistic becomes significantly smaller. **Figures 2.43** and **2.44** show a comparison between two profiles with different values for PSD intercept (*PSDi*) and the logarithm of PSD slope (*pPSDs*), respectively. The top row shows the profiles in mm, and the bottom row shows their PSD in the logarithm scale.

70
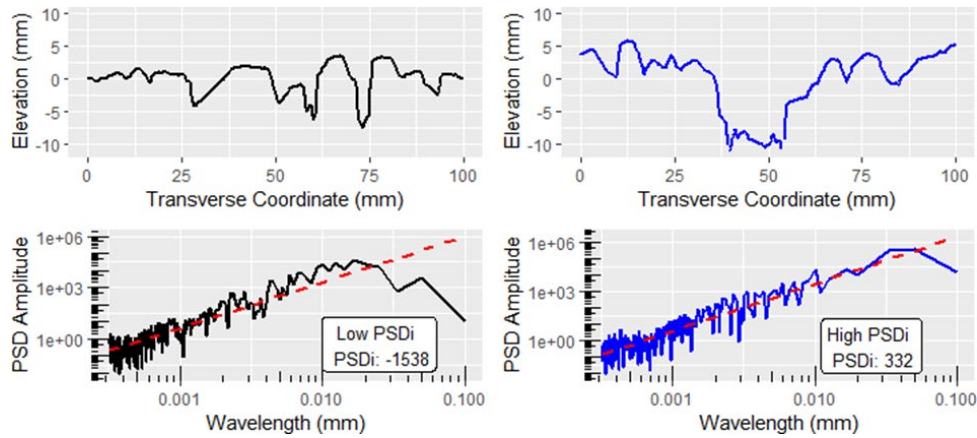
**Figure 2.43** : *Profiles with high $PSD_i$ (blue) and one with low $PSD_i$ (black).*
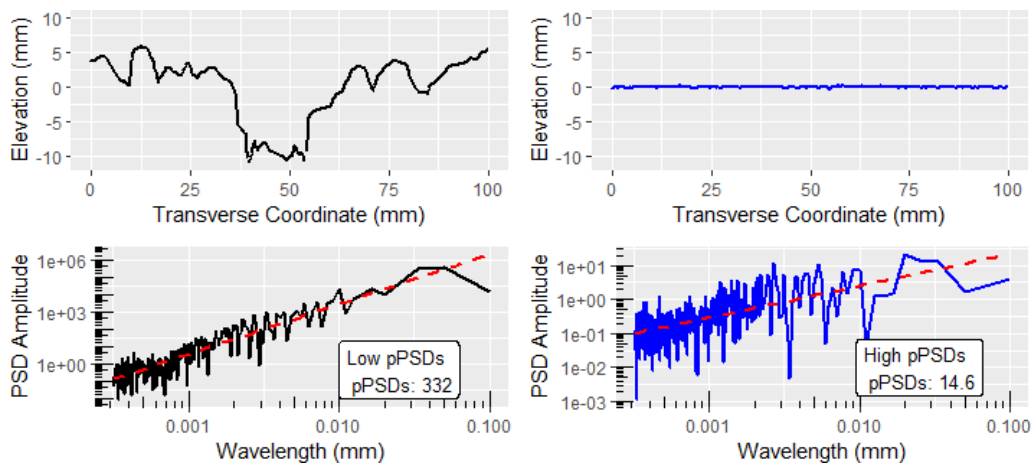


**Figure 2.44** *Profiles with high $pPSD_s$ (blue) and one with low $pPSD_s$ (black)*

## 2.4.2 Filtering High Noise Profiles

The noise removal and imputation processes mentioned in Sections 2.3.2.2 and 2.3.2.3 are essential to remove any spikes that would bias the results. Nonetheless, some of the profiles presented too much noise and most of the data were removed before it got imputed to the extent that the level of uncertainty in the data was too high. In fact, statisticians who study the effects of imputation in different fields of science recommend that when a single variable has more than 60% missing data, this variable should be discarded (Jacobsen et al., 2017; Dong and Peng, 2013; Lee and Huber, 2011). In this case, that would be equivalent to the amount of data that was removed because it was deemed as noise by the SOFA. Thus, it is important to set a threshold of how much noise and imputation is considered allowable.

In the context of pavement profiles, some standards state the amount of noise to be tolerated should be 10% or at most 20% (ISO 13473, 2008; ASTM E2157, 2015; ASTM E1845, 2008; ISO 4287,1997). These thresholds are usually used for profiles that are collected using stationary equipment like the LLS or CTM,

which is expected to have a high level of precision and little to no interference from the environment, such as light saturation or mechanical vibrations. However, the prototype developed for this project collects continuous data at highway speeds. This implies that the sensor is subjected to vehicle vibrations (induced by the engine and pavement roughness), inconsistent lighting, pavement reflectivity, debris, and distresses on the road. For all these reasons, the threshold at which a profile is considered invalid was increased to 33%. Any profile with a percentage of noise higher than the threshold was discarded. The 33% threshold corresponds to more than 205 data points out of 622. Notice that this threshold is particularly high when compared to all other standards, but for the time being scanning chip seals with high macrotexture or dark slurry seals can yield high noise levels, where using 10% or even 20% would remove all the data on these pavement surfaces.

## 2.4.3 Profile Averaging

Once the filtered profiles and their statistics were computed. The next task consists of collapsing groups of 25 consecutive profiles by computing the average of their statistics. This is because the friction data was collected every meter, whereas the texture data was taken every 0.04 meters (25 profiles per meter). This allows the research team to have a one-to-one relationship between the friction and texture statistics. Alternatively, the 25 consecutive profiles could be combined to obtain a 3D surface and compute 3D texture statistics, however, 3D statistics are mostly experimental and are not so popular in practice.

## 2.4.4 Statistic Normalization

Several machine learning algorithms could be applied find trends in the data by analyzing the sample space and comparing every observation in the dataset. An issue arises when the features have different scales. Variables that are measured at different scales do not contribute equally to the model fitting and might end up creating a bias, especially those that are orders of magnitude bigger than the rest. Thus, feature-wise scale reduction techniques are used prior to model fitting to deal with this problem.

Min-max normalization is one of the most common ways to normalize data. For every feature, the minimum value of that feature gets transformed into a zero, the maximum value gets transformed into a one, and every other value gets transformed into a decimal between zero and one using the transformation in **Equation 2.8.**

$$U_i = \frac{x_i - x_1}{x_n - x_1} \tag{2.8}$$

where $U_i$ is the standard uniform random variable, x is the value of the statistic, $x_1$ is the minimum in the statistic's distribution, and $x_n$ is the maximum in the statistic's distribution. Nonetheless, min-max normalization has one significant disadvantage: it does not handle outliers very well. If the data happens to have numerous outliers, then a different normalization technique must be used. Z-score normalization is a strategy for normalizing data that avoids the issues caused by outliers. The formula for Z-score normalization is provided in **Equation 2.9**.

$$Z_i = \frac{x_i - \bar{x}}{s_n} \tag{2.9}$$

where $Z_i$ is the standard normal score, $s_n$ is the sample standard deviation, and $\bar{x}$ is the sample mean. If a value is exactly equal to the mean of all the values of the feature, it is normalized to zero. If it is below the mean, it will be a negative number; if it is above the mean, it will be a positive number. The size of those negative and positive numbers is determined by the standard deviation of the original feature. If the unnormalized data had a small standard deviation, the normalized values will be closer to zero.

The sets of statistics used in this project have very different scales. The top of **Figure 2.45** illustrates the dissimilarities in the scales of four statistics used in this analysis. As can be seen, some of this statistic have multiple outliers; thus, it was deemed appropriate to normalize the scales by using Z-score normalization. Once done, all statistics were transformed into standard normal variables with similar scales, as shown in the bottom of **Figure 2.45**.
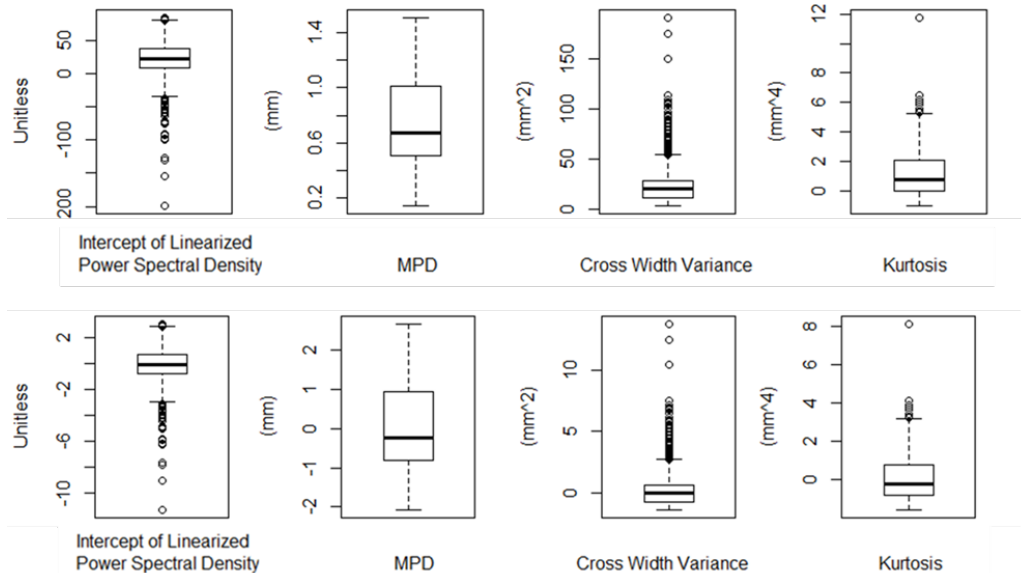


**Figure 2.45** *Boxplot of four unnormalized statistics (top), boxplot of the same statistics after being converted to standard normal variables (bottom).*

## 2.5　Pavement Surface Prediction

Previous research has shown that incorporating surface information into a regression model to predict skid resistance can drastically improve the predictive power of the model from 0.50 to 0.70 in adjusted R2. However, in practice, there is a major shortcoming to this approach. Often, the surface information for the pavement is not known at a network level. Even at a project level this information is still not easy to obtain. For this reason, the research team investigated methods of predicting the pavement surface using the collected data.

### 2.5.1 Pavement Surface Picture Collection

The first step in predicting the surface type of the scanned pavements is assembling a comprehensive training set. This set is meant to have the major classes of pavement seen in Texas. For this project, this includes dense mixes (fine and coarse); open and gap-graded mixes (including SMAs and PFCs); and different surface treatments, such as chip seals of different grades, thin overlays, slurry seals, and microsurfacings. To achieve this, the research team surveyed multiple pavements around the city of Austin and photographed their surfaces, taking a close-up and a slightly zoomed-out photo of each surface. Each photograph includes a quarter coin for scale. **Figure 2.46** shows clear examples of some pavement surfaces that were observed and collected for training the algorithms. Pictures of each pavement section are shown in **Appendix A**.
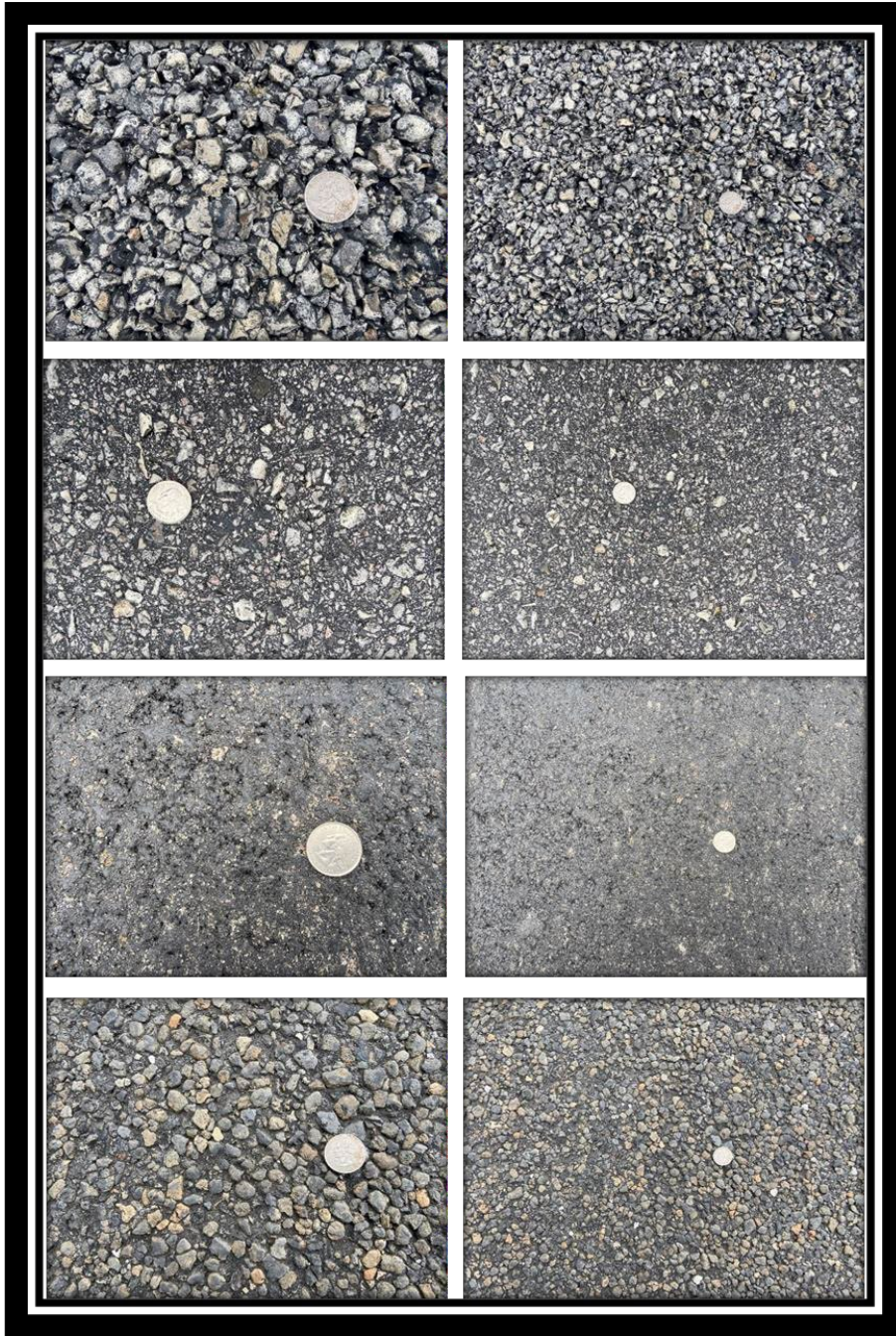
**Figure 2.46** *From top to bottom: PFC, dense coarse mix surface, microsurfacing, and chip seal*

## 2.5.2 Expert Opinion

The research team reached out to experts from TxDOT's Maintenance Division (MNT) and Material and Testing Division (MTD) to have the most educated guess of what mix type corresponded with each of the pictures of the surveyed sections. Specifically, the research team contacted Dr. Andre Smit and Dr. Feng Hong to have them inspect every picture collected from the test sites. From their

visual inspection, it was concluded that at least six different pavement sections were surveyed: dense coarse mixes, dense fine mixes, open graded mixes, gap-graded mixes, and different types of chip seals. This information was critical as it provided the research team with a better understanding of the data, but most importantly, it was used to train and better understand the output of machine learning algorithms to predict both the surface type and the pavement friction.

## 2.5.3 Unsupervised Learning Techniques

Once the research team had a better understanding of the pavement surfaces that were tested, the next step involved using unsupervised machine learning techniques to assess if the texture statistics naturally clustered into their respective surface types. The techniques used in this analysis were k-means clustering and agglomerative hierarchical clustering. A cluster refers to a collection of data points aggregated together because of certain similarities. These clustering implementations are said to have an unsupervised learning phase because the dataset does not contain the true surface type of the pavement. In machine learning, this variable would be known as the label. Thus, the algorithm analyzes the data in such a way that it finds naturally occurring clusters by determining the similarities and differences between the texture statistics. These statistics are referred to as features in the machine learning context.

### 2.5.3.1     K-means Clustering

K-means clustering is one of the simplest and most popular unsupervised machine learning algorithms. The algorithm clusters data by trying to separate samples into $k$ groups of equal variances by minimizing a criterion known as the inertia or the within-cluster sum of squares (**Expression 2.10**).

$$\sum_{i=0}^{k} \min_{\mu_j \in C} \left( \left\| x_i - \mu_j \right\|^2 \right) \qquad \textbf{(2.10)}$$

where $x_i$ is the feature vector for the ith observation, $\mu_j$ is the centroid of cluster j, $C$ is the cluster space, and the operator $\| \|$ is the norm. Inertia is a measure of the variability of the observations within each cluster. In general, a cluster that has a small inertia is more compact than a cluster that has a large inertia. K is a quantity that must be defined by the user before running the algorithm and refers to the number of centroids needed to create the clusters. Each cluster is characterized by the mean $\mu_j$ of the samples in the cluster. The means are commonly called the cluster "*centroids*" and they can be the imaginary or real locations representing the center of each cluster.

The algorithm has three steps. The first step chooses the initial centroids, with the most basic method being to choose $k$ samples from the dataset. After initialization, the algorithm loops between the two other steps. The second step assigns each sample to its nearest centroid. In this step, typically "nearest" means the shortest Euclidean distance to the centroid. The third step creates new centroids by taking the mean value of all samples assigned to each previous centroid.The difference between the old and the new centroids are computed, and the algorithm repeats these last two steps until this value is less than a threshold. In other words, it repeats until the centroids do not move significantly (Choromanska and Monteleoni, 2012).

Given enough time, k-means always converges; however, this may be to a local minimum. This is highly dependent on the initialization of the centroids. As a result, the computation is often done several times, with different initializations of the centroids. One method to help address this issue is the k-means++ initialization scheme. This initializes the centroids to be generally distant from each other, leading to generally better results than random initialization (Choromanska and Monteleoni, 2012).

### 2.5.3.1.1    *Choosing K: The Elbow Method*

Finding the optimal initialization points for the centroids is one of the two challenges when implementing k-means; the other involves determining how many clusters should the algorithm find. That is, how do you find the optimal "k" for the analysis?

The elbow method is a heuristic but commonly used approach to determine this optimal value of k. This method consists of plotting different values for k against their corresponding distortion value. In this case the distortion is calculated as the average inertia of all clusters. As k increases, the average distortions tend to decrease since each cluster has fewer constituent instances, and the instances get closer to their respective centroids. However, the improvements in average distortion declines as k increases. The value of k at which improvement in distortion declines the most is called the elbow. The elbow is the point of diminishing returns for the number of clusters in the data. One can see that all the distortions proceeding the elbow decrease in an almost linear fashion. **Figure 2.47** shows the elbow plot generated from the field data collected.
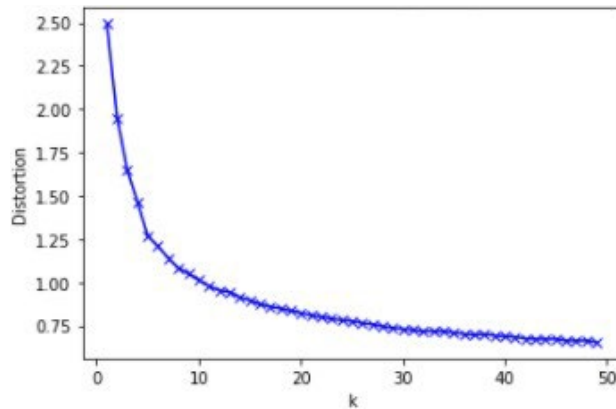
**Figure 2.47** *: Elbow method plot to find the optimal k, generated from field texture data*

## 2.5.3.2 Agglomerative Hierarchical Clustering

Hierarchical clustering is a general family of clustering algorithms that build nested clusters by merging or splitting them successively. There are two main variations of this clustering technique: the agglomerative and the divisive approach. For this project, the agglomerative approach was selected. In the agglomerative approach each observation starts in its own cluster, and pairs of clusters are merged as one moves up the hierarchy. This hierarchy of clusters is represented as a tree (or dendrogram). The root of the tree is the unique cluster that gathers all the samples, the leaves being the clusters with only one sample (Rokach et al, 2005). Upon visual inspection, one can have an estimate of the "optimal" number of naturally occurring clusters in the data, but it is recommended to use the elbow method to corroborate this number. **Figure 2.48** shows the dendrogram generated from the field data collected.
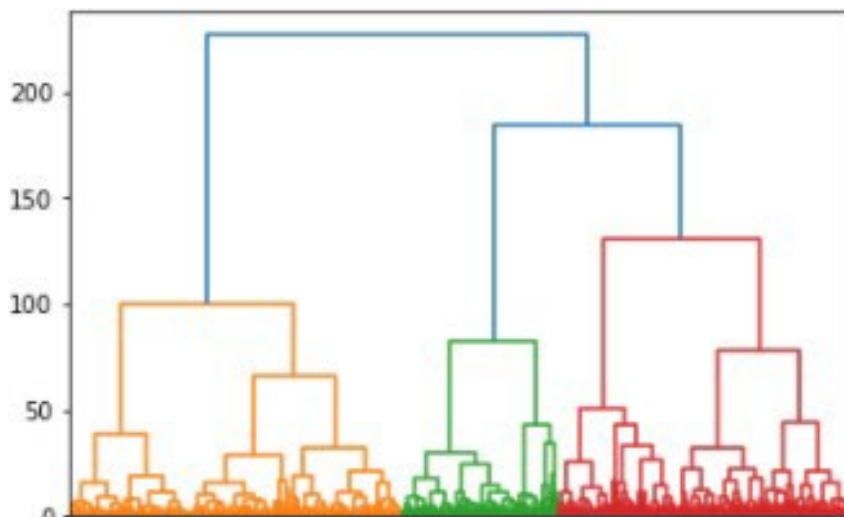


**Figure 2.48** *Dendrogram generated from the field texture data*

To decide which clusters should be combined, a measure of dissimilarity between sets of observations is required. In most methods of hierarchical

78

clustering, this is achieved using an appropriate metric, a measure of distance between pairs of observations, and a linkage criterion that specifies the dissimilarity of sets as a function of the pairwise distances of observations in the sets. The Euclidean distance is generally the most widely used metric to measure distances between two points when the number of features in the data is not too high. In terms of the linkage criterion, there are multiple options, but the one used for this analysis is known as Ward linkage criterion. Ward minimizes the sum of squared differences within all clusters. It is a variance-minimizing approach and in this sense is like the k-means objective function (Rokach et al., 2005).

In general, the merges and splits are determined in a greedy manner. This implies that the algorithm follows the problem-solving heuristic of making the locally optimal choice at each stage. In many problems, a greedy strategy does not usually produce an optimal solution, but nonetheless, a greedy heuristic may yield locally optimal solutions that approximate a globally optimal solution in a reasonable amount of time (Nielsen, 2016).

The main drawback of this approach is its computation time. The time complexity of the algorithm is of the order $O(N3)$; that is, the computation of the algorithm cubes with the size of the dataset. However, running agglomerative hierarchical clustering with a specified metric and linkage criterion is guaranteed to converge onto the same unique solution every time (Sibson, 1973).

## 2.5.4 Supervised Learning Techniques

The research team assigned labels to the pavement surfaces based on the results from the unsupervised learning analysis. As of now, there are six pavement surfaces that are easily distinguished by the clustering models:

1.  Chip seals with high macrotexture (HM CS)
2.  Dense fine mixes (DFM)
3.  Chip seals with low macrotexture (LM CS)
4.  Open mixes or PFCs (OM)
5.  Dense coarse mixes (DCM), and
6.  Stone matrix asphalt (SMA)

These labels were used to train a supervised learning model to classify different pavement surfaces. Supervised machine learning algorithms are designed to learn by example. This type of learning is called "supervised" because the model is given the correct label for each observation when learning the patterns of the data. During its training phase, the algorithm searches for patterns in the data that correlate with the desired outputs. After training, a supervised learning algorithm can take in new unseen inputs and determine which label to assign the

new inputs based on the prior training data. For this project, a decision tree classifier was utilized.

Decision trees are a type of non-parametric supervised learning method used for classification and regression. This classifier uses a decision tree as a predictive model to go from observations about an item, represented by the branches, to conclusions about the item's target value, represented by the leaves. Tree models where the target variable can take a discrete set of values are called classification trees. In these tree structures, leaves represent class labels and branches represent conjunctions of features that lead to those class labels. Decision trees where the target variable can take continuous values (typically real numbers) are called regression trees. The goal is to create a model that predicts the value of a target variable by learning simple decision rules inferred from the data features. Decision trees are among the most popular machine learning algorithms, given their intelligibility and simplicity (Wu et al, 2007; Piryonesi and El-Diraby, 2020). **Figure 2.49** shows one of the decision trees generated in the preliminary stages of this project.
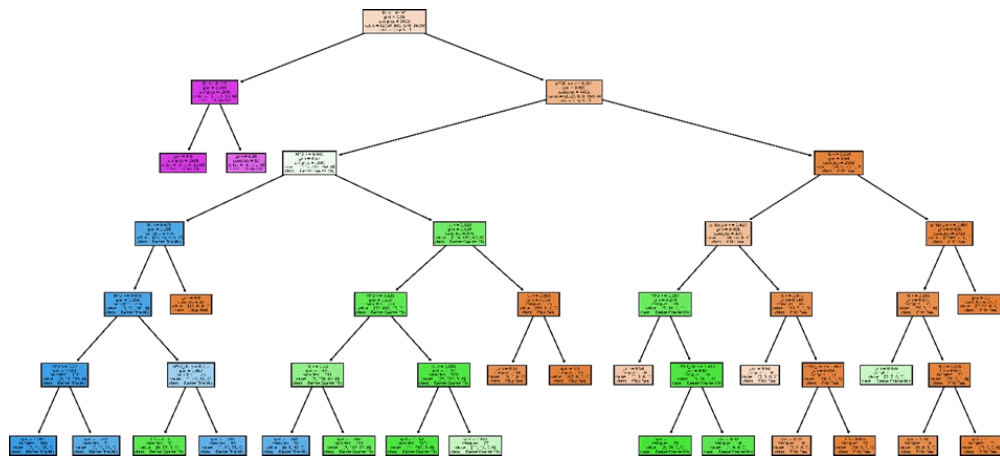


**Figure 2.49** : *Decision tree generated in preliminary development to classify four surfaces*

## 2.6   Skid Prediction Modelling

This section presents the statistical methods used to develop a mathematical model to predict pavement skid resistance from a pavement texture profile.

### 2.6.1 Multiple Regression Analysis

Regression analysis was used to quantify the relationship between measured friction and texture statistics related in a nondeterministic fashion. The most straightforward deterministic mathematical relationship between two variables X and Y is a linear relationship. This relationship is also known as the simple linear regression equation. However, a simple linear regression may not be good enough to obtain a consistent and accurate prediction of the dependent variable.

This is likely because the variance of the parameter of interest cannot be fully explained with a single independent variable, but rather by the combination of multiple parameters. Hence, a multiple regression analysis (MRA) was proposed. In MRA, the objective is to build a probabilistic model that relates a dependent variable to more than one explanatory variable (Devore, 2015). The general additive multiple regression model is defined by **Equation 2.11**:

$$\hat{Y} = \beta_0 + \beta_1 x_1 + \beta_2 x_2 + \cdots + \beta_k x_k + \epsilon \qquad \textbf{(2.11)}$$

where $\hat{Y}$ is the predicted random variable, $\beta_k$ are correlation parameters, $x_k$ are the explanatory/independent variables and $\epsilon$ is the random deviation term. Linear regression models use the coefficient of determination, $R^2$, as a comparative measure of the correlation between $Y$ and $X$ values. $R^2$ measures how close the data are to the fitted regression line or, more precisely, how much of the variability of $Y$ can be explained by the variability of $X$. However, $R^2$ is not an appropriate statistic to compare multiple regression models because its value increases every time an additional predictor variable is added to the model. To deal with this problem, the coefficient of multiple determination ($R^2_{adj}$) is used instead. The adjusted coefficient quantifies how well the model fits the data but punishes the user for each additional parameter added to the model. Thus, this statistic is more appropriate to compare models with a different number of predictors.

## 2.6.1.1 Hypothesis Testing

A two-tailed hypothesis test was used to determine whether the independent variables included in the models had a statistically significant influence on skid resistance. The confidence level selected was 95%. The null hypothesis, ($H_0$), establishes that the coefficient ($\beta_i$) was equal to zero; that is, the corresponding independent variable did not have a significant impact on the dependent variable. The alternative hypothesis, ($H_A$), states that the coefficient is different from zero, which means that the variable did have a statistically significant influence on the dependent variable. The null hypothesis needs to be rejected to be able to conclude that the coefficients are different than zero. That means the corresponding texture statistics had a statistically significant influence on the friction with a confidence level of 95%.

$$H_0: \beta_i = 0$$
$$H_A: \beta_i \neq 0$$

For the hypothesis test, the information was analyzed using the p-value of each coefficient. The p-value represents the probability, assuming that the null hypothesis is true, of obtaining a value of the t-statistic at least as contradictory

to the null hypothesis as the value calculated from the available sample. The p-value was used to make the final decision of whether to reject the null hypothesis by comparing it with the significance level, which is the probability of making a Type I error. Type I errors occur when the null hypothesis is rejected when it is true. The p-values must be lower than 0.05 to reject the null hypothesis.

## 2.6.2 Panel Data Analysis

Panel data combines cross-sectional and time-series data. It is a dataset in which the behavior of several entities is observed across time, or in this case, across a given length of highway. Under the context of pavement management, the panel data analysis is composed of cross-sectional information of pavement sections (information like pavement type or geographical location), combined with performance indicators, condition or distress measurements over the length of a highway. The main difference that distinguishes the panel model from the cross-sectional regression model is that the panel model incorporates heterogeneity among the pavement sections. This means this model can incorporate different mix-type specific parameters. There are two major types of panel models: fixed-effects and random-effects; however, this project focused solely on the former. In the fixed-effects model, mix-type specific parameters are treated as fixed parameters to be estimated.

### 2.6.2.1 Fixed-Effects Regression

Fixed-effects regression explores the relationship between predictor and outcome variables within an entity. In this case, that entity happens to be the pavement surface information. Each entity has its own individual characteristics that may or may not influence the predictor variables. In the fixed-effects model (**Equation 2.12**), the subject specific variable, $c_i$, is a fixed and unknown parameter. The variable represents the omitted variables that are unknown to the data analyst, but constant over time $\mu_{it}$ is assumed to vary non-stochastically over i or t (Li et al., 2017):

$$Y_{it} = x_{it,1}\beta_1 + x_{it,2}\beta_2 + \cdots + x_{it,k}\beta_k + c_i + u_{it} \qquad \textbf{(2.12)}$$

where $x_{it}$ is the independent random variable at a time *t*, $c_i$ is an unknown intercept for each entity, and $u_{it}$ is the error term. The fixed effect model can also be formulated as a dummy variable regression model (**Equation 2.13**). This is useful as dummy variable regression allows the user to see where the surface type variable is incorporated into the prediction for friction (Li et al., 2017):

$$Y_{it} = x_{it,1}\beta_1 + x_{it,2}\beta_2 + \cdots + x_{it,k}\beta_k + v_1\gamma_1 + \cdots + v_n\gamma_n + u_{it} \qquad \textbf{(2.13)}$$

where $v_j$ is a binary dummy representing the surface type, and $\gamma_j$ is the regression coefficient for $v_j$.

The research team used the dummy variable representation of fixed effects panel data analysis to develop a prediction model. Previous research showed that prediction models that incorporate surface information have much more predictive power compared to a multiple regression model that solely uses texture as its predictors (Zuniga, 2017).

## 2.7  Stationary Field-Testing Data Processing

This section explains the methodology employed to compute the summary statistics using the static and smaller scale measuring equipment. The data collected with this equipment was used for validation of the measurements collected with the data collection prototype.

The DFT measurements are easy to process given that the software automatically computes the friction force at 20, 40, 60, and 80 km/h. For the SPT, the method involves applying a known volume, which is typically 25 $mm^3$, of either solid glass spheres of uniform size or Ottawa natural silica sand on a relatively uniform, not distressed section of the pavement surface. The sand is later spread in a circular pattern with a standardized spreading tool. Once the roughly circular patch of sand is made, four equally spaced diameters are measured and averaged to compute the area of the sand patch. The known volume of sand is then divided by the area of the circle using **Equation 1.1** and reported as the MTD. The CTM measurements are similar to the DFT in the sense that the software automatically computes the MPD and RMS along a circular path of a pavement surface. The only quality control that must be performed to guarantee good-quality data is that the percentage of spikes within the data obtained must never exceed 10%; otherwise, the entire dataset is considered invalid. Data collected with the LLS was subjected to the same data processing described under Section 2.3, given that the laser software in this device is similar to the sensor used in the data collection prototype.

# Chapter 3:   Validation of Proposed Friction Prediction Methods

## 3.1   Field Test Design

### 3.1.1 Dynamic Testing

After developing a methodology to process and analyze the texture and friction data, the research team selected a total of twenty-nine pavement sections close to the city of Austin that cover a wide range of different textures and skid numbers encountered in Texas (**Figure 3.1**). These sections were used to validate the methodology established in Chapter 2. A tabulation specifying the highway and the surface present at each section is presented in **Table 3.1**.
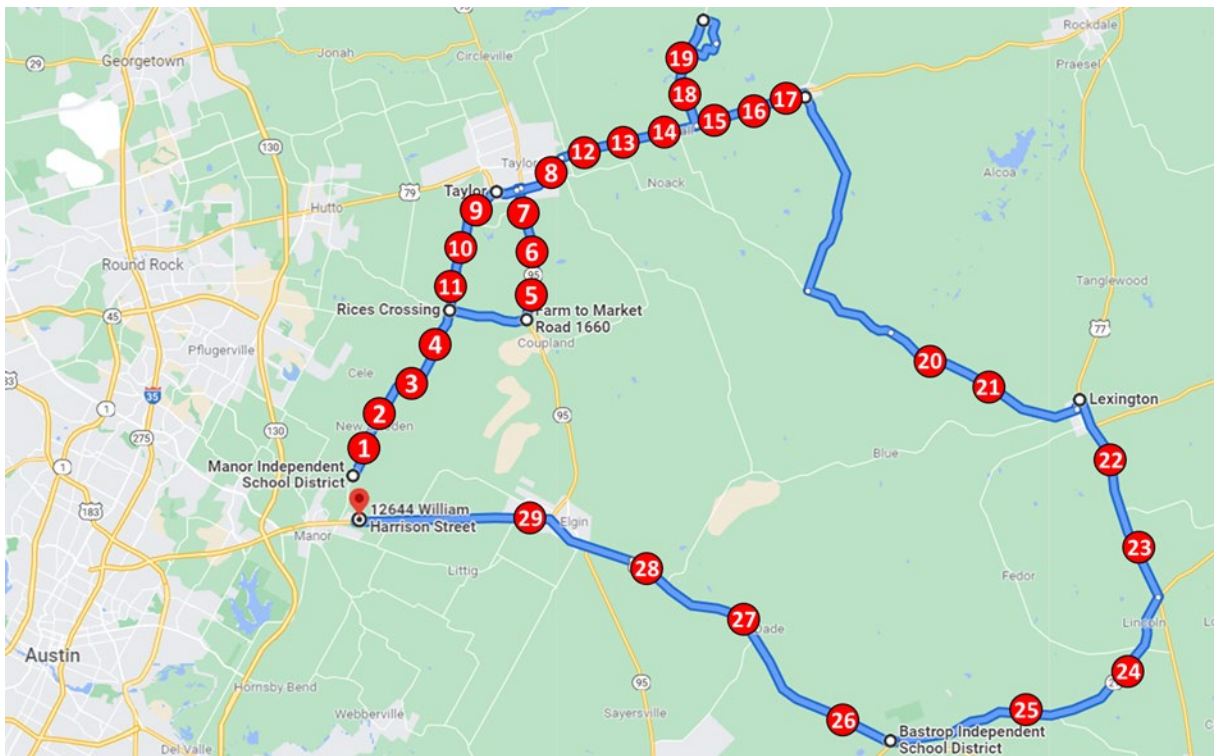


**Figure 3.1** Map location of tested pavement section

Out of the twenty-nine sections, fifteen were surveyed using only the data collection prototype. These sections were tested to ensure it worked as expected. Once it was proven to be fully operational, the research team selected fourteen other sections with varying pavement surfaces to be tested simultaneously with the prototype and TxDOT's LWT. The GripTester from the prototype and LWT characterized the skid of the road in terms of GN and SN, respectively. Both measurements have a scale from 0.0 to 1.0, where zero represents a frictionless surface and one is a surface with maximum friction. These data was used to validate the friction measurements obtained with the GripTester. Lastly, a group of three sections that had been tested by both TxDOT and CTR was selected.

The goal of these sections was to validate the readings obtained by the texture and friction measuring devices used by the performing and receiving agencies.

**Table 3.1 Final selection of pavement surfaces tested with data collection prototype**

| Highway | Pavement Surface | Number ofSamples |
|---------|------------------|------------------|
| FM 0973 | Chip Seals | 6 |
| FM 0973 | Dense Fine Mix | 1 |
| SH 0095 | Dense Coarse Mixes | 3 |
| US 0079 | Chip Seal | 1 |
| US 0079 | Porous Friction Coarse | 5 |
| US 0079 | Dense Fine Mix | 1 |
| FM 1063 | Chip Seal | 2 |
| FM 0112 | Chip Seal | 2 |
| US 0077 | Stone Matrix Asphalt | 1 |
| US 0077 | Dense Coarse Mix | 1 |
| SH 0021 | Stone Matrix Asphalt | 1 |
| SH 0021 | Chip Seal | 1 |
| US 0290 | Porous Friction Coarse | 2 |
| US 0290 | Microsurfacing | 1 |
| US 0290 | Stone Matrix Asphalt | 1 |

## 3.1.2 Stationary Testing

Several tests were performed with stationary equipment on the inner wheel path of the outer lane where TxDOT's LWT and the GripTester had previously tested. The stationary equipment involved in the test were:

- CTM (ASTM E 2157),
- SPT (ASTM E 965),
- LLS, and
- DFT (ASTM E 1911).

Section 1.1.3 describes these equipment devices in detail. Due to the test being stationary, traffic control was requested with the aid of TxDOT to help the researchers conduct the test safely along SH95, US79, and US290. The testing for all three sites was performed over the course of three days where SH95 and US79 were tested on the same day. The time of testing was in the morning starting at 8:00 AM and ending at 11:00 AM, the temperature at each site ranged between 70 and 80°F, and the pavement was completely dry at the moment of testing.

At each test location, measurements were taken 30 meters in the direction of travel from a known GPS position where the LWT and GripTester started measuring. The additional 30 meters are based on the LWT needing approximately 30 meters from their software initialization to the stage that it starts collecting skid measurements. This guarantees that all stationary testing was done within the region that the LWT collected skid measurements. The research team tested three times along the inner wheel path in a span of 20 meters, that is, 10 meters between each measurement spot as shown in the schematic on **Figure 3.2**.
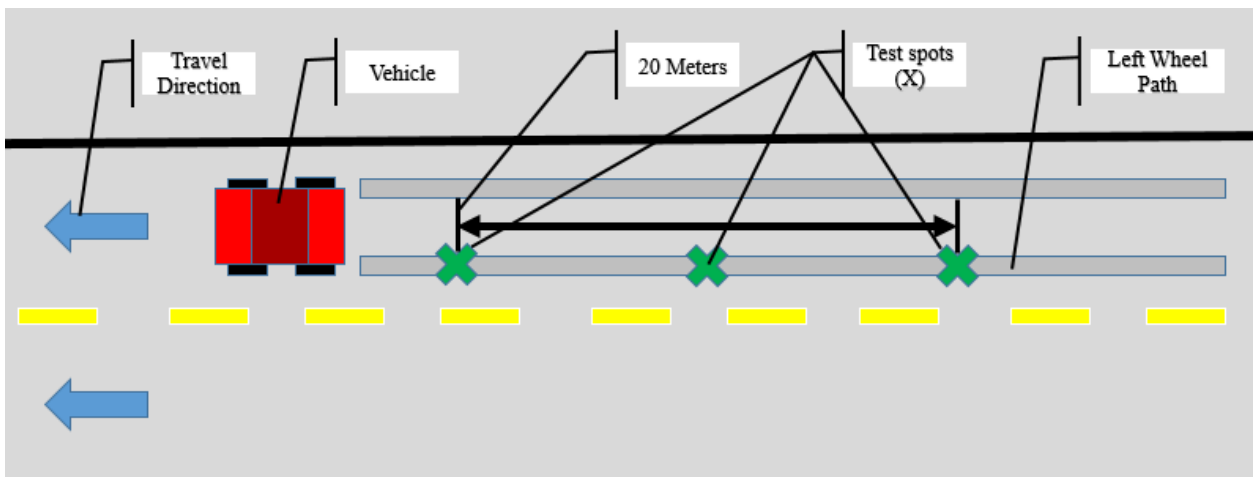


*Figure 3.2 Schematic showing the set up for the three locations tested with stationary equipment*

The order and procedure for testing went as follows: a researcher started with the CTM, carefully positioning the instrument along the inner wheel path. Chalk was used to mark the perimeter of the CTM's chassis for the rest of the devices to collect in the same spot. This was done for all three locations spaced apart by 10 meters. Once the CTM collected data in the first location and moved on to the second one, the LLS followed and collected texture data on the first marked spot. Once the LLS testing was completed and moved on the second location, the DFT followed and tested the marked spot. In parallel to these tests, another researcher performed the SPT adjacent to the marked spots, approximately 0.5 meters in-front. **Figure 3.3** shows a schematic visually describing the location of each testing device. Performing the full battery of testing at each location would take approximately 1.5 hours to complete.
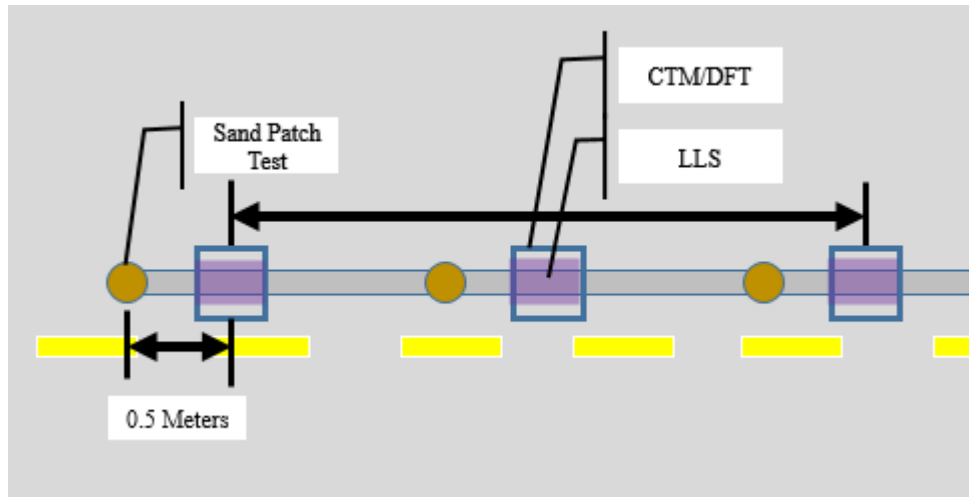
*Figure 3.3 Schematic with locations of each device where the tests would be run*

The texture measurements collected with the in-motion laser sensor were later cross-verified with readings from the CTM, LLS, and SPT. The skid measurements collected with the GripTester and LWT were correlated with the DFT. **Figure 3.4** shows each of the stationary pieces of equipment operating in field conditions.
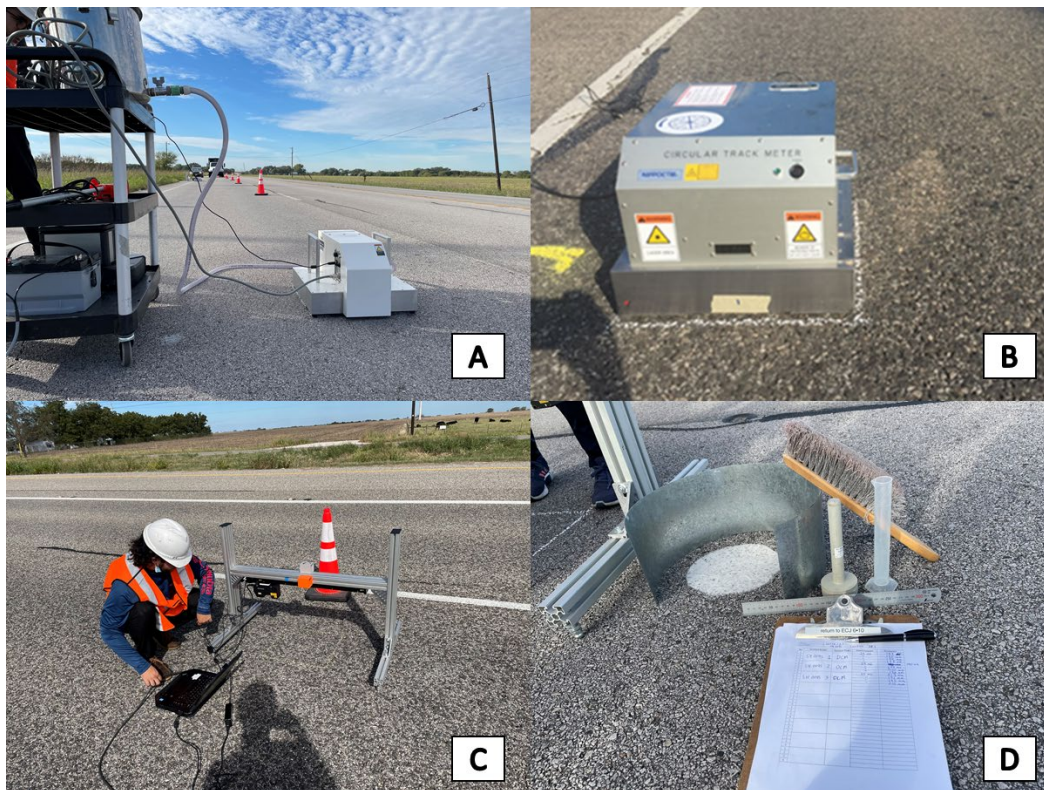


*Figure 3.4: Stationary testing conducted, DFT (A), CTM (B), LLS (C) and SPT (D)*

## 3.2   Data Collected

This section presents all the summary statistics for texture and friction that were collected during the experiment. Multiple statistics were computed from the two-dimensional profiles of the pavement to characterize the pavement texture when using the laser sensor from the prototype. These statistics are summarized in **Tables 3.2 and 3.3.** Not all of the statistics are included in the final specification for the mathematical models, but this is the full set of statistics that were computed and tested to find the ideal combination that yielded most accurate prediction of pavement skid resistance. The average of all texture statistics for the twenty-nine sections have been summarized in **Tables 3.4** and **3.5**.

**Table 3.2 List of summary texture statistics (amplitude statistics)**

| Statistic | Equation |
|---|---|
| Maximum Height ($R_z$) | $R_z = \max(h_i) - \min(h_i), i = 1,2,...,N$ |
| Absolute Height Average ($R_a$) | $R_a = \dfrac{1}{N}\displaystyle\sum_{i=1}^{N}\lvert h_i \rvert$ |
| Height Variance ($R_v$) | $R_v = \dfrac{1}{n-1}\displaystyle\sum_{i=1}^{n}\left(h_i - \bar{h}_i\right)^2$ |
| Root Mean Square ($RMS$) | $RMS = \sqrt{R_v}$ |
| Skewness ($R_s$) | $R_s = \dfrac{n}{(n-1)(n-2)}\displaystyle\sum_{i=1}^{n}\dfrac{\left(h_i - \bar{h}_i\right)^3}{RMS^3}$ |
| Kurtosis ($R_k$) | $R_k = \dfrac{n(n+1)}{(n-1)(n-2)(n-3)}\displaystyle\sum_{i=1}^{n}\dfrac{\left(h_i - \bar{h}_i\right)^4}{RMS^4} - \dfrac{3(n-1)^2}{(n-2)(n-3)}$ |
| Profile Solidity Factor ($R_r$) | $R_r = \dfrac{\min(h_i)}{\max(h_i)}$ |
| Ten-Point Mean Roughness ($R_t$) | $R_t = \dfrac{1}{5}\displaystyle\sum_{j=1}^{5}(h_{pj} - h_{vj})$ |
| Mean Profile Depth ($MPD$) | $MPD = \dfrac{1}{2}\left[\max\left(h_1,...,h_{N/2}\right) + \max\left(h_{N/2},...,h_N\right)\right]$ |

**Table 3.3 List of summary texture statistics (spacing, hybrid and spectral statistics)**

| Statistic | Equation |
|---|---|
| Mean Cross Width ($C_m$) | $$C_m = \frac{1}{n} \sum_{i=1}^{n} x_i$$ |
| Cross Width Variance ($C_v$) | $$C_v = \frac{1}{n-1} \sum_{i=1}^{n} (x_i - \bar{x}_i)^2$$ |
| Cross Width Skewness ($C_s$) | $$C_s = \frac{n}{(n-1)(n-2)} \sum_{i=1}^{n} \frac{(x_i - \bar{x}_i)^3}{RMS^3}$$ |
| Two-Point Slope Variance (SV2) | $$SV_2 = \sqrt{\frac{1}{N} \sum_{i=1}^{N} \left( \frac{h_i - h_{i+1}}{\Delta x} \right)^2}$$ |
| Six-Point Slope Variance (SV6) | $$SV_6 = \sqrt{\frac{1}{N} \sum_{i=1}^{N} \left( \frac{h_{i+3} - 9h_{i+2} + 45h_{i+1} - 45h_{i-1} + 9h_{i-2} - h_{i-3}}{60\Delta x} \right)^2}$$ |
| PSD Intercept | The intercept of the linearized PSD plot (Description provided in TM3) |
| PSD Slope | The slope of the linearized PSD plot (Description provided in TM3) |

## 3.2.1 Skid-Texture Prototype Data

### Table 3.4 Summary texture statistics for all pavement surfaces using data collection prototype

| Section Number | $R_z$ (mm) | $R_a$ (mm) | $R_v$ (mm²) | RMS (mm) | $R_s$ (mm³) | $R_k$ (mm⁴) | $R_r$ (unitless) | $R_t$ (mm) | MPD (mm) |
|---|---|---|---|---|---|---|---|---|---|
| 1 | 3.80 | 0.64 | 0.75 | 0.80 | 0.10 | 0.24 | -1.06 | -0.06 | 1.57 |
| 2 | 4.49 | 0.77 | 1.01 | 0.96 | -0.10 | 0.03 | -0.92 | -0.27 | 1.78 |
| 3 | 4.83 | 0.87 | 1.21 | 1.07 | 0.13 | -0.21 | -1.08 | 0.07 | 2.08 |
| 4 | 3.38 | 0.53 | 0.52 | 0.68 | 0.10 | 0.47 | -1.05 | -0.06 | 1.38 |
| 5 | 2.77 | 0.40 | 0.29 | 0.52 | -1.04 | 1.56 | -0.50 | -0.93 | 0.81 |
| 6 | 2.49 | 0.34 | 0.22 | 0.45 | -1.10 | 1.88 | -0.49 | -0.86 | 0.71 |
| 7 | 2.64 | 0.36 | 0.25 | 0.48 | -1.07 | 1.85 | -0.50 | -0.90 | 0.76 |
| 8 | 3.30 | 0.51 | 0.51 | 0.66 | 0.09 | 0.60 | -0.97 | -0.14 | 1.31 |
| 9 | 4.28 | 0.70 | 0.83 | 0.88 | -0.14 | 0.20 | -0.87 | -0.34 | 1.66 |
| 10 | 1.90 | 0.23 | 0.11 | 0.31 | -1.28 | 2.84 | -0.46 | -0.71 | 0.50 |
| 11 | 5.06 | 0.91 | 1.35 | 1.12 | 0.02 | -0.21 | -1.01 | -0.06 | 2.12 |
| 12 | 6.51 | 1.11 | 2.06 | 1.40 | -0.99 | 0.84 | -0.50 | -2.19 | 1.87 |
| 13 | 1.98 | 0.24 | 0.12 | 0.32 | -1.45 | 3.53 | -0.41 | -0.83 | 0.48 |
| 14 | 6.95 | 1.23 | 2.51 | 1.54 | -0.80 | 0.41 | -0.57 | -1.89 | 2.19 |
| 15 | 7.01 | 1.23 | 2.52 | 1.55 | -0.82 | 0.45 | -0.57 | -1.94 | 2.18 |
| 16 | 6.08 | 1.02 | 1.76 | 1.29 | -1.08 | 1.09 | -0.47 | -2.21 | 1.68 |
| 17 | 6.37 | 1.08 | 1.98 | 1.37 | -1.01 | 0.93 | -0.50 | -2.14 | 1.83 |
| 18 | 3.88 | 0.66 | 0.74 | 0.82 | -0.49 | 0.20 | -0.71 | -0.69 | 1.40 |
| 19 | 4.26 | 0.71 | 0.88 | 0.89 | -0.48 | 0.28 | -0.72 | -0.71 | 1.54 |
| 20 | 5.45 | 1.09 | 1.86 | 1.31 | -0.23 | -0.50 | -0.86 | -0.45 | 2.23 |
| 21 | 6.93 | 1.38 | 2.84 | 1.66 | -0.02 | -0.59 | -0.92 | -0.35 | 2.89 |
| 22 | 4.13 | 0.60 | 0.66 | 0.79 | -1.38 | 2.25 | -0.39 | -1.78 | 1.02 |
| 23 | 2.05 | 0.25 | 0.13 | 0.34 | -1.21 | 2.73 | -0.47 | -0.73 | 0.56 |
| 24 | 3.28 | 0.42 | 0.36 | 0.58 | -1.77 | 4.03 | -0.33 | -1.62 | 0.69 |
| 25 | 3.19 | 0.53 | 0.51 | 0.67 | -0.37 | 0.17 | -0.80 | -0.46 | 1.18 |
| 26 | 6.53 | 1.03 | 1.87 | 1.33 | -1.06 | 1.28 | -0.49 | -2.25 | 1.82 |
| 27 | 3.12 | 0.39 | 0.30 | 0.52 | -1.36 | 3.50 | -0.46 | -1.18 | 0.78 |
| 28 | 6.71 | 1.26 | 2.54 | 1.55 | -0.78 | 0.21 | -0.57 | -1.86 | 2.10 |
| 29 | 4.12 | 0.59 | 0.64 | 0.78 | -1.46 | 2.62 | -0.38 | -1.83 | 0.98 |

**Table 3.5 Summary texture statistics and friction for all pavement surfaces using data collection prototype, continuation**

| Section Number | $C_m$ (mm) | $C_v$ (mm²) | $C_s$ (mm³) | $SV_2$ (mm) | $SV_6$ (mm) | PSD_int (unitless) | PSD_slo (unitless) |
|---|---|---|---|---|---|---|---|
| 1 | 4.26 | 31.0 | 1.84 | 0.74 | 0.69 | 13.4 | 10.2 |
| 2 | 5.10 | 35.6 | 1.51 | 0.82 | 0.78 | 12.2 | 10.7 |
| 3 | 5.52 | 36.4 | 1.41 | 0.85 | 0.82 | 18.4 | 10.9 |
| 4 | 4.08 | 33.7 | 2.00 | 0.60 | 0.55 | 5.95 | 9.97 |
| 5 | 2.68 | 9.24 | 1.67 | 0.69 | 0.65 | 13.6 | 9.06 |
| 6 | 2.46 | 8.62 | 1.80 | 0.60 | 0.56 | 10.5 | 8.77 |
| 7 | 2.47 | 8.38 | 1.75 | 0.63 | 0.60 | 11.8 | 8.87 |
| 8 | 4.03 | 31.2 | 2.01 | 0.60 | 0.56 | 4.18 | 9.87 |
| 9 | 5.03 | 31.4 | 1.46 | 0.74 | 0.72 | 13.4 | 10.5 |
| 10 | 2.04 | 8.04 | 2.17 | 0.50 | 0.46 | 4.89 | 8.07 |
| 11 | 5.56 | 34.7 | 1.36 | 0.88 | 0.85 | 15.9 | 11.0 |
| 12 | 5.49 | 25.7 | 1.12 | 1.32 | 1.28 | 61.3 | 11.3 |
| 13 | 2.07 | 8.39 | 2.16 | 0.53 | 0.48 | 5.47 | 8.09 |
| 14 | 6.14 | 32.2 | 1.09 | 1.27 | 1.24 | 51.1 | 11.6 |
| 15 | 6.25 | 33.3 | 1.07 | 1.25 | 1.23 | 45.8 | 11.6 |
| 16 | 5.26 | 22.8 | 1.14 | 1.24 | 1.22 | 62.6 | 11.1 |
| 17 | 5.67 | 26.1 | 1.10 | 1.23 | 1.20 | 57.8 | 11.3 |
| 18 | 3.79 | 18.2 | 1.53 | 0.79 | 0.75 | 22.8 | 10.2 |
| 19 | 3.99 | 19.4 | 1.52 | 0.84 | 0.80 | 25.4 | 10.4 |
| 20 | 5.13 | 25.7 | 1.25 | 1.12 | 1.08 | 39.1 | 11.2 |
| 21 | 6.01 | 34.7 | 1.21 | 1.31 | 1.28 | 33.3 | 11.9 |
| 22 | 3.22 | 10.4 | 1.46 | 1.05 | 1.01 | 37.5 | 9.85 |
| 23 | 1.97 | 6.35 | 1.97 | 0.58 | 0.53 | 6.06 | 8.10 |
| 24 | 2.99 | 11.4 | 1.71 | 0.82 | 0.78 | 20.1 | 9.20 |
| 25 | 3.89 | 26.4 | 1.79 | 0.66 | 0.61 | 6.35 | 9.87 |
| 26 | 5.06 | 24.5 | 1.18 | 1.25 | 1.21 | 58.4 | 11.2 |
| 27 | 2.39 | 9.17 | 1.97 | 0.81 | 0.74 | 14.0 | 9.01 |
| 28 | 6.12 | 30.8 | 1.08 | 1.33 | 1.31 | 49.6 | 11.6 |
| 29 | 3.39 | 12.6 | 1.52 | 0.99 | 0.95 | 34.0 | 9.87 |

## 3.2.2 Summary of Skid Measured by TxDOT and CTR

The research team also compared the skid data that TxDOT collected with the LWT. **Table 3.6** shows the average skid reading of GripTester and the LWT for the fourteen section that were surveyed using both pieces of equipment. It should be noticed that the correlation is very high even though both pieces of equipment measure skid resistance at different transverse positions. The few sections with higher discrepancies were found were those where the surface texture on the inner wheel path and along the centerline were significantly different. Although the friction prediction models were developed for the GripTester, they could be easily recalibrated to predict SN as measured by the LWT used by TxDOT.

**Table 3.6 Average skid measurements collected with data collection prototype and LWT**

| Highway | Surface | Average Grip Number (GN) | Average Skid Number (SN) |
|---------|---------|--------------------------|--------------------------|
| FM 0973 | Chip Seal | 0.38 | 0.21 |
| FM 0973 | Chip Seal | 0.35 | 0.23 |
| SH 0095 | Dense Mix | 0.45 | 0.35 |
| US 0079 | Porous Friction Coarse | 0.57 | 0.44 |
| FM 0112 | Chip Seal | 0.92 | 0.75 |
| FM 0112 | Chip Seal | 0.94 | 0.59 |
| US 0077 | Stone Matrix Asphalt | 0.67 | 0.44 |
| US 0077 | Dense Mix | 0.48 | 0.23 |
| SH 0021 | Stone Matrix Asphalt | 0.76 | 0.48 |
| SH 0021 | Chip Seal | 0.66 | 0.39 |
| US 0290 | Porous Friction Coarse | 0.50 | 0.37 |
| US 0290 | Dense Mix | 0.53 | 0.33 |
| US 0290 | Porous Friction Coarse | 0.25 | 0.23 |
| US 0290 | Stone Matrix Asphalt | 0.62 | 0.46 |

## 3.2.3 Stationary Field-Testing Data

This sub-section presents all the results from the stationary testing devices. The SPT summarized the texture of the pavement surface using the MTD (**Table 3.7**). The CTM summarized the texture of the pavement sections by providing an average MPD and RMS (**Table 3.8**). The DFT summarized the skid of the pavement section using the F20, F40, F60 and F80 measurements. That is, the equivalent skid number at a speed of 20, 40, 60 and 80 kph (**Table 3.9**). The LLS device was used to compute and validate all the statistics computed using the data collection prototype, every statistic shown in **Tables 3.2** and **3.3** was recomputed using this stationary laser sensor. However, due to complications in the field, the LLS was not used on US-290. Results from the LLS are summarized in **Tables 3.10** and **3.11**.

**Table 3.7 Summary data collected using the SPT**

| Highway Name | Surface Type | Volume (mm³) | Average Diameter (mm) | Mean Texture Depth (mm) |
|---|---|---|---|---|
| SH 0095 #1 | Dense Coarse Mix | 25,000 | 194 | 0.84 |
| SH 0095 #2 | | | 197 | 0.82 |
| SH 0095 #3 | | | 202 | 0.78 |
| US 0079 #1 | Porous Friction Coarse | 25,000 | 121 | 2.21 |
| US 0079 #2 | | | 128 | 1.95 |
| US 0079 #3 | | | 130 | 1.91 |
| US 0290 #1 | Porous Friction Coarse | 25,000 | 121 | 2.21 |
| US 0290 #2 | | | 115 | 2.41 |
| US 0290 #3 | | | 117 | 2.33 |

**Table 3.8 Summary data collected using the CTM**

| Highway Name | Surface Type | MPD (std deviation) | RMS (std deviation) |
|---|---|---|---|
| SH 0095 #1 | Dense Coarse Mix | 0.78 mm (0.08 mm) | 0.53 mm (0.08 mm) |
| SH 0095 #2 | | 0.87 mm (0.15 mm) | 0.57 mm (0.23 mm) |
| SH 0095 #3 | | 0.72 mm (0.13 mm) | 0.45 mm (0.11 mm) |
| US 0079 #1 | Porous Friction Coarse | 1.95 mm (0.27 mm) | 1.50 mm (0.36 mm) |
| US 0079 #2 | | 1.85 mm (0.15 mm) | 1.36 mm (0.18 mm) |
| US 0079 #3 | | 1.89 mm (0.55 mm) | 1.63 mm (0.75 mm) |
| US 0290 #1 | Porous Friction Coarse | 1.99 mm (0.39 mm) | 1.63 mm (0.42 mm) |
| US 0290 #2 | | 1.86 mm (0.17 mm) | 1.51 mm (0.26 mm) |
| US 0290 #3 | | 1.83 mm (0.36 mm) | 1.46 mm (0.31 mm) |

**Table 3.9 Summary data collected using the DFT**

| Highway Name | Surface Type | Speed km/h (mph) | DFT Skid Number | | |
|---|---|---|---|---|---|
| | | | Section #1 | Section #2 | Section #3 |
| SH 0095 | Dense Coarse Mix | 20 (12) | 0.36 | 0.40 | 0.39 |
| | | 40 (24) | 0.36 | 0.41 | 0.38 |
| | | 60 (36) | 0.34 | 0.39 | 0.38 |
| | | 80 (48) | 0.14 | 0.10 | 0.13 |
| US 0079 | Porous Friction Coarse | 20 (12) | 0.35 | 0.39 | 0.35 |
| | | 40 (24) | 0.36 | 0.39 | 0.33 |
| | | 60 (36) | 0.35 | 0.38 | 0.32 |
| | | 80 (48) | 0.16 | 0.17 | 0.12 |
| US 0290 | Porous Friction Coarse | 20 (12) | 0.21 | 0.19 | 0.21 |
| | | 40 (24) | 0.22 | 0.20 | 0.22 |
| | | 60 (36) | 0.23 | 0.21 | 0.22 |
| | | 80 (48) | 0.08 | 0.08 | 0.15 |

**Table 3.10 Summary texture statistics (amplitude) for all pavement surfaces using the LLS**

| Section Number | $R_z$ (mm) | $R_a$ (mm) | $R_v$ (mm²) | RMS (mm) | $R_s$ (mm³) | $R_k$ (mm⁴) | $R_r$ (unitless) | $R_t$ (mm) | MPD (mm) |
|---|---|---|---|---|---|---|---|---|---|
| SH 0095 #1 | 2.86 | 0.37 | 0.25 | 0.49 | -0.79 | 1.46 | -0.61 | -0.71 | 0.76 |
| SH 0095 #2 | 2.80 | 0.36 | 0.23 | 0.47 | -0.83 | 1.60 | -0.57 | -0.76 | 0.75 |
| SH 0095 #3 | 2.50 | 0.31 | 0.18 | 0.41 | -0.86 | 1.88 | -0.57 | -0.69 | 0.66 |
| **Avg. SH 0095** | 2.72 | 0.35 | 0.22 | 0.46 | -0.83 | 1.65 | -0.58 | -0.72 | 0.72 |
| US 0079 #1 | 9.86 | 1.45 | 4.04 | 1.89 | -0.95 | 1.82 | -0.48 | -3.44 | 2.49 |
| US 0079 #2 | 8.78 | 1.37 | 3.37 | 1.73 | -0.84 | 1.20 | -0.52 | -2.66 | 2.21 |
| US 0079 #3 | 7.98 | 1.19 | 2.56 | 1.53 | -1.01 | 1.65 | -0.48 | -2.78 | 1.87 |
| **Avg. US 0079** | 8.87 | 1.34 | 3.32 | 1.72 | -0.93 | 1.56 | -0.49 | -2.96 | 2.19 |

**Table 3.11 Summary texture statistics (spacing, hybrid and spectral) and friction for all pavement surfaces using the LLS**

| Section Number | $C_m$ (mm) | $C_v$ (mm²) | $C_s$ (mm³) | $SV_2$ (mm) | $SV_6$ (mm) | PSD_int (unitless) | PSD_slo (unitless) |
|---|---|---|---|---|---|---|---|
| SH 0095 #1 | 4.22 | 18.3 | 1.66 | 0.37 | 0.36 | 23.0 | 8.79 |
| SH 0095 #2 | 3.90 | 17.1 | 1.86 | 0.38 | 0.37 | 23.2 | 8.64 |
| SH 0095 #3 | 3.82 | 14.5 | 1.62 | 0.35 | 0.34 | 19.6 | 8.35 |
| **Avg. SH 0095** | 3.98 | 16.6 | 1.71 | 0.37 | 0.36 | 21.9 | 8.59 |
| US 0079 #1 | 10.2 | 111 | 1.44 | 1.17 | 1.16 | 229 | 11.7 |
| US 0079 #2 | 11.0 | 135 | 1.43 | 1.13 | 1.12 | 189 | 11.6 |
| US 0079 #3 | 10.1 | 116 | 1.47 | 1.01 | 1.00 | 166 | 11.3 |
| **Avg. US 0079** | 10.4 | 121 | 1.45 | 1.10 | 1.09 | 195 | 11.5 |

## 3.3   Statistical Analysis

This section presents all the analyses and mathematical models that were developed using the data presented in Section 3.2.

### 3.3.1 Comparison of Skid Measuring Devices

The first analysis conducted was a comparison between the skid measurements collected with the LWT and the GripTester. The standard deviation and mean of all skid measurements were computed for each pavement section tested with both pieces of equipment and summarized in **Table 3.12**. Note that the mean GN of the GripTester is always higher than the mean SN from the LWT. This is because of two reasons: 1) The LWT fully locks its measuring wheel before collecting skid, whereas the GripTester's tire uses a 15% fixed slip to collect friction measurements. The physics behind measuring skid with a fully locked wheel and one with a fixed slip imply that the wheel with a fixed slip will have more grip with the pavement than the wheel that is fully locked. 2) The LWT measures the inner wheel path of the lane its testing, whereas the GripTester measures the part of the lane that is in between the inner and outer wheel paths. The aggregates on the inner and outer wheel paths experience significant polishing from the constant flow of traffic relative to the aggregates located in between the wheel paths. That polishing action results in the aggregates along the inner wheel path having a smoother texture and thus a reduced skid compared to the less polished aggregates in between the wheel paths.

**Table 3.12 Comparison between the LWT and GripTester skid measurements**

| Highway | Surface | Mean SN | Std. Dev. SN | Mean GN | Std. Dev. GN |
|---------|---------|---------|--------------|---------|--------------|
| FM 0973 | Chip Seal | 0.21 | 0.05 | 0.38 | 0.06 |
| FM 0973 | Chip Seal | 0.23 | 0.04 | 0.35 | 0.03 |
| SH 0095 | Dense Mix | 0.35 | 0.02 | 0.45 | 0.02 |
| US 0079 | Porous Friction Coarse | 0.44 | 0.01 | 0.57 | 0.03 |
| FM 0112 | Chip Seal | 0.75 | 0.12 | 0.92 | 0.04 |
| FM 0112 | Chip Seal | 0.59 | 0.11 | 0.94 | 0.02 |
| US 0077 | Stone Matrix Asphalt | 0.44 | 0.02 | 0.67 | 0.01 |
| US 0077 | Dense Mix | 0.23 | 0.02 | 0.48 | 0.03 |
| SH 0021 | Stone Matrix Asphalt | 0.48 | 0.04 | 0.76 | 0.04 |
| SH 0021 | Chip Seal | 0.39 | 0.07 | 0.66 | 0.15 |
| US 0290 | Porous Friction Coarse | 0.37 | 0.01 | 0.50 | 0.03 |
| US 0290 | Dense Mix | 0.33 | 0.03 | 0.53 | 0.02 |
| US 0290 | Porous Friction Coarse | 0.23 | 0.01 | 0.25 | 0.04 |
| US 0290 | Stone Matrix Asphalt | 0.21 | 0.05 | 0.62 | 0.06 |
| TxDOT's LWT Standard Deviation | | | | | 0.04 |
| UT's GripTester Trailer Standard Deviation | | | | | 0.04 |

Furthermore, notice that in **Table 3.13** the standard deviations for GN and SN are quite similar with the exception of three pavement sections. In sections along FM112, notice that standard deviation for the SN is much higher than that of the GN. This is because these two sections are chip seals with coarse aggregates that are high in macrotexture and also have some of the highest skids, relative to the other sections. The LWT's measuring wheel has problems fully locking on pavements with high macrotexture and high skid, hence why the standard deviations are so high. In the case of one of the sections along SH0021, the standard deviation of GN is much higher than the SN. The reason for this disparity lies in the fact that this section had asphalt patches that cover most of the right lane. Many of these patches do not go up to the inner wheel path, thus TxDOT's LWT was not capturing the pavement patches, whereas the GripTester was capturing the multiple changes in skid from alternating between asphalt patches and the chip seal. However, even when including those three sections with high standard deviations, we can see that the average standard deviation across all section from the GripTester from the prototype and TxDOT's LWT are almost identical.

## 3.3.2 Skid along Different Locations in the Lane

Given the difference in the mean value of skid between the GN and SN measurements, the research team decided to investigate the difference in skid between the inner wheel path and the pavement in between wheel paths. Three sections with different pavement surfaces were selected to assess this difference, these sections were #6 which is a PFC, #4 which is a chip seal with minor flushing and #25 which is also a chip seal, but with multiple asphalt patches. **Figure 3.5** shows plots of each section where the grip number is mapped against the distance travelled for the equipment. Notice that in all three plots the skid for the in between wheel path is always either about equal or higher than the skid in the inner wheel path. This corroborates the suspicion that the in-between wheel path aggregates have reduced polishing and thus a skid that at least as high as the one present in the inner wheel path. The research team also believes that the magnitude of the difference between the in between and inner wheel path can also be a function of the type of mix, the traffic volume and the age of the pavement.
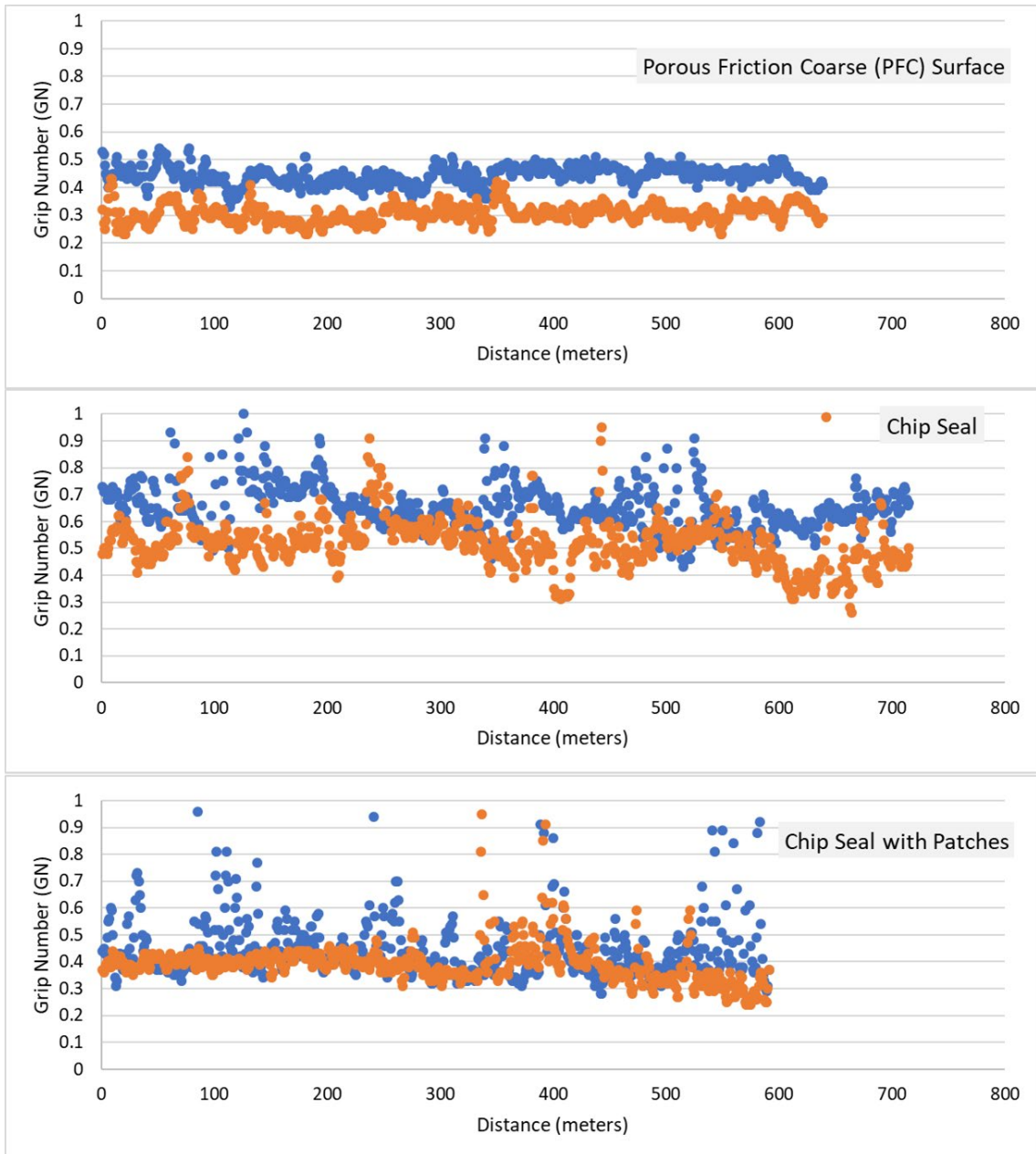
*Figure 3.5: Distance versus friction plot for FM 0973 (top), US 0079 (middle), and SH 0021 (bottom)*

The research team wanted to further investigate this phenomenon, thus, for section #6, a survey was done where the GripTester alternated between surveying the inner wheel path (IW) and the pavement in between wheel paths (IBW). **Figure 3.6** shows the different grip numbers obtained as the skid trailer alternated between wheel paths. The plot further confirms that the pavement in between wheel paths always has on average a higher skid number than the inner wheel path and that the magnitude of that difference in skid is dependent on other factors such as age of the pavement or traffic volume.

99
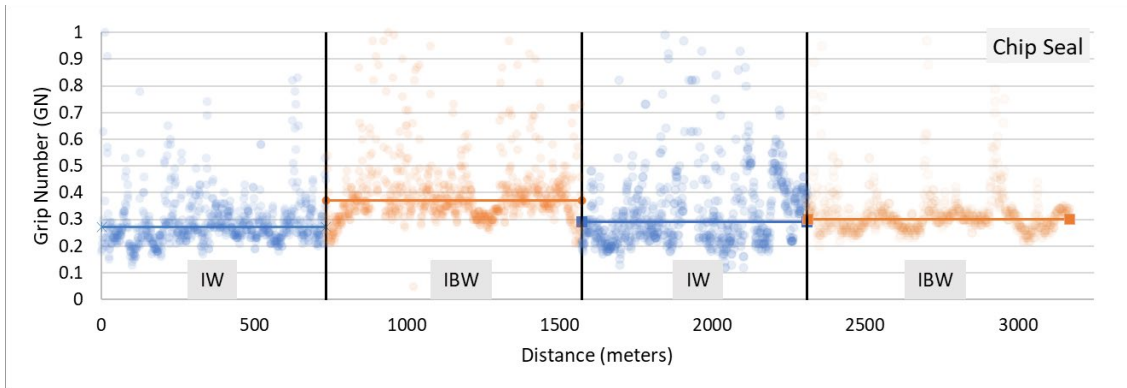
**Figure 3.6**: *Distance versus friction plot for FM973 travelling southbound alternating between the inner wheel path and the pavement in between wheel paths*

### 3.3.3 Influence of Speed of Vehicle on Skid Measurements

A common assumption often made when assessing skid resistance is that skid reduces as the speed of the vehicle increases. The research team quantified the impact that speed has on the measured GN by driving on a straight roadway at varying speeds while measuring the skid resistance. The research team started the test by driving increments of 0.5 miles at speeds of 40, 50 and 60 mph, which tend to be typical highway speeds across the United States. The skid number was then plotted against the speed of the measuring vehicle **(Figure 3.7)** and a regression analysis was performed on the data. The resulting equation that captures the effect of speed on GN for the range of speeds tested is shown in **Equation 3.1**.

$$GN = 0.58 - 0.003 * Speed \qquad\qquad \textbf{(3.01)}$$
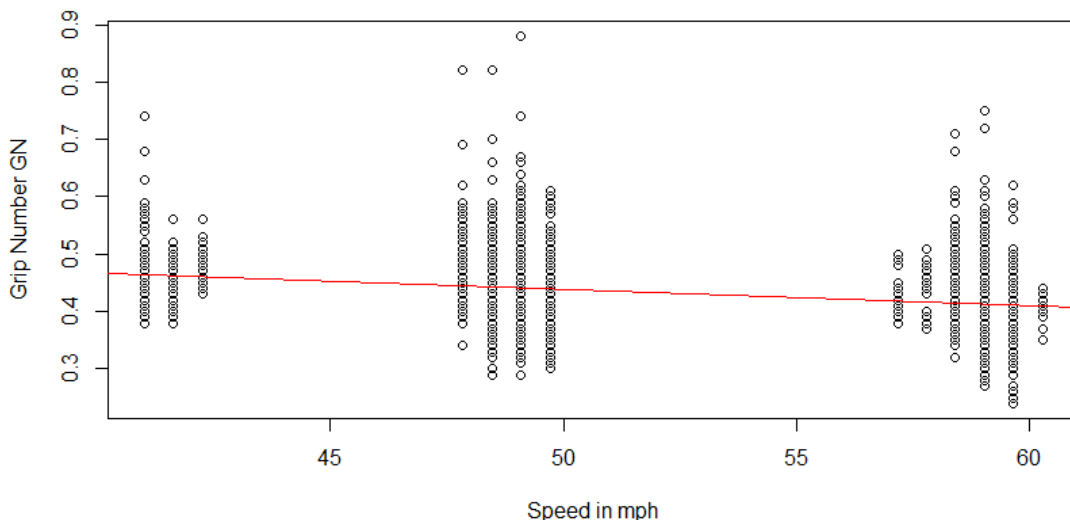


**Figure 3.7**: *Regression plot between the speed of measuring vehicle and the GN*

100

In **Equation 3.1**, the constant 0.58 represents the skid on the pavement associated with all the factors that are not considered in the regression analysis. That would include factors such as the surface type, the texture on the surface, wetness of the surface, etc. The coefficient for speed can be interpreted as the effect that a unit increment in the speed of the measuring vehicle has on the pavement's GN. The data indicates that for every additional mph in the speed of the vehicle (starting at 40 mph and ending at 60 mph), the GN is reduced by 0.003. Even though the data shows with 95% confidence that this reduction in skid due to increasing speeds is statistically significant, the value of 0.003 is too low to cause any dramatic drop in the skid of the road for the range of speeds being measured. Even if the vehicle went from 40 to 60 mph, the predicted reduction in skid would be equal to 0.06, which is not a significant difference. However, it should also be noted that it is possible that once a vehicle drives faster than 60 mph, the reduction in skid becomes much more drastic than 0.003 for every unit increment in speed. However, due to safety concerns and the posted speed limit of the roadway tested, the research team was unable to test this hypothesis

## 3.3.4 Comparison between stationary and dynamic data

To validate the measurements collected with prototype, a series of tests of hypothesis were conducted to check if the average texture or skid measurement is significantly different from the average measurements taken with the stationary equipment. The null hypothesis for this test is that the measurement from the prototype is identical to the measurement from the stationary equipment. In statistical notation this test can be written as:

$$H_0: \hat{\beta}_p - \hat{\beta}_S = 0$$
$$H_A: \hat{\beta}_p - \hat{\beta}_S \neq 0$$

where $\hat{\beta}_P$ is the average measurement computed using data from the prototype and $\hat{\beta}_S$ is the average measurement computed using data from stationary equipment. Since every piece of equipment collected more than 500 profiles per section tested, it is reasonable to assume that the sample average measurement of each piece of equipment follows a normal distribution, by the central limit theorem. These tests were conducted with a significance level of 5%. If the P-value of the test statistic is lower than the significance level, then the null hypothesis is rejected. This means there is strong evidence to prove that the statistics computed with the prototype are different from those of the statistic equipment. Tables showing all the average values that were tested for each piece of equipment and every statistic is shown in **Appendix B**. The results for the hypothesis conducted can be seen in **Table 3.13** for all the skid measurements, and **Table 3.14** for all the relevant texture measurements.

From the hypothesis tests, it can be seen that the measurements from both the LWT and GripTester closely resemble the F60 skid measurements for the DFT. Surprisingly, the DFT measurements at 80 km/h are drastically different from the SN and GN measurements. Furthermore, the LWT appears to be more in line with the DFT than the GripTester, but this outcome is a result of the GripTester outputting higher values of GN relative to the SN. This result indicates that it is probably best to convert the measurements of GN to SN using linear regression. This analysis is discussed in Section 3.3.7. In terms of texture, it appears that the prototype measurements are consistent with the LLS for most of the statistics. The statistics where these metrics differ the most is the cross-width variance, where the measurements of the LLS are an order of magnitude larger than those of the prototype. It should also be noticed that the MPD measured by the CTM was significantly different than the once collected by the LLS and the prototype. This was an unusual result since the LLS and CTM have been tested in the past and results show that their estimates of MPD are quite common.

**Table 3.13 Summary of hypothesis tests conducted**

| Test | Highway | P-value | Conclusion |
|---|---|---|---|
| GripTester's GN and DFT's F20 | SH 0095 | 0.002 | Reject null |
| | US 0079 | 0.000 | Reject null |
| | US 0290 | 0.254 | Fail to reject null |
| LWT SN and DFT's F20 | SH 0095 | 0.364 | Fail to reject null |
| | US 0079 | 0.000 | Reject null |
| | US 0290 | 0.879 | Fail to reject null |
| GripTester's GN and DFT's F40 | SH 0095 | 0.001 | Reject null |
| | US 0079 | 0.000 | Reject null |
| | US 0290 | 0.978 | Fail to reject null |
| LWT SN and DFT's F40 | SH 0095 | 0.995 | Fail to reject null |
| | US 0079 | 0.000 | Reject null |
| | US 0290 | 0.923 | Fail to reject null |
| GripTester's GN and DFT's F60 | SH 0095 | 0.002 | Reject null |
| | US 0079 | 0.000 | Reject null |
| | US 0290 | 0.975 | Fail to reject null |
| LWT SN and DFT's F60 | SH 0095 | 0.774 | Fail to reject null |
| | US 0079 | 0.021 | Reject null |
| | US 0290 | 0.973 | Fail to reject null |
| GripTester's GN and DFT's F80 | SH 0095 | 0.000 | Reject null |
| | US 0079 | 0.000 | Reject null |
| | US 0290 | 0.000 | Reject null |
| LWT SN and DFT's F80 | SH 0095 | 0.000 | Reject null |
| | US 0079 | 0.000 | Reject null |
| | US 0290 | 0.000 | Reject null |

**Table 3.14 Summary of hypothesis tests conducted**

| Test | Highway | P-value | Conclusion |
|---|---|---|---|
| MPD from Prototype and CTM | SH 0095 | 0.025 | Reject null |
| | US 0079 | 0.018 | Reject null |
| | US 0290 | 0.033 | Reject null |
| MPD from Prototype and LLS | SH 0095 | 0.099 | Fail to reject null |
| | US 0079 | 0.152 | Fail to reject null |
| | US 0290 | ~ | ~ |
| RMS from Prototype and CTM | SH 0095 | 0.354 | Fail to reject null |
| | US 0079 | 0.004 | Reject null |
| | US 0290 | 0.654 | Fail to reject null |
| RMS from Prototype and LLS | SH 0095 | 0.785 | Fail to reject null |
| | US 0079 | 0.004 | Reject null |
| | US 0290 | ~ | ~ |
| SV2 from Prototype and LLS | SH 0095 | 0.028 | Reject null |
| | US 0079 | 0.367 | Fail to reject null |
| | US 0290 | ~ | ~ |
| Rs from Prototype and LLS | SH 0095 | 0.158 | Fail to reject null |
| | US 0079 | 0.000 | Reject null |
| | US 0290 | ~ | ~ |
| Rr from Prototype and LLS | SH 0095 | 0.233 | Fail to reject null |
| | US 0079 | 0.687 | Fail to reject null |
| | US 0290 | ~ | ~ |
| Rt from Prototype and LLS | SH 0095 | 0.167 | Fail to reject null |
| | US 0079 | 0.214 | Fail to reject null |
| | US 0290 | ~ | ~ |
| Cv from Prototype and LLS | SH 0095 | 0.000 | Reject null |
| | US 0079 | 0.000 | Reject null |
| | US 0290 | ~ | ~ |

## 3.3.5 Cluster Analysis

Based on the elbow plot and dendrogram of the data shown in **Figures 2.47** and **2.48**, there appears to be six clusters that correspond to six different flexible pavement surfaces. Upon closer inspection of these clusters, the six surfaces were identified to be:

1. Chip seals with medium to low macrotexture (raveling, flushing or aggregate polishing)
2. Chip seals with high macrotexture (good condition)
3. Dense coarse mixes (Types D and C)
4. Dense fine mixes (Type F and TOM)
5. Open Friction Coarse surfaces (PFC)
6. Stone Matrix Asphalts (SMA)

This information was then corroborated with the expert opinion of the TxDOT's Maintenance Division personnel. This further demonstrated that the texture data alone appears to have enough information such that six distinct asphalt pavement surfaces can be accurately identified solely using texture statistics computed from 2D pavement profiles. Furthermore, the cluster analysis showed that both algorithms yield similar results, meaning that regardless of which of the two algorithms is chosen, pavement surface classification is almost identical. Nonetheless, the research team recommends using agglomerative hierarchical clustering with a "ward" linkage method. This is because, hierarchical clustering is always guaranteed to converge on the same final output, whereas the output of K-means can vary depending on the initial guess for cluster centroids.

The results of the clustering analysis are promising as they indicate that the texture information can be used to predict the type of asphalt surface present in a highway. Using this information, the research team developed a decision tree classifier that predicts pavement surface type using texture statistics.

## 3.3.6 Decision Tree Classifier

To determine whether a classification decision tree model is accurate or not, a statistic known as the F1 score is computed. The F1 score is the harmonic mean between the precision and the recall of the model. Precision is the proportion of correctly classified groups over the total number of observations for each group. Recall is the proportion of correctly classified groups over the total number of predictions for each group. The reason for which classification models favor the F1 score as opposed to the accuracy of the model, is because the F1 score is the most robust measure of accuracy for imbalanced datasets. That is, if one of the groups being classified has significantly more representation than the other groups. This happens to be the case in this analysis since there are few data points for high macrotexture chip seals compared to the open mixes and dense mixes in the dataset. Only four sections out of the six that can be detected are used for the pavement surface classifier, this is because in terms of their surface skid properties SMA, dense fine mixes and dense coarse mixes behave in similar ways, thus they can be categorized together into a single group. Thus, the four pavement surfaces the classifier will predict are:

1. High macrotexture chip seals (HM CS)
2. Low to medium macrotexture chip seals (LM CS)
3. Dense mix surfaces and SMA (DMS), and
4. Open-graded mix surfaces (OMS)

The set of all statistics shown in Section 2.4.1 was used to train the first decision tree. However, only the most relevant statistics were kept for the final decision

tree in a process of elimination by trial and error. Furthermore, 80% of the data was used to train the model and the remaining 20% was used to test the model. The results of this testing are summarized in **Table 3.15**

**Table 3.15 Classification report obtained for the most recent decision tree model**

| Surface | Precision | Recall | F1 Score | # of Data Points |
|---------|-----------|--------|----------|------------------|
| HM CS | 0.81 | 0.83 | 0.82 | 431 |
| LM CS | 0.91 | 0.92 | 0.92 | 801 |
| DMS | 0.99 | 0.99 | 0.99 | 910 |
| OMS | 0.99 | 0.98 | 0.99 | 700 |
| | | | Overall Model Accuracy | 0.94 |

**Table 3.14** shows that at an individual level, the smallest accuracy the decision tree model has is 82%, in F1 Score, when classifying HM CS. This means that on average, it is expected that out of 100 sections that are HM CS, 82 of them will be accurately classified as HM CS. This percentage is relatively low compared to the other F1 scores because as soon as chip seal with high macrotexture start experiencing aggregate polishing after years of wear and tear, they start behaving more like a LM CS. In the few instances where HM CS is misclassified, it is misclassified as a LM CS, and this can be confirmed by looking at the confusion matrix shown in **Figure 3.8**. The confusion matrix is a visual way of assessing the accuracy of the model. The confusion matrix is read row by row. To know if the model is accurate, the main diagonal of the confusion matrix should be populated with a high percentage of the observations. The observations on the main diagonal indicate that the predictions made by the model are correct. Observations off of the main diagonal are false positives or false negatives. On the aggregate, the overall accuracy of model measured in terms of F1 score is 94%. This value is extremely high and proves that there is enough information obtained from the texture profile alone, to make a model that is applicable and reliable for predicting the pavement surface at a network level.

**Figure 3.8**: *Unnormalized confusion matrix (left), normalized confusion matrix (right)*

## 3.3.7 Conversion from GN to SN

The ultimate goal of this study is to estimate skid in terms of SN using texture data. Therefore, it is important for the research team to convert the measured GN into SN. A linear regression suggests that the relation between GN and SN is linear and can be estimated by **Equation 3.2**. In this equation, the parameter $\gamma_0$ represents characteristics of the skid number that are not captured in the regression model. For example, the difference in skid between the inner wheel path and the aggregates in between wheel paths. Whereas the parameter $\gamma_1$ captures the effect that a unit increment in the measured GN has on the SN of the road. The data indicate that for every unit increment in GN, the SN increases by 0.634. The goodness of fit of this relation is 0.69 in $R^2$ which from a statistical point of view is a good fit to the data. A summary of the regression analysis is shown in **Table 3.16** and a visualization of the average grip number versus the skid number for the sections is shown in **Figure 3.9**.

$$SN = \gamma_0 + \gamma_1 * GN \tag{3.02}$$

**Table 3.16 Linear regression summary analysis for transforming GN to SN**

| Regression Summary | | |
|---|---|---|
| Parameter | Coefficient | Influence (P-value) |
| Intercept | $\beta_0$ | 0.025 (0.240) |
| Grip Number | $\beta_1$ | 0.634 (0.000) |
| **Goodness of Fit** | | |
| Multiple R | | 0.831 |
| Adjusted $R^2$ | | 0.691 |
| Residual Standard Error | | 8.71 |

This linear transformation on the GN does not affect the goodness of fit statistics obtained when regressing the predicted SN on the texture and surface

information parameters. This is because linear transformations on the random variable being predicted does not affect the correlation between the random variables. This linear transformation merely changes the magnitude of the regression coefficients.
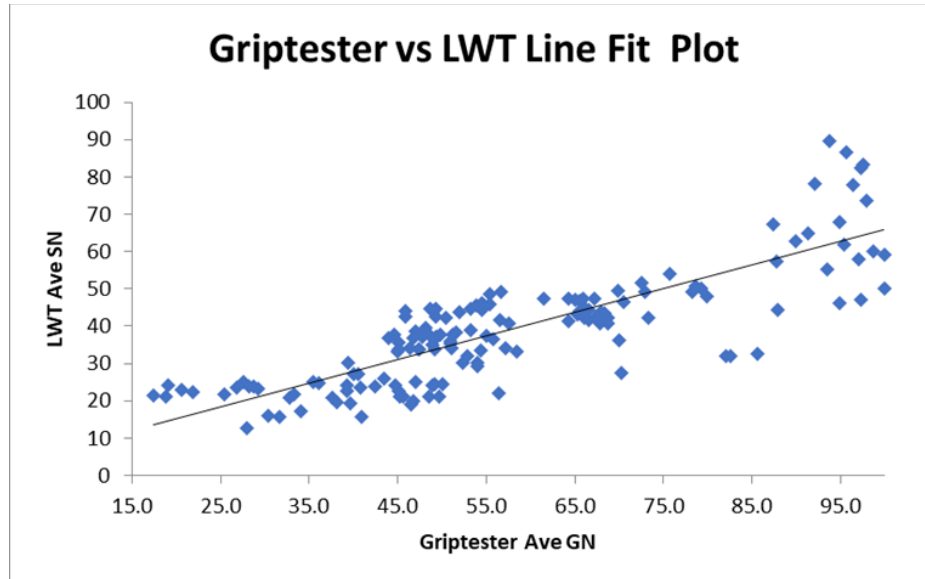


**Figure 3.9**: Scatterplot of the average GN versus the average SN collected across all pavement sections

## 3.3.8 Skid Prediction: Multiple Linear Regression

Once the pavement surface has been predicted, several multiple linear regression analyses were conducted to identify the variables that could capture friction more accurately. The regression model finally chosen is one that combines two macro-texture statistics ($R_s$ and RMS) and three dummy variables that represent the different types of surfaces:

1. Chip seals with high macrotexture (these are the base case),
2. Chip seals with medium to low macrotexture (LM CS),
3. Dense Mix Surfaces (DMS)
4. Open Mix Surfaces (OMS)

There are two reasons why this model uses four pavement surfaces as opposed to the six that could be predicted with the decision tree classifier. First, the regression analysis showed that, at least in terms of skid resistance, there only appears to be a significant difference between LM CS, HM CS, OMS and DMS. The influence of texture in dense fine mixes and stone matrix asphalts appears to have the same effects on skid resistance as the dense coarse mixes, thus they were all combined into a single surface category called "Dense Mix Surfaces". Second, the multiple regression equation is capable of achieving a predictive

power in order of 0.80 in adjusted $R^2$ just by using these four surfaces, including the other two surfaces does not appear to have a significant improvement in predictive power and also increases the likelihood of overfitting the regression model. The final regression equation to predict skid using field texture data is shown in **Equation 3.3.**

$$SN = \beta_0 + \beta_1(R_s) + \beta_2(RMS) + \beta_3(LM\ CS) + \beta_4(DMS) + \beta_3(OMS)$$ **(3.03)**

**Equation 3.3** is a combination of dummy variables and continuous random variables. This means the intercept $\beta_0$ represents the pavement surface type that will be used as a baseline. The baseline surface in **Equation 4.3** are chip seals with high macrotexture. However, the magnitude of $\beta_1$ does not have a direct physical interpretation. The intercept term is just the point at which the regression line for chip seals with high macrotexture crosses the y-axis when extrapolated backwards. The coefficient $\beta_1$ represents the effect that a unit increment in skewness has on the skid of the pavement. The data indicate that for every unit increment in skewness, the skid is reduced by 0.207. This means that regardless of the surface type, the more negative texture present at the pavement surface, the more skid resistance the roadway provides. The coefficient $\beta_2$ represents the effect that a unit increment in RMS has on the skid of the pavement. The data indicates that for every unit increment in RMS, the skid is increased by 0.147. This means that pavements with lots of high variability (high deviations from the horizontal plane) offer, on average, more skid resistance than pavements with smaller deviations. The coefficient $\beta_3$ represents the differential effect between a LM CS and HM CS. The data indicates LM CS have on average 0.167 less skid than HM CS. The coefficient $\beta_4$ represents the differential effect between a DMS and HM CS. The data indicates dense mixes have on average 0.302 less skid than HM CS. Lastly, the coefficient $\beta_5$ represents the differential effect between OMS and HM CS. The data indicates that OMS have on average 0.418 less skid than HM CS. A summary of the regression model and the goodness of fit statistics is provided in **Table 3.17.**

**Table 3.17 Linear regression summary analysis for predicting SN**

| Regression Summary | | |
|---|---|---|
| Parameter | Coefficient | Influence (P-value) |
| Intercept | $\beta_0$ | 0.318 (0.000) |
| Skewness ($R_s$) | $\beta_1$ | -0.207 (0.000) |
| Root Mean Square (RMS) | $\beta_2$ | 0.147 (0.000) |
| Chip Seal Surface (LM CS) | $\beta_3$ | -0.167 (0.003) |
| Dense Mix Surface (DMS) | $\beta_4$ | -0.302 (0.000) |
| Open Mix Surface (OMS) | $\beta_5$ | -0.418 (0.000) |
| Goodness of Fit | | |
| Multiple R | 0.837 | |
| Adjusted $R^2$ | 0.801 | |
| Residual Standard Error | 0.05 | |

# Chapter 4:  Conclusions and Recommendations

## 4.1  Recommendations

Based on the results of the various analyses presented in this report, the research team compiled the following conclusions and recommendations for the estimation of pavement friction using field profile data.

### 4.1.1 Texture and Skid Measuring Equipment

The research team recommends TxDOT to conduct their texture and skid data collection simultaneously by attaching a line laser scanner that collects transverse pavement profiles along the inner wheel path of the lane. This is to ensure that high quality texture data are collected on the same wheel path that the LWT tests for skid. The sampling rate of this laser must be such that at least 100 pavement profiles are collected for every skid measurement collected to replicate the results obtained with the prototype equipment. Current laser technology is unable to capture the full first decade of microtexture while driving at highways speeds. However, this component of texture is not required to achieve a high enough prediction of skid. Its incorporation in the future, will undoubtedly improve the friction prediction model.

For the short- to medium-term, TxDOT should continue to collect skid using the same protocols currently in place. The skid and texture data collected every fiscal year can be used to validate the skid prediction model proposed in this study. Once TxDOT is convinced that the model performs as expected, then the LWT can be kept for project level skid collection and forensic investigations; while at the network level, a surveying vehicle equipped with a fast, high-definition laser sensor can be used to collect the texture data needed to predict the SN with a high degree of accuracy.

### 4.1.2 Data Processing

Once data are collected, a thorough data processing must take place. Quality control criteria for the skid data and texture data must be enforced to ensure that the data used in the mixed model is of the highest possible quality. TxDOT already has good quality control measures to ensure their skid measurements are valid, so this recommendation will not address that aspect. The texture data should be processed using a four-step protocol to ensure the texture data are of good quality before computing summary statistics. This process should include the following steps:

1. Invalid point removal
2. Noise detection and removal

3. Data imputation
4. Profile detrending

The research team carried out a meticulous investigation in each of those areas and developed robust algorithms capable of performing all these tasks. The first step is critical: to separate dropout values from valid measurements. The next step requires having an algorithm that can consistently and reliably detects and removes noise from profiles to prevent outliers from biasing the texture statistics. A robust imputation algorithm capable of handling missing data values to remove any bias that could be introduced by missing data, i.e., the noise that was removed at the previous step. Finally, an efficient detrending algorithm that centers all the profiles to an elevation of 0.0 mm in the shortest amount of time. Data transformation was not deemed necessary as spectral parameters were not used in the final model specification.

The research team developed the SOFA to perform to automate the processing of all the texture profile collected. SOFA is a self-calibrating algorithm. This means that once new data are collected, the algorithm assesses the data and determine what the best thresholds are to eliminate all the noise from the signal. Once calibrated, SOFA automatically trims the profile to remove invalid data points and denoise the profile using an eight-stage filtering process. Once all dropouts, spike and flat lines have been removed, the missing data points are imputed using linear interpolation as it has been proven the most efficient and simplest imputation algorithm. Finally, SOFA executes a regression detrending algorithm to remove any linear trends from the pavement profile. The output of the SOFA is a pavement profile with a minimal amount of noise (if any), that is centered around a flat horizontal plane at an elevation of 0.0 mm. The processed pavement profiles are then fed to a different algorithm that automatically computes all the summary texture statistics that are used for predicting the surface and skid resistance of the pavement. These statistics must be computed for each individual profile and then averaged across each 0.1-mile section, in such a way that there is one of each texture statistic for each skid measurement in Pavement Analyst (PA).

### 4.1.3 Surface Prediction

Decision trees work using binary decisions, are easy to code and are commonly used in PA's current framework. The research team highly encourages their use as the pavement surface classifier of preference. The decision tree developed was trained using over 10,000 pavement profiles coming from different types of flexible pavement surfaces and tested with over 4,000 profiles. The research team meticulously conducted pre-pruning and post-pruning on the decision tree model to avoid overfitting and have a robust classifier with a high degree of accuracy. The classifier requires the following texture statistics:

- Cross-Width Variance ($C_v$)
- Ten Point Mean Roughness ($R_t$)
- Solidity Factor ($R_r$)
- Two-Point Slope Variance ($SV2$)

Using these statistics, the decision tree will output one out of four flexible pavement surfaces: HM CS for a chip seal with high macrotexture, LM CS for a chip seal with low macrotexture, DMS for stone matrix asphalts or dense mixes (both coarse or fine), and OMS for the open graded mixes or PFCs. The pavement surface should be predicted using the decision tree framework shown in **Figure 4.1.**
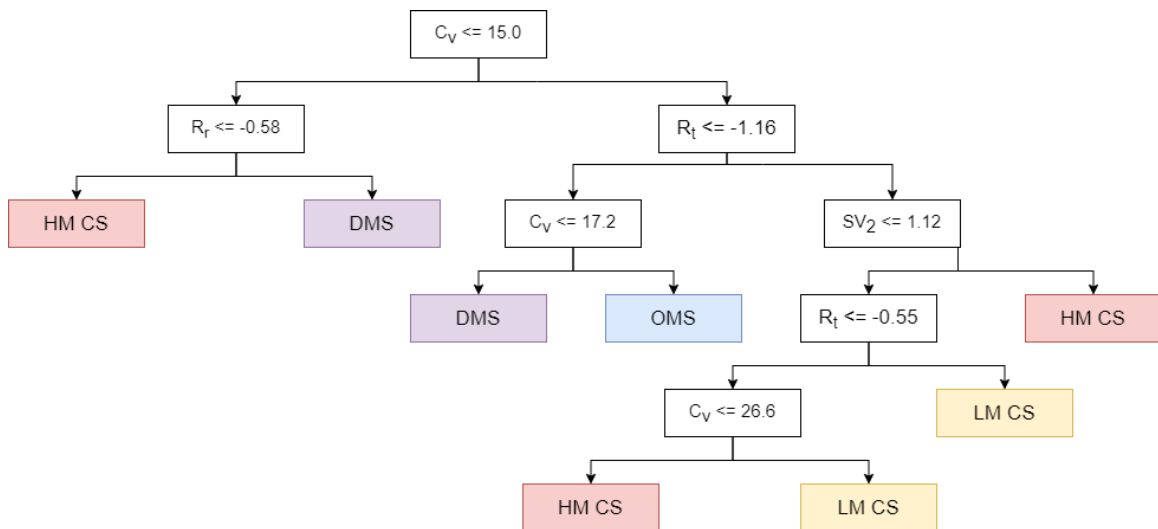


Figure 4.1: Final decision tree classifier framework

This model was proven to have a global accuracy of 94% in F1-score, meaning that out of 100 different flexible pavements surface that it encounters, it accurately predicts the surface type of 94 of them. The pavement surface must be predicted across all the profiles collected within each PA pavement section. The mode of all predictions within each section is assigned as the pavement surface for that whole section. Finally, the dummy variable for LM CS, DMS and OMS must be created. These dummy variables take the value of one if the prediction for the 0.1-mile section matches the surface type of that dummy variable and zero otherwise.

## 4.1.4 Skid Prediction

The regression model of preference to predict the skid resistance of the pavement with an accuracy of 0.80 measured in adjusted $R^2$ is a dummy variable multiple regression that uses two summary texture statistics and three surface information dummy variables. The statistics required to run the regression model are:

- Third Moment of Profile Elevation or Skewness (Rs),
- Standard Deviation of Profile Elevation or Root Mean Square (RMS),
- Dummy variable for LM CS (LCMS),
- Dummy variable for Dense Mixes and SMAs (DMS), and
- Dummy variable for Open Mixes or PFCs (OMS).

The regression model generates exactly four lines, as shown in **Figure 4.2**. One is the predicted SN for HM CS which are the base case given the texture statistics, the predicted SN for LM CS given the texture statistics, the predicted SN for DMS given the texture statistics and the predicted SN for OMS given the texture statistics. This regression model assumes that effect of skewness and root mean square on the skid of the pavement are linear and constant. Moreover, that relation is also dependent upon the material and gradation properties of the type of surface of each pavement and that effect is captured by the dummy variables. The final regression model is presented in **Equation 4.1.**

$$SN = 0.238 - 0.282(R_s) + 0.196(RMS) - 0.130(LMCS) - 0.346(DMS) - 0.478(OMS) \qquad \textbf{(4.01)}$$
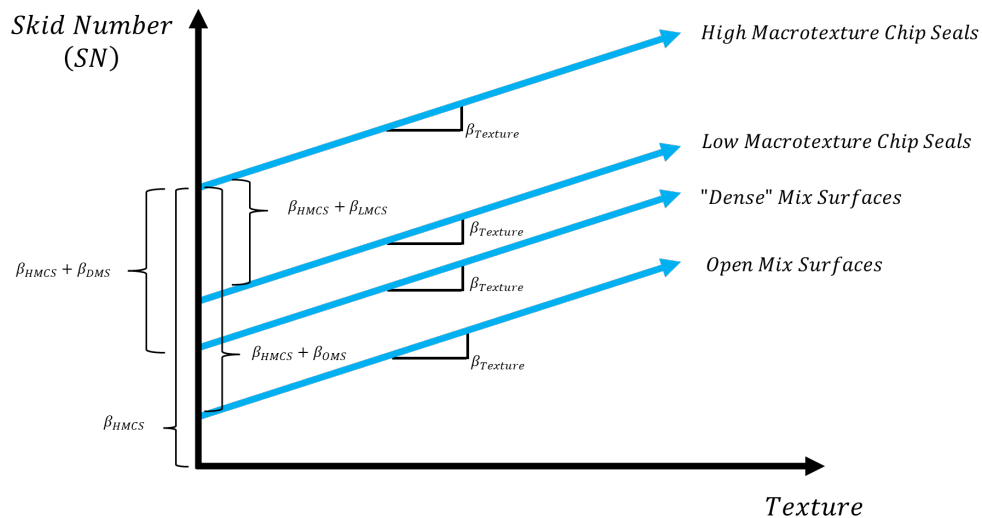


**Figure 4.2** *Visual depiction of the dummy variable multiple regression equation*

## 4.2   Conclusion

During this study a new prototype system for simultaneously collecting high-definition texture and skid resistance data at highway speeds was developed. With the data collected, effective prediction models for pavement skid resistance in terms of SN were developed as a function of texture statistics and pavement

surface information. Currently, the equipment and associated hardware and software perform data acquisition only. The data processing is performed aposteriori using the algorithms developed in this project. It is recommended that research is continued or implemented to develop a system that can perform both data acquisition and data processing on real time. Multiple texture statistics were calculated and regressed against the SN to find the best correlations between the explanatory variables and the dependent variable. The major advantages of the equipment developed can be summarized as follows:

- It eliminates uncertainty due to a time gap between the data collection for pavement texture and skid,
- Both types of data are collected on the same wheel path,
- The equipment has been proven to work at the same speed the locked wheel testers operate (80 kph or 50 mph), and
- The laser sensor used is powerful enough the capture the full spectrum of macrotexture and, with future advancements in technology, it is expected that the first decade of microtexture could be captured in the near future.

A meticulous cluster analysis showed that a combination of amplitude, spacing and hybrid statistics is required in order to create a pavement surface classifier. This study showed that $R_r$, $R_t$, $C_v$ and $SV2$ were the minimum numbers of statistics capable of reaching a predictive power in the order of 94% in F1 Score using a decision tree framework. The implications of having such a strong predictive power for pavement surface could go far beyond just predicting pavement friction. That type of information could also be used in models that predict rolling resistance, splash and spray, pavement/noise, among many other pavement surface interactions.

This research study has demonstrated that texture statistics computed using high-definition texture profile instrumentation have a statistically significant influence on pavement skid resistance and can be used for two major purposes: 1) the prediction of the pavement surface and 2) the prediction of friction with a high degree of accuracy. In fact, these technological advances and the incorporation of artificial intelligence allowed for the development of predictive friction models more powerful than previously possible. Based on the analyzed data, there appears to be a clear relationship between the texture statistics and friction; however, this relationship is not unique and depends on the surface type. Strong correlation can be found among these two factors, but texture statistics alone can only explain up to 50% of the variance within the skid resistance of flexible pavements when all mixtures are considered together. Accounting for the surface type and clustering pavement sections based on a prediction of the

pavement surface increases the explanatory power of texture statistics as high 80% in adjusted $R^2$.

To further improve this study, the research team recommends exploring the use of 3D texture statistics in predicting pavement friction or a complete new set of statistics. Furthermore, the research team encourages repeating this type of study on rigid pavement to assess if texture statistics are capable of distinguishing between different types of concrete pavement surface finishings or texturing, as well as predicting their skid resistance with an accuracy that is at least as good as the one found in this study. Lastly, the research team recommends repeating this study once laser technology has a high enough resolution and sampling rate to capture the first decade of microtexture. Accounting for macro and microtexture, as well as the surface information is bound to increase the predictive power of the models to 90% in adjusted $R^2$.

# References

American Association of State Highway and Transportation Officials (AASHTO). (2008). *AASHTO Guide for Pavement Friction*, first ed., Washington DC.

ASME B46.1 (2009). *Surface Texture (Surface Roughness, Waviness, and Lay)*. American Society of Mechanical Engineers (ASME).

ASTM E1845-15 (2015). *Standard Practice for Calculating Pavement Macrotexture Mean Profile Depth*. West Conshohocken, PA; American Society for Testing and Materials (ASTM).

ASTM E1960-07 (2015). *Standard Practice for Calculating International Friction Index of a Pavement Surface*. West Conshohocken, PA; American Society for Testing and Materials (ASTM).

ASTM E2157 (2015). *Standard Test Method for Measuring Pavement Macrotexture Properties Using the Circular* Track Meter. West Conshohocken, PA; American Society for Testing and Materials (ASTM).

ASTM E2340 (2015). *Standard Test Method for Measuring the Skid Resistance of Pavements and Other Trafficked Surfaces Using a Continuous Reading, Fixed-Slip Technique*. West Conshohocken, PA; American Society for Testing and Materials (ASTM).

ASTM E2380 (2015). *Standard Test Method for Measuring Pavement Texture Drainage Using an Outflow Meter*. West Conshohocken, PA; American Society for Testing and Materials (ASTM).

ASTM E274/E274M-15 (2015). *Standard Test Method for Skid Resistance of Paved Surfaces Using a Full-Scale Tire*. West Conshohocken, PA; American Society for Testing and Materials (ASTM).

ASTM E303 (1998). *Standard Test Method for Measuring Surface Frictional Properties Using the British Pendulum Tester*. West Conshohocken, PA; American Society for Testing and Materials (ASTM).

ASTM E524-08 (2015). *Standard Specification for Standard Smooth Tire for Pavement Skid-Resistance Tests*. West Conshohocken, PA; American Society for Testing and Materials (ASTM).

ASTM E965-15 (2019). *Standard Test Method for Measuring Pavement Macrotexture Depth Using a Volumetric Technique*. West Conshohocken, PA; American Society for Testing and Materials (ASTM).

British Standard Institution (BSI) (2013). *Aggregates for Bituminous Mixtures and Surface Treatments for Roads, Airfields and Other Trafficked Areas*. BS EN 10343. Brussels: European Committee for Standarization.

Choubane, B., Holzschuher, C.R., and Gokhale, S. (2004). *Precision of Locked-Wheel Testers for Measurement of Roadway Surface Friction Characteristics*. Transportation Research Record, 1869.

Choromanska, A. and Monteleoni, C., (2012). Online Clustering with Experts. *Journal ofMachine Learning Research*, 26.

Devore, J., and Farnum, N. (2015). *Applied Statistics for Engineers and Scientists*, Belmont,California: Duxbury.

Dong, Y. and Peng, C.,(2013). Principled missing data methods for researchers. *SpringerPlus*,2(1).

Frank Nielsen (2016). "Chapter 8: Hierarchical Clustering". *Introduction to HPC with MPIfor Data Science*. Springer.

Flintsch, G., McGhee, K., de Leon Izeppi, K. and Najafi, S. (2012). *The Little Book of Tire Pavement Friction*. Pavement Surface Properties Consortium.

Fuentes, L. and Gunaratne, M. (2011). Revised Methodology for Computing International Friction Index. Transportation Research Record: Journal of the Transportation Research Board, 2227(1), pp.129-137.

Gadelmawla, E., Koura, M., Maksoud, T., Elewa, I. and Soliman, H., (2002). Roughnessparameters. *Journal of Materials Processing Technology*, 123(1), pp.133-145.

Hall, J., Smith, K. and Littleton, P. (2008). *Texturing of Concrete Pavements*. Project No. 10-67. Washington, DC: National Cooperative Highway Research Program.

Hall, J.W., K.L. Smith, J.C. Wambold, T.J. Yager and Z. Rado (2009). *Guide for Pavement Friction*. NCHRP Web-Only Document 108. National Cooperative Highway Research Program, Washington, D.C.

Henry, J.J. (2000). *Evaluation of Pavement Friction Characteristics*. NCHRP Synthesis291. National Cooperative Highway Research Program, Washington, D.C.

Huang, H. and Pan, J., (2006). *Speech pitch determination based on Hilbert–Huang transform. Signal Processing*, 86 (4), 792 – 803. doi: 10.1016/j.sigpro.2005.06.01

ISO 4287 (1997). *Geometrical Product Specifications (GPS) — Surface texture: Profile method — Terms, definitions and surface texture parameters*. International Organisation forStandardisation (ISO), Geneve, Switzerland.

ISO 13473-4 (2008). *Characterization of Pavement Texture by Use of Surface Profiles – Part4: Spectral Analysis of Surface Profiles*. International Organisation for Standardisation (ISO),Geneve, Switzerland.

Jakobsen, J., Gluud, C., Wetterslev, J. and Winkel, P., (2017). When and how should multipleimputation be used for handling missing data in randomised clinical trials – a practical guidewith flowcharts. *BMC Medical Research Methodology*, 17(1).

Kane, M., Rado, Z. and Timmons, A. (2015) '*Exploring the texture–friction relationship: from texture empirical decomposition to pavement*

*friction'*, International Journal of Pavement Engineering, 16(10), pp. 919–928. doi: 10.1080/10298436.2014.972956.

Kang, H., (2013). The prevention and handling of the missing data. *Korean Journal ofAnesthesiology*, 64(5), p.402.

Kogbara, R.B., Masad E.A., Kassem, E. Sparpas A.T., Anupam, K. (2016). *A State of Art Review of Parameters Influencing Measurements and Modeling of Skid Resistance of Asphalt Pavements*. Construction and Building Materials 114 602–617.

Lee, J. and Huber, J., (2011). Multiple imputation with large proportions of missing data: Howmuch is too much?

Li, Q., Zhan, Y., Yang, G., Wang, K. and Wang, C., (2017). Panel data analysis of surface skidresistance for various pavement preventive maintenance treatments using long term pavement performance (LTPP) data. *Canadian Journal of Civil Engineering*, 44(5), pp.358-366.

Li, Q., G. Yang, Y. Zhan, K. Wang, and C. Wang. (2017). "*Novel Macro- and Microtexture Indicators for Pavement Friction by Using High-Resolution Three-Dimensional Surface Data."* Transp. Res. Rec. 2641 (3): 164–176. https://doi.org/10.3141/2641-19.

Little, D., Allen, D. and Bhasin, A. (2018). *Modeling and Design of Flexible Pavements and Materials*. Cham: Springer International Publishing.

Maguire, D.J., & Carme, C. (2015). "*LOUDNESS tells you nothing*", Ishn, vol. 49, no. 8, pp. 34.

Mandelbrot, B. (2004). *Fractals and Chaos*. Berlin: Springer.

Mandelbrot, B. (1983). *The Fractal Geometry of Nature*. New York: Macmillan.

Masad, E. (2005). *Aggregate Imaging System (AIMS): Basics and Applications*. Texas: Texas Transportation Institute. FHWA/TX-05/5-1707-01-1.

McGhee, K.K., and Flintsch, G.W. (2003). *High-speed Texture Measurement of Pavements*. Final Report VTRC 3-R9. Virginia Transportation Research Council. Charlottesville, Virginia

Miller, T., Swiertz, D., Tashman, L., Tabatabaee, N. and Bahia, H. (2011). *Characterization of Asphalt Pavement Surface Texture*. Madison: Transportation Research Board.

National Academies of Sciences, Engineering, and Medicine (NASEM) (2009). *Guide for Pavement Friction*. Washington, DC: The National Academies Press. *https://doi.org/10.17226/23038*.

Nielsen, F., (2016). *Introduction to HPC with MPI for Data Science*. Bern: SpringerInternational Publishing.

Noyce, D. A., H. U. Bahia, J. M. Yambó, and G. Kim (2005)*. Incorporating Road Safety into Pavement Management: Maximizing Asphalt Pavement Surface Friction for Road Safety Improvements*. Draft Literature Review

and State Surveys. Midwest Regional University Transportation Center, Madison, Wis.

Piryonesi, S. and El-Diraby, T., 2020. Data Analytics in Asset Management: Cost-EffectivePrediction of the Pavement Condition Index. *Journal of Infrastructure Systems*, 26(1), p.04019036.

Pms.ie. (2017). SCRIM® - *PMS Pavement Management Services Ltd*. [online] Available at: http://www.pms.ie/scrim/4567237776 [Accessed 16 Jan. 2020].

Roe, P. and Hartshorne, S. (1998). *The Polished Stone Value of aggregates and in-service skidding resistance*. TRL Report 322. Berkshire: Transport Research Laboratory.

Rado, Z. and Kane, M., (2014). *An initial attempt to develop an empirical relation between texture and pavement friction using the HHT approach.* Wear, 309 (1–2), 233 – 246.

Rajaei, S., Chatti, K., and Dargazany, R. (2017). *A Review: Pavement Surface Microtexture and its Contribution to Surface Friction*. Transportation Research Board 96th Annual Meeting, Paper 17-06773.

Rokach, L., and Oded M..(2005.) "Clustering methods." Data mining and knowledgediscovery handbook. Springer US, 321-352.

Rubin, D., (1974). Inference and missing data. *Biometrika*, 63(3), pp.581–592.

Sandberg, U. (1987), *"Road traffic noise—The influence of the road surface and its characterization"*, Applied Acoustics, vol. 21, no. 2, pp. 97-118.

Sandberg, U., and Descornet, G. (1980). *Road Surface Influence on Tyre/Road Noise – Parts I and II*. Proceedings of Inter-Noise 80, Miami, Florida, pages 259–272.

Sayers, M.W., Gillespie, T.D., and Paterson, D.O. (1986). *Guidelines for Conducting and Calibrating Road Roughness Measurements*. Work Bank Technical Paper Number 46. The World Bank, Washington, D.C.

Sayers, M. and Karamihas, S. (1998). *The Little Book of Profiling*. New York, NY: Regent of the University of Michigan.

Serigos, P., De Fortier Smit, A. and Prozzi, J. (2014). *Incorporating Surface Microtexture in the Prediction of Skid Resistance of Flexible Pavements*. Transportation Research Record: Journal of the Transportation Research Board, 2457(1), pp.105-113.

Serigos, P., Buddhavarapu, P., Gorman, G., Hong, F. and Prozzi, J. (2016). *The contribution of Micro and Macro-Texture to the Skid Resistance of Flexible Pavement*. Austin: Center for Transportation Research, Report No. SWUTC/16/600451-00085-1.

Sibson, R., 1973. SLINK: An optimally efficient algorithm for the single-link clustermethod. *The Computer Journal*, 16(1), pp.30-34.

Smit, A. (2008). Synthesis of NCAT Low Noise HMS Studies, NCAT Report 0801, Auburn University, Auburn, AL, March 2008.

Smit, A., Prozzi, J., Manuel, T., Natalia, Z. and Buddavarapu, P. (2016). *Designing Quieter Pavement Surfaces*. Austin: Center for Transportation Research, Technical Report No: 0-6819-1

Szatkowski, W. and Hosking, J. (1972). *The Effect of Traffic Aggregate on the Skidding Resistance of Bituminous Surfacings*. TRRL Rept. LR 504. London: U.K. Transport and Road Research Laboratory.

Thomas, L. (2008). *MK2 D-type Maintenance Manual*. Issue 4, Findlay, Irvine Limited, Scotland.

TxDOT, 2014. *Standard Specifications for Construction and Maintenance of Highways,Streets and Bridges*. Austin: Texas Department of Transportation.

Villani, M., Scarpas, A., Bondt, A., Khedoe, R. and Artamendi, I. (2014). *Application of Fractal Analysis for Measuring the Effects of Rubber Polishing on the Friction of Asphalt Concrete Mixtures.* Wear, pp.179-188.

VTI (2021) *Road Surface Tester.* [https://www.vti.se/en/services/highway-engineering-and-geotechnics/on-road-measurement/measurement-of-road-surface](https://www.vti.se/en/services/highway-engineering-and-geotechnics/on-road-measurement/measurement-of-road-surface)*. Accessed November 2021.*

Wambold, J. C., Antle, C. E., Henry, J. J., Rado, Z., Descornet, G., Sandberg, U., Gothié, M. and Huschek S. (1995). *International PIARC Experiment to Compare and Harmonize Skid        Resistance and Texture Measurements* (Paris: PIARC) Publication number 01.04.T.

Wei, L., Fwa, T. and Zhe, Z. (2002). *Pavement roughness analysis using wavelet theory*. 6th International Conference on Managing Pavements. Queensland.

Wu, X., Kumar, V., Ross Quinlan, J., Ghosh, J., Yang, Q., Motoda, H., McLachlan, G., Ng,A., Liu, B., Yu, P., Zhou, Z., Steinbach, M., Hand, D. and Steinberg, D., (2007). Top 10 algorithms in data mining. *Knowledge and Information Systems*, 14(1), pp.1-37.

Zuniga-Garcia, N. (2017). *Predicting Friction with Improved Texture Characterization* (Master's Thesis). The University of Texas at Austin, Austin, TX, United States.

# Appendix A (Images of Pavement Sections)



**Highway:** FM 0973

**Predicted Surface:** Low Macrotexture Chip Seal

**MPD:** 1.57 mm.

**RMS:** 0.80 mm.



**Highway:** FM 0973

**Predicted Surface:** Low Macrotexture Chip Seal

**MPD:** 1.78 mm.

**RMS:** 0.96 mm.



**Highway:** FM 0973

**Predicted Surface:** Low Macrotexture Chip Seal

**MPD:** 2.08 mm.

**RMS:** 1.07 mm.

**Highway:** FM 0973

**Predicted Surface:** Low Macrotexture Chip Seal

**MPD:** 1.38 mm.

**RMS:** 0.68 mm.



**Highway:** FM 0973

**Predicted Surface:** Low Macrotexture Chip Seal

**MPD:** 0.76 mm.

**RMS:** 0.48 mm.



**Highway:** FM 0973

**Predicted Surface:** Low Macrotexture Chip Seal

**MPD:** 1.31 mm.

**RMS:** 0.66 mm.

**Highway:** FM 0973

**Predicted Surface:** Low Macrotexture Chip Seal

**MPD:** 1.66 mm.

**RMS:** 0.88 mm.



**Highway:** FM 0973

**Predicted Surface:** Dense Fine Mix

**MPD:** 0.50 mm.

**RMS:** 0.31 mm.



**Highway:** SH 0095

**Predicted Surface:** Dense Coarse Mix

**MPD:** 0.81 mm.

**RMS:** 0.68 mm.

**Highway:** SH 0095

**Predicted Surface:** Dense Coarse Mix

**MPD:** 0.71 mm.

**RMS:** 0.52 mm.



**Highway:** SH 0095

**Predicted Surface:** Dense Coarse Mix

**MPD:** 0.76 mm.

**RMS:** 0.45 mm.



**Highway:** US 0079

**Predicted Surface:** Porous Friction Coarse

**MPD:** 2.12 mm.

**RMS:** 1.12 mm.

**Highway:** US 0079

**Predicted Surface:** Porous Friction Coarse

**MPD:** 1.87 mm.

**RMS:** 1.54 mm.



**Highway:** US 0079

**Predicted Surface:** Porous Friction Coarse

**MPD:** 2.19 mm.

**RMS:** 1.55 mm.



**Highway:** US 0079

**Predicted Surface:** Dense Fine Mix

**MPD:** 0.48 mm.

**RMS:** 0.32 mm.

**Highway:** US 0079

**Predicted Surface:** Porous Friction Coarse

**MPD:** 2.18 mm.

**RMS:** 1.29 mm.



**Highway:** US 0079

**Predicted Surface:** Porous Friction Coarse

**MPD:** 1.68 mm.

**RMS:** 1.37 mm.



**Highway:** FM 1063

**Predicted Surface:** High Macrotexture Chip Seal

**MPD:** 2.19 mm.

**RMS:** 1.54 mm.

126

**Highway:** FM 1063

**Predicted Surface:** High Macrotexture Chip Seal

**MPD:** 2.18 mm.

**RMS:** 1.55 mm.



**Highway:** FM 0112

**Predicted Surface:** High Macrotexture Chip Seal

**MPD:** 2.23 mm.

**RMS:** 1.31 mm.



**Highway:** FM 0112

**Predicted Surface:** High Macrotexture Chip Seal

**MPD:** 2.89 mm.

**RMS:** 1.66 mm.

**Highway:** US 0077

**Predicted Surface:** Stone Matrix Asphalt

**MPD:** 1.02 mm.

**RMS:** 0.79 mm.



**Highway:** US 0077

**Predicted Surface:** Dense Coarse Mix

**MPD:** 0.56 mm.

**RMS:** 0.34 mm.



**Highway:** SH 0021

**Predicted Surface:** Stone Matrix Asphalt

**MPD:** 0.69 mm.

**RMS:** 0.58 mm.

**Highway:** SH 0021

**Predicted Surface:** Low Macrotexture Chip Seal

**MPD:** 1.18 mm.

**RMS:** 0.67 mm.



**Highway:** US 0290

**Predicted Surface:** Porous Friction Coarse

**MPD:** 1.82 mm.

**RMS:** 1.33 mm.



**Highway:** US 0290

**Predicted Surface:** Dense Fine Mix

**MPD:** 0.78 mm.

**RMS:** 0.52 mm.

**Highway:** US 0290

**Predicted Surface:** Porous Friction Coarse

**MPD:** 2.10 mm.

**RMS:** 1.55 mm.



**Highway:** US 0290

**Predicted Surface:** Stone Matrix Asphalt

**MPD:** 0.98 mm.

**RMS:** 0.78 mm.

# Appendix B (Cross Validation Tables)

Comparison of skid measurements

| Highway | GripTester (GN) | LWT (SN) | DFT (F60) | | |
|---|---|---|---|---|---|
| | | | Section #1 | Section #2 | Section #3 |
| SH 0095 | 0.45 | 0.35 | 0.34 | 0.39 | 0.38 |
| US 0079 | 0.57 | 0.44 | 0.35 | 0.38 | 0.32 |
| US 0290 | 0.25 | 0.23 | 0.23 | 0.21 | 0.22 |

Comparison of MPD measurements

| Highway | Prototype MPD (mm) | LLS MPD (mm) | | | CTM MPD (mm) | | |
|---|---|---|---|---|---|---|---|
| | | Section #1 | Section #2 | Section #3 | Section #1 | Section #2 | Section #3 |
| SH 0095 | 0.71 | 0.76 | 0.75 | 0.66 | 0.78 | 0.87 | 0.72 |
| US 0079 | 2.12 | 2.49 | 2.21 | 1.87 | 1.95 | 1.85 | 1.89 |
| US 0290 | 2.1 | ~ | ~ | ~ | 1.99 | 1.86 | 1.83 |

Comparison of RMS measurements

| Highway | Prototype RMS (mm) | LLS RMS (mm) | | | CTM RMS (mm) | | |
|---|---|---|---|---|---|---|---|
| | | Section #1 | Section #2 | Section #3 | Section #1 | Section #2 | Section #3 |
| SH 0095 | 0.45 | 0.49 | 0.47 | 0.41 | 0.53 | 0.57 | 0.45 |
| US 0079 | 1.12 | 1.89 | 1.73 | 1.53 | 1.5 | 1.36 | 1.63 |
| US 0290 | 1.55 | ~ | ~ | ~ | 1.63 | 1.51 | 1.46 |

Comparison of SV2 measurements

| Highway | Prototype SV2 (mm) | LLS SV2 (mm) | | |
|---|---|---|---|---|
| | | Section #1 | Section #2 | Section #3 |
| SH 0095 | 0.6 | 0.37 | 0.38 | 0.35 |
| US 0079 | 1.32 | 1.17 | 1.13 | 1.01 |

Comparison of $R_r$ measurements

| Highway | Prototype $R_r$ (unitless) | LLS $R_r$ (unitless) | | |
|---|---|---|---|---|
| | | Section #1 | Section #2 | Section #3 |
| SH 0095 | -0.49 | -0.61 | -0.57 | -0.56 |
| US 0079 | -0.5 | -0.48 | -0.52 | -0.49 |

Comparison of $R_t$ measurements

| Highway | Prototype $R_t$ (mm) | LLS $R_t$ (mm) | | |
|---|---|---|---|---|
| | | Section #1 | Section #2 | Section #3 |
| SH 0095 | 0.6 | 0.37 | 0.38 | 0.35 |
| US 0079 | 1.32 | 1.17 | 1.13 | 1.01 |

Comparison of $R_s$ measurements

| Highway | Prototype $R_s$ (mm³) | LLS $R_s$ (mm³) | | |
|---|---|---|---|---|
| | | Section #1 | Section #2 | Section #3 |
| SH 0095 | -1.1 | -0.79 | -0.83 | -0.86 |
| US 0079 | -0.99 | -0.95 | -0.84 | -1.01 |

Comparison of $C_v$ measurements

| Highway | Prototype $C_v$ (mm²) | LLS $C_v$ (mm²) | | |
|---|---|---|---|---|
| | | Section #1 | Section #2 | Section #3 |
| SH 0095 | 8.62 | 18.3 | 17.1 | 14.5 |
| US 0079 | 25.7 | 111 | 135 | 116 |

# Appendix C (Value of Research)

A detailed analysis of the economic benefits brought about by TxDOT Research Project 0-7031 is explained in this appendix. The analysis on a macroeconomic level evaluates the long-term effects of sponsoring this research project are examined. The monetary savings obtained at both the macro and microeconomic levels are utilized in a net present value (NPV) cost-benefit analysis using the template provided by TxDOT.

Motor-vehicle accidents can occur due to numerous reasons; however, the most common potential causes can be classified into three broad categories: driver-related, vehicle-related and highway condition-related. Driver related accidents involve drivers being distracted, sleepy or in a state that impairs their ability to drive a vehicle safely. It is not possible for TxDOT to fully prevent driver-related, vehicle-related, or environmental-related accidents, as many of those causes are beyond their control. However, TxDOT can mitigate crashes across all three categories by improving the pavement surface friction.

The ultimate goal of this project is to improve safety across Texas' highway network by having complete information of the friction conditions on a annual basis, which allows for proper maintenance scheduling whenever friction falls below a given threshold. The reduction in skid due to wet-weather conditions is of particular interest, given that reduced skid under wet conditions increases the probability of accidents to occur and increases the likelihood of hydroplaning. In the United States, a significant number of wet-weather crashes occur on a yearly basis that not only result in large economic losses but could even result in the death or full incapacitation of individuals involved. It is because of this that ensuring adequate skid resistance is essential to improve public safety. The macroeconomic analysis quantifies an estimate of the average economic loss that is associated with motor-vehicle accidents in Texas and predict the monetary savings that can be obtained by having full coverage of friction levels on an annual basis, which results in better allocation of funds to preventive maintenance projects to bring the skid back to serviceable levels and ultimately reduces the number of crashes.

## Average Economic Loss Associated with Motor Vehicle Accidents

The National Safety Council in the United States has developed a guide to calculating the average costs associated with motor-vehicle injury based on accident severity, as shown in **Table C.1**. These average cost estimates account for wage and productivity losses, medical expenses, administrative expenses, motor-vehicle damage, and employer's uninsured costs. However, these

quantities are conservative as they do not account for the value of lost quality of life, which has to be empirically calculated (Injury Facts, 2021). All costs are based on 2019 dollars thus, they were converted to 2021 dollars using a consumer price index of 8.19% based on current inflation trends.

**Table C.1: Average Economic Cost by Injury Severity or Crash 2019 (Injury Facts, 2021)**

| Accident Severity | Ave. Economic Cost in 2019 (in millions of dollars) | Ave. Economic Cost in 2021 (in millions of dollars) |
|---|---|---|
| Death | $1.704 | $1.840 |
| Disabling | $0.098 | $0.106 |
| Evident | $0.029 | $0.031 |
| Possible | $0.023 | $0.025 |
| No Injury | $0.012 | $0.014 |
| Property Damage | $0.004 | $0.005 |

To estimate the total monetary costs of motor-vehicle accidents in Texas, the research team used the TxDOT yearly report on "Urban and Rural Crashes and Injuries by Severity for 2020". The research team does not know what the current trend for crashes in Texas is, thus the values for 2020 were used in this analysis. The total expected cost of motor-vehicle accidents in Texas across all levels of accident severity was computed by multiplying the average economic cost in 2021 dollars by the number of accidents for each level of accident severity. A table summarizes the number of crashes in the state of Texas by crash severity and the expected monetary cost for each accident is shown in **Table A.2.**

**Table C.2: Summary of Urban and Rural Crashes and Injuries by Severity for 2020 in Texas**

| Accident Severity | Number of crashes | Expected Monetary Cost (in millions of dollars) |
|---|---|---|
| Death | 3,542 | $6,520 |
| Disabling | 12,107 | $1,280 |
| Evident | 46,209 | $1,420 |
| Possible | 82,663 | $2,090 |
| No Injury | 308,136 | $4,160 |
| Property Damage | 21,892 | $109 |
| **Total Expected Cost (in millions of dollars)** | | **$15,579** |

Assuming that the number of crashes in Texas across each category remain relatively unchanged from 2020, the total expected cost incurred by both the state and its constituents is estimated to be about $15.579 billion.

## Potential Outcome of Project Implementation

Consider the case where the products from this project are implemented, enabling TxDOT to have reliable friction estimates across the entire highway network. Having complete friction information on their network allows the maintenance division to identify hot spots in along the network with low skid resistance and address the issue by applying a high-friction courses of chip seals to improve the road's friction. Based on the regression analysis conducted in this study, it was seen that the average difference between a chip seal with low macrotexture and one with high macrotexture is in the order of 13 in SN. It can be conservatively assumed that this is the average increase in SN once a seal coat is laid on top of a low friction road. This is a conservative estimate because the average difference between a high macrotexture chip seal and the other mixes a much higher. From data collected by the research team, the lowest skid that was found from a sample of 20 pavement surfaces was SN = 25. Once a seal coat is laid, the pavement section is expected to have a skid number of 38.

To translate this improvement in skid to a reduction in crashes, the study by Burchett and Rizenbergs (1982) was utilized. The study sought to quantify the effect that the level of skid resistance had on wet weather accidents. The study found that a significant increase in the percentage of wet pavement accidents occurs when SN70R drops below 27. SN70R stands for the skid number measured at 70 km/h using a ribbed tire. Their fitted model can be found in **Figure C.1.** The equation for the fitted model in **Figure C.1** was used to estimate the average percentage of wet weather accidents expected to occur on a road given its skid number. The percentage of wet weather accidents before and after the treatment were computed to be 33.6% and 23.8%, respectively. This means that by applying a seal coat to improve the skid, we could expect an average reduction of 9.7% in wet weather accidents on every pavement section that is treated. Being conservative, it can be assumed that the average reduction in wet weather crashes due to all the maintenance work across the network is 5%, half of what the equation in **Figure C.1** estimates.
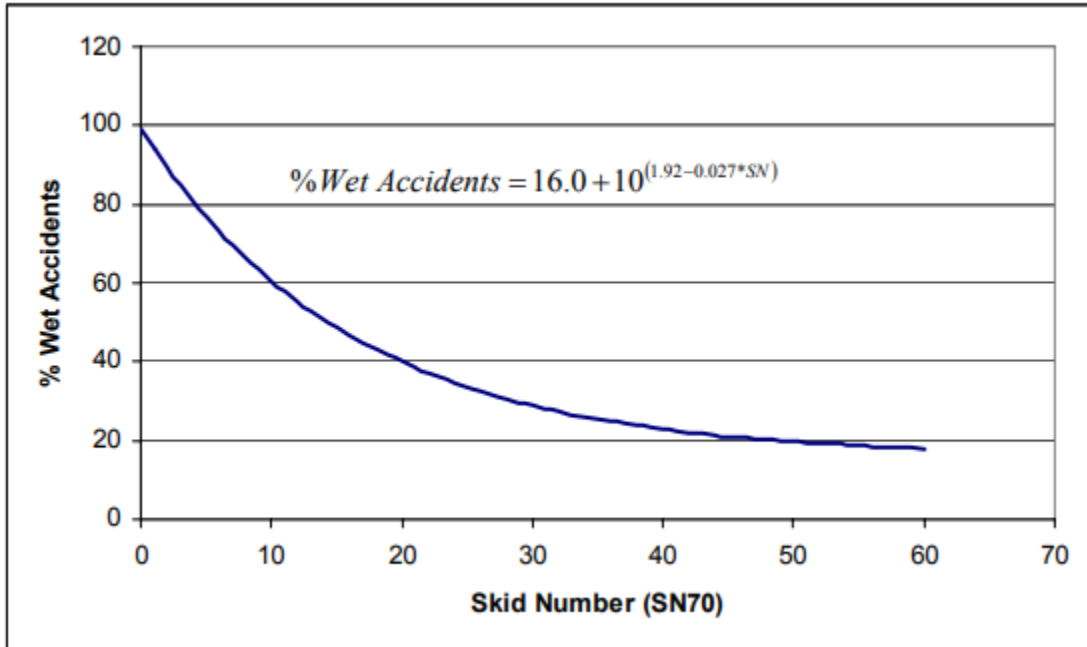
$$\%Wet\ Accidents = 16.0 + 10^{(1.92-0.027*SN)}$$

*Figure C.1: Percentage of Wet Crashes Varying with SN70R (Burchett and Rizenbergs, 1982)*

Data from the Crash Records Information System (CRIS for short) indicates that out of the total crashes that occurred in Texas in 2020, about 16% occurred during wet weather conditions (TxDOT, 2021). Meaning that out of the total of 398,622 crashes 75,927 were wet weather-related crashes. It is now assumed that dry weather crashes remain unchanged. Given these assumptions, the number of wet and total accidents after TxDOT treats low skid sections are 72,130 and 470,752, respectively. All that remains is to match the proportion of crashes across each category to the ones observed in 2020 and the expected monetary cost after treatment can be computed. **Table C.3** summarizes all the information needed to compute the total expected monetary cost after implementation.

**Table C.3: Summary of information to compute total expected monetary cost after implementation**

| Parameter | Value |
|---|---|
| Number of accidents in 2020 | 474,549 |
| Wet weather accidents | 75,927 |
| Avg. reduction in wet weather accidents | 5% |
| Wet weather accidents after treatment | 72,130 |
| Number of accidents after treatment | 470,752 |

| Accident Severity | Proportion of total | New Number of Crashes | Expected Monetary Cost (in millions of dollars) |
|---|---|---|---|
| Death | 0.01 | 3,514 | $6,510 |
| Disabling | 0.03 | 12,010 | $1,280 |
| Evident | 0.10 | 45,839 | $1,420 |
| Possible | 0.17 | 82,002 | $2,090 |
| No Injury | 0.65 | 305,671 | $4,150 |
| Property Damage | 0.05 | 21,717 | $109 |
| Total Cost (in millions of dollars) | | | $15,559 |

After maintenance improvement, the total cost for the state and its constituents is $15.559 billion. This is a total savings of almost $20 million dollars at a macroeconomic state-wide level.

## NPV Cost Benefit analysis

The final economic analysis was conducted by using the Excel template provided by TxDOT. This template performs a net present value (NPV) cost-benefit analysis by considering:

1. Project budget: the total amount of money allocated to finance this research project, measured in dollars,
2. Project duration: the agreed upon timeframe for project completion, measured in years,
3. Expected value per year: An estimation of the annual savings incurred by TxDOT after implementing the project's products, measured in dollars,

4. <u>Expected value duration</u>: the timeframe over which this economic analysis is conducted, measured in years, and

5. <u>Discount rate</u>: the interest rate used in discounted cash flow analysis to determine the present value of future cash flows, measured as a percentage.

Many of the inputs were dictated by TxDOT or could not be varied as they were based on values from the contract; however, there are two terms, Exp. Value (per Yr) and Expected Value Duration (Yrs), which the research team had full freedom to vary. The values associated with those two terms (highlighted in yellow at the top of **Figure C.2**) governed the outputs of the economic analysis.

## Inputs for the economic analysis

The project budget was set to $348,740. This value was the agreed upon budget as stipulated in the project's contract team. The inputted project duration was 2.3326 years. The University Handbook (2016) states that the project duration is not rounded. The project commenced on January 1, 2019 and the termination date is December 31, 2021. There are 852 days from the start date of the project to the end date (with the end date included), which equates to 2.3326 years. The expected value per year was $20 million. This input is the total savings that was computed for the macro analysis. As mentioned in the previous sections most of the values used in both analyses were as conservative as possible. The expected value duration of the project was assumed to be 10 years to reflect a potential timeframe between the inception of this project and the time it takes for it to be fully implemented. Finally, the input for the discount was 5% as recommended by the University Handbook (2016). The inputs and outputs of this economic analysis can be seen at the top of **Figure C.2** and a graphical representation of the NPV measured in millions of dollars over the timeframe of the economic analysis can be seen at the bottom of **Figure C.2.**

| Project # | 0-7031 | | |
|---|---|---|---|
| Project Name: | Develop Efficient Prediction Model of Highway Friction on an Annual Bassis on Texas Network | | |
| Agency: | CTR | Project Budget | $ 348,740 |
| Project Duration (Yrs) | 2.33 | Exp. Value (per Yr) | $ 20,000,000 |
| Expected Value Duration (Yrs) | 10 | Discount Rate | 5% |

**Economic Value**

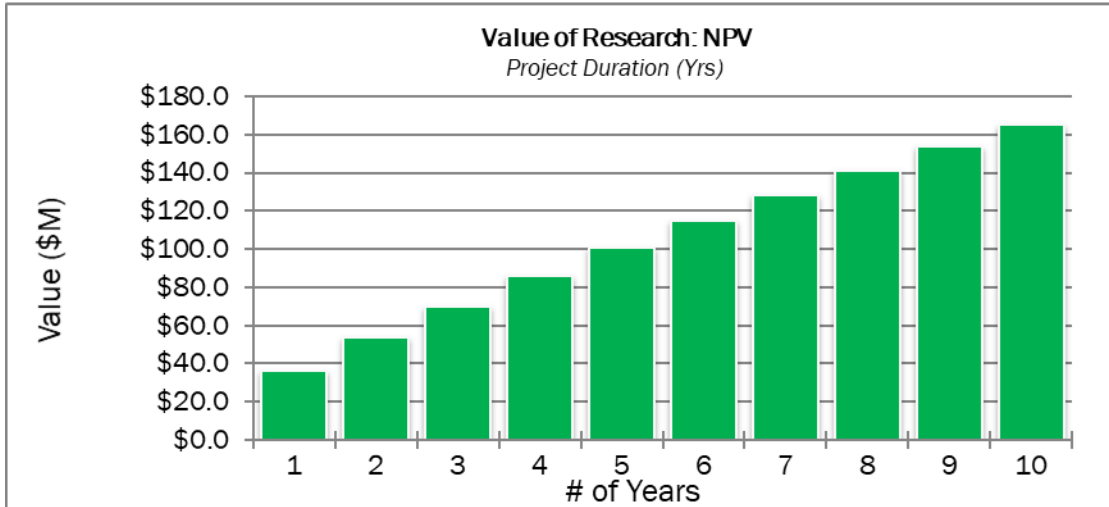| Total Savings: | $ 199,651,260 | Net Present Value (NPV): | $ 165,353,534 |
|---|---|---|---|
| Payback Period (Yrs): | 0.017437 | Cost Benefit Ratio (CBR, $1 : $___): | $ 474 |



**Figure C.2** *Inputs and outputs of NPV cost-benefit analysis (top), graphical representation of NPV over the course of ten years (bottom)*

## Conclusion

The expected economic savings that this project could generate for road users and TxDOT as a whole was estimated to be $200 million over the course of 10 years. From a purely mathematical point of view, this project is paid back in a small fraction of a year (0.017) and has a cost benefit ratio of 474. These extremely high values are not uncommon given for projects that deal with driver safety. The recommended technology from this project allows for more information of skid along any given section on the TxDOT network by providing measurements at any distance, continuously. Giving TxDOT added information on skid to identify and apply corrective measures. A tool that saves money for the agency and lives on the road.